

ABSTRACT

Title of dissertation: THE OPTICAL KERR EFFECT OF LIQUIDS

Xiang Zhu, Doctor of Philosophy, 2007

Dissertation directed by: Professor John T. Fourkas
Department of Chemistry and Biochemistry

Optical Kerr effect (OKE) spectroscopy has found broad use in monitoring ultrafast dynamics in transparent media. I demonstrated that by using two pump pulses with independently-controllable polarizations, intensity and timing, different contributions to the OKE signal in liquids can be enhanced and suppressed, and I characterize in detail perpendicularly-polarized pulses used for the excitation step in OKE spectroscopy. The results indicate that the signal can be described well as arising from the sum of independent third-order responses initiated by each pump pulse.

OKE spectroscopy has been used to study the orientational dynamics of benzene and benzene-d₆ confined in nanoporous sol-gel glass monoliths with a range

of average pore sizes. The orientational dynamics are described well by the sum of two exponentials, one of which depends on pore size. Comparison to Raman linewidth data suggests that the liquid exhibits significant structuring at the pore walls, with the benzene molecules lying flat on the surfaces of unmodified pores. OKE spectroscopy has also been used to study the temperature-dependent orientational dynamics of a series of nitriles with n-alkyl chains ranging from one to 11 carbons in length. In all cases the orientational diffusion is found to be described by a single-exponential decay. Analysis of the orientational correlation times using the Debye–Stokes–Einstein equation suggests that the molecules adopt extended configurations and reorient as rigid rods. The liquids with shorter alkyl chains undergo an apparent ordering transition as they are cooled.

THE OPTICAL KERR EFFECT OF LIQUIDS

by

Xiang Zhu

Dissertation submitted to the Faculty of the Graduate School of the
University of Maryland, College Park in partial fulfillment
of the requirements for the degree of
Doctor of Philosophy
2007

Advisory Committee:

Professor Amy Mullin, Chair
Professor Howard M. Milchberg
Professor John Weeks
Professor Robert Walker
Professor John T. Fourkas

©Copyright by

Xiang Zhu

2007

Acknowledgements

My work presented in this thesis cannot be accomplished without the assistance, guidance and support of many individuals. Unfortunately it is impossible to directly acknowledge all of the people to whom I am indebted, however, the following deserve mention for their extraordinary contributions to my research and my life.

First and foremost, I must thank my wife, Yan, who persuaded me to attend graduate school in United States. During the past 5 years, she provided unwavering love and support for all of my endeavors. In the first few years when I was in Boston College, it was her who sometimes helped to align the laser beam. I am very extremely luck to have such a loving family- I love you, and could never have done it without you.

I am deeply indebted to my advisor, Prof. John Fourkas, for invaluable discussion and much needed encouragement in order to complete this project. His uncanny ability to obtain funding allowed us to build a truly state of the art laboratory. Dr. Rick Farrer taught me everything about the experiment setup and laser adjustment in detail when I was at Boston College. He alone is responsible for all the Labview programming that made data acquisition and analysis seem so perfect. I am truly grateful to Tommaso Baldacchini, Chris Lafratta, Qin Zhong, Linjie Li for eternal discussions about optics, lasers and life. Thanks goes to everyone else in Fourkas group, especially Erez

Gershgoren, The more I got to know Eriz, the more I realized that he is the model of a Scholar for me. Last but not least, thanks for G. Finkenbiner for outstanding scientific glassblowing, Alan Vashon of the B.C machine shop, and Steve Smith at Coherent.

Most of the work presented in this thesis was supported by funds from the National Science Foundation, the Camille and Henry Dreyfus foundation.

Contents

1. Introduction

1.1	Motivation.....	1
1.2	Early origins and background.....	2
1.3	Advantages of our configuration.....	8
1.4	The Deconvolution procedure and heterodyne detection.....	10
1.5	Impulsive stimulated Raman scattering.....	12
1.6	Surface dynamics of liquids in Nanopores.....	16
1.7	Outline of thesis.....	22
1.8	Endnotes.....	23

2. Methods

2.1	The optical experimental set-up.....	26
2.2	Data acquisition.....	29
2.3	Sol –gel preparation and characterization.....	30
2.4	Endnotes.....	35

3. Mode selective OKE spectroscopy

3.1	Introduction.....	36
3.2	Experimental section.....	37

3.3	Theory.....	38
3.4	Results.....	42
3.5	Conclusion.....	47
3.6	Endnotes.....	48

4. OKE spectroscopy using time delayed pairs of pump pulses with orthogonal polarizations

4.1	Introduction.....	49
4.2	Experimental section.....	50
4.3	Theory.....	51
4.4	Results.....	55
4.5	Discussion.....	65
4.6	Conclusion.....	71
4.7	Endnotes.....	72

5. Ultrafast orientational dynamics of nanoconfined benzene

5.1	Introduction.....	73
5.2	Experimental section.....	75
5.3	Results.....	76
5.4	Discussion.....	84

5.5	Conclusion.....	93	
5.6	Endnotes.....	95	
6. Orientational diffusion of n-alkyl cyanides			
6.1	Introduction.....	97	
6.2	Experimental section.....	99	
6.3	Results.....	101	
6.4	Discussion.....	103	
6.5	Conclusion.....	120	
6.6	Endnotes.....	121	
7. New OKE technique for microscopy			
7.1	Introduction.....	123	
7.2	Experimental section.....	123	
7.3	Results.....	129	
7.4	Conclusions.....	132	
7.4	Endnotes.....	134	
8. Conclusions.....			135
9. Appendix.....			139
10. References.....			141

List of figures

1.1	Optical Kerr effect Geometry.....	4
1.2	OKE data for propionitrile in 290K.....	7
1.3	Mechanisms for impulsive stimulated scattering.....	13
1.4A	Schematic diagram illustrating the spontaneous Raman (A)	15
1.4B	Schematic diagram illustrating the OKE experiment (B).....	15
2.1	Schematic of OKE experiment.....	26
2.2	Sol-Gel nanoporous glass monoliths.....	34
3.1	Schematic of the optics for creation of dual pump pulses.....	37
3.2	Mechanisms for mode selective of coherent vibrational motion, represented in the figure by coherent wavepacket propagation.....	41
3.3	Mode-selective OKE decays for propionitrile.....	44
3.4	Semilog plots to demonstrate the complete suppression of the reorientational signal.....	44
3.5	OKE decays for S ₂ Cl ₂	46
4.1	Experimental setup for creating perpendicularly polarized pump pulses.....	51
4.2	Ladder diagram representations of processes that contribute to the OKE decay..	52
4.3	OKE decays for benzene.....	56
4.4	Ratio of pump beam intensities required to cancel the orientational diffusion component.....	58
4.5	OKE decays for iodobenzene at room temperature.....	60
4.6	OKE decays for chloroform.....	61
4.7	Ratio of pump beam intensities required to suppress the contribution of one mode in chloroform.....	63
4.8	Mode-selective for iodobenzene.....	64
4.9	OKE decay for mixture of chloroform and chlorobenzene.....	65

4.10	Imaginary portion of the Fourier transform of OKE decays of mixture of chloroform and chlorobenzene.....	66
5.1	Collective orientational correlation functions for benzene in the bulk (bottom trace) and, from top to bottom, confined in 24 Å, 34 Å, 49 Å, 60 Å and 73 Å pores. All data were obtained at 293K and the correlation functions have been offset for clarity.....	77
5.2	Collective orientational correlation functions for benzene-d ₆ in the bulk (bottom trace) and, from top to bottom, confined in 27 Å, 34 Å, 42 Å, 49 Å, 50 Å, 60 Å, and 73 Å pores. All data were obtained at 293 K and the correlation functions have been offset for clarity.....	77
5.3	Fastest decay time (τ_1) as a function of the pore curvature (inverse of the pore diameter) for benzene (solid circles) and benzene-d ₆ (open circles). The data points at zero curvature are for the bulk liquids, and the lines are linear least-squares fits to the data.....	82
5.4	Calculated surface-layer thickness for benzene (solid circles) and benzene-d ₆ (open circles) as a function of pore diameter.....	82
5.5	Representative OKE decays for benzene in 34-Å pores that are untreated (solid line) and that have surface methyl groups (dashed line).....	83
5.6	Fastest decay time (τ_1) as a function of the pore curvature (inverse of the pore diameter) for benzene (solid circles) and benzene-d ₆ (open circles) in silanized pores. The data points at zero curvature are for the bulk liquids, and the lines are linear least-squares fits to the data.....	83
5.7	Calculated surface-layer thickness for benzene (solid circles) and benzene-d ₆ (open circles) as a function of pore diameter in silanized pores.....	85
5.8	Estimated values of g_2 , surface as a function of pore curvature.....	85
6.1.	Collective orientational correlation function (solid line) and biexponential fit (dottedline) for butyl cyanide at 366.5 K. The lower panel shows the residual derived by subtracting the fit from the data.....	101

6.2	Collective orientational correlation functions for butyl cyanide as a function of temperature.....	102
6.3	Plot of τ_2 versus τ_1 from all of the OKE decays reported previously for methyl cyanide and for all of those summarized here in tables 6-2 to 6-11.....	112
6.4	Debye–Stokes–Einstein plot for butyl cyanide.	114
6.5	Value of η/T at the transition in slopes in the DSE plot for alkyl cyanides as a function of number of carbons in the alkyl chain.....	115
6.6	Slope of the DSE plots as a function of molecular volume for methyl cyanide and the liquids studied here. Circles denote slope 1 and squares slope 2.....	115
6.7	Slope of the DSE plots as a function of hydrodynamic volume assuming fully extended alkyl chains for methyl cyanide and the liquids studied here.	116
7.1	First-generation antiresonant-ring OKE spectrometer.....	125
7.2	Schematic diagram of the second-generation ARKS spectrometer.....	128
7.3	$R_{xxxx}(\tau)$ response of CS ₂ at room temperature.....	130
7.4	$R_{xxyy}(\tau)$ response of CS ₂ at room temperature.....	131
7.5	Isotropic $R_{xxmm}(\tau)$ response of CS ₂ at room temperature.....	131
7.6	Depolarized $R_{xxyy}(\tau)$ response of CS ₂ at room temperature.....	132

List of tables

1-1 Collective reorientational times(τ_R) for several liquids at 290 K. All relaxation times are measured in picoseconds. The approximate uncertainty in each time is ± 5 in the last digit.....	7
5-1 Fit Parameters and Surface Layer Thickness for Benzene in Unmodified Pores.....	79
5-2 Fit Parameters and Surface Layer Thickness for Benzene- d_6 in Unmodified Pores.....	79
5-3 Fit Parameters and Surface Layer Thickness for Benzene in Modified Pores.....	80
5-4 Fit Parameters and Surface Layer Thickness for Benzene- d_6 in Modified Pores....	80
5-5 Comparison of Raman and OKE Data for Benzene- d_6 in Unmodified Pores.....	90
6-1 Melting points, boiling points, and slopes of Debye–Stokes–Einstein plots for the liquids studied here.....	100
6-2 Normalized amplitudes and decay times for biexponential fits to $C_{\text{coll}}(\tau)$ for ethylcyanide as a function of temperature.....	103
6-3 Normalized amplitudes and decay times for biexponential fits to $C_{\text{coll}}(\tau)$ for propyl cyanide as a function of temperature.....	104
6-4 Normalized amplitudes and decay times for biexponential fits to $C_{\text{coll}}(\tau)$ for butyl cyanide as a function of temperature.....	104

6-5. Normalized amplitudes and decay times for biexponential fits to $C_{\text{coll}}(\tau)$ for pentyl cyanide as a function of temperature.....	105
6-6 Normalized amplitudes and decay times for biexponential fits to $C_{\text{coll}}(\tau)$ for hexyl cyanide as a function of temperature.....	105
6-7 Normalized amplitudes and decay times for biexponential fits to $C_{\text{coll}}(\tau)$ for heptyl cyanide as a function of temperature.....	106
6-8 Normalized amplitudes and decay times for biexponential fits to $C_{\text{coll}}(\tau)$ for octyl cyanide as a function of temperature.....	106
6-9 Normalized amplitudes and decay times for biexponential fits to $C_{\text{coll}}(\tau)$ for nonylcyanide as a function of temperature.....	107
6-10 Normalized amplitudes and decay times for biexponential fits to $C_{\text{coll}}(\tau)$ for decylcyanide as a function of temperature.....	107
6-11 Normalized amplitudes and decay times for biexponential fits to $C_{\text{coll}}(\tau)$ for undecyl cyanide as a function of temperature.....	108
7-1 The different tensor elements by changing the timing and polarization of all pulses.....	130

Chapter 1

Introduction

1.1 Motivation

Nonlinear optical techniques are revolutionizing optical microscopy by increasing its sensitivity and resolution and by providing new types of image contrast.¹⁻⁴ We are still in the infancy of this revolution, and many powerful nonlinear optical techniques remain to be explored fully in the context of microscopy. One such technique is optical Kerr effect (OKE) spectroscopy.⁵⁻⁸

Optical Kerr effect (OKE) spectroscopy has found broad use in monitoring ultrafast dynamics in transparent media.⁹⁻¹² In recent years, this technique has been applied to the study of simple,¹³⁻¹⁹ supercooled,²⁰⁻²³ ionic,²⁴⁻²⁶ and confined²⁷⁻³⁰ liquids, liquid mixtures,³¹⁻³⁶ polymers,³⁰⁻³⁷ biomolecules,³⁸⁻⁴⁰ and complex fluids.⁴¹⁻⁴⁵ Interest is also developing in using OKE spectroscopy as a means of achieving contrast in nonlinear microscopy.⁴⁶ Such contrast could in principle be based on any of the contributions to the OKE signal, which include electronic hyperpolarizability, impulsively excited intermolecular modes, impulsively excited, Raman-active intramolecular vibrations, and molecular reorientation. In practice, however, separating these different contributions from one another is often difficult due to a considerable degree of overlap in the time scales of the processes that are involved. Recently I introduced a technique that allows for the selective enhancement or suppression of specific contributions to the OKE

signal.⁴⁷ This method draws its inspiration from the work of Weiner, Nelson, and co-workers,⁴⁸⁻⁵⁰ who demonstrated that by employing trains of pulses with a spacing equal to the period of a specific Raman-active vibration for excitation the contribution of that mode to the OKE signal is strongly enhanced. While in that work all of the excitation pulses were of the same polarization, Wefers, Kawashima, and Nelson more recently demonstrated that with two perpendicularly polarized excitation pulses control could be exerted over the Raman-active lattice vibrations in crystalline quartz.⁵¹ Gershgoren et al. have also demonstrated a related technique with electronically resonant, parallel-polarized pump pulses on I_3^- in solution.⁵² I reported the application of a similar technique to liquids⁴⁷ and demonstrated that with two pump pulses with independently controllable timing, intensity, and polarization it is possible to suppress or enhance the contribution of a specific intramolecular vibrational mode or of reorientation to the OKE signal. While it is possible to exert a considerable amount of control over the contributions to the OKE signal with just two pump pulses, for microscopy and other applications ultimately it will be desirable to employ trains of pulses with arbitrary time delays, intensities, and polarizations to isolate the contributions of individual modes. To be able to design appropriate excitation pulse sequences, it is necessary to develop a detailed understanding of the dual-pulse-excitation scheme. With that goal in mind, in this thesis I will present a detailed study of the OKE spectroscopy of liquids using two excitation pulses.

1.2 Early origins and background

The Kerr effect was discovered in 1875 when it was suggested that an isotropic transparent medium becomes birefringent when placed in an electric field. In the electric field, the medium resembles a crystal whose optical axis corresponds to the direction of the applied field.⁵³ The two indices of refraction, $n_{//}$ and n_{\perp} are associated with the directions parallel and perpendicular to the applied field. The birefringence, ($\Delta n = n_{//} - n_{\perp}$) is found to be experimentally

$$\Delta n = \lambda_0 K E^2 \quad (1.1)$$

where K is the Kerr constant and λ_0 is the wavelength of light in vacuum.⁵³ Figure 1.1 demonstrates the experiment. The polarizers are aligned perpendicularly to one another so that no light is transmitted initially. When a voltage is applied across the sample, birefringence is induced. The alignment of molecules creates different phase velocities for the parallel and perpendicular components of the polarization. Thus, elliptically polarized light is obtained, which has a component that is transmitted by the analyzer. The Kerr effect has been used to create shutters in high-speed photography and choppers for light beams. Almost a century after its discovery, theoretical work by Mayer and Gires showed it was possible to use optical pulses instead of traditional electrical pulses to induce a birefringence in liquids.⁵⁴ The simplified optical Kerr effect geometry is in Figure 1.1. In 1969 Duguay and Hansen expanded this theory and produced the first experimental evidence of the Optical Kerr Effect (OKE) in the quadratic (homodyned) configuration using CS_2 and nitrobenzene.⁵⁵ They measured the orientational effects of a

liquid by creating an “ultrafast gate” using high-intensity picosecond pulses. In this configuration the transmitted signal (T) became quadratic in the pump intensity (I_{pump}) and linear in the probe intensity (I_{probe}):

$$T(\tau) = \int_{-\infty}^{\infty} dt I_{probe}(t - \tau) \times \left| \int_{-\infty}^t R^{(3)}(t - t') E_k^*(t') E_l(t') \right|^2 \quad (1.2)$$

where τ is the delay time, $R^{(3)}$ is the nonlinear-optical impulse response function of the material and $E_k^*(t')$ and $E_l(t')$ represent the electric field of the pump pulse. All the purely electronic hyperpolarizability degrees of freedom as well as the single-molecule intramolecular polarizabilities and collective intermolecular polarizabilities, are incorporated in $R^{(3)}$. Any detailed knowledge of the microscopic dynamics of liquids entails, therefore, an understanding of $R^{(3)}$.

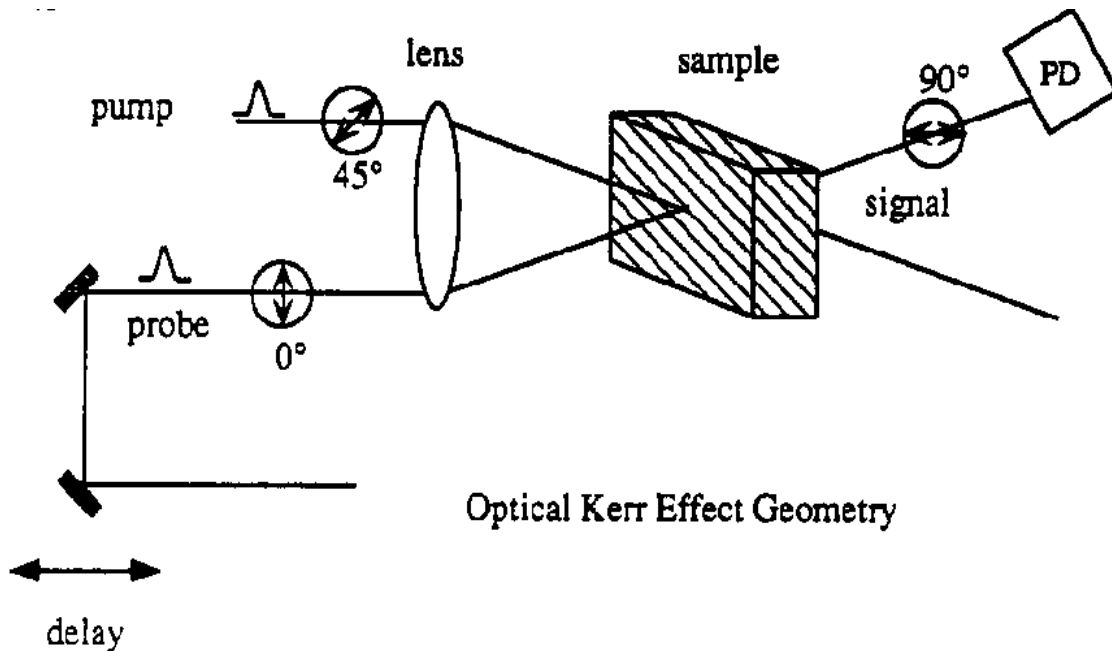


Figure 1.1 Optical Kerr Effect Geometry

In 1975 Ippen and Shank created the first heterodyne-detected optical Kerr gate to eliminate possible effects of pulse asymmetry in the Kerr signal.⁵⁶ The orientational correlation time of CS₂ was measured in “biased mode” with a quarter-wave plate slightly rotated. This technique, which consists of the coherent mixing at the detector of the local oscillator with signal field, resulted in a transmission that was linear in both pump and probe intensities and is given by :

$$T(\tau) = \int_{-\infty}^{\infty} R^{(3)}(t) I_{pump}(t) I_{probe}(\tau - t) dt \quad (1.3)$$

Though not recognized at the time of publication, the heterodyne-detected scheme dramatically increases the sensitivity of the experiment and, as discussed in section 1.3, allows for straightforward data analysis.

Because of poor signal to noise and relatively long laser pulses, quantitative information to this point was limited to orientational correlation times. The development of femtosecond lasers brought entirely new possibilities in our ability to utilize OKE spectroscopy. Utilizing amplified laser pulses from a CPM ring dye laser, a prominent sub-picosecond, yet noninstantaneous, response was first identified by Green and Farrow in 1983.⁵⁷ With significantly shorter pulses Kenney-Wallace and co-workers,⁵⁸ as well as Nelson and co-workers⁵⁹⁻⁶¹ independently confirmed the broad, low frequency vibrational character of intermolecular modes. They were able to observe directly three different components of the OKE signal that arose due to coupling between the radiation field and $R^{(3)}$, the third order susceptibility of the sample. One, an instantaneous off-resonant hyperpolarizability component, follows the temporal profile of the laser pulses (near time zero). The second, a slow picosecond diffusive component, was attributed to the

molecular orientational relaxation of the sample (delay > 2 ps). Finally, a sub-picosecond contribution was attributed to a variety of different molecular motions available to a liquid, including intramolecular vibrations, hindered rotations (librations), and collision-induced (dipole-induced dipole) interactions.

Figure 1.2 shows OKE data for propionitrile at 290 K. All the microscopic molecular motions described above are interrogated directly in real time. Evident in data is a clear separation of the instantaneous electronic response (near zero delay) followed by the slower nuclear response of the sample. Non-exponential intermolecular relaxation continues out to about two picoseconds delay. The damped sinusoidal oscillations superimposed on this decay are characteristic of intramolecular vibrational modes in the sample. Since OKE spectroscopy reveals details of the fast librational and collision induced effects as well as the slow reorientational motions in a single experiment, it is ideally suited for the interpretation of the complex dynamics that occur in liquids.

Decay times for several liquids are summarized in Table 1-1.

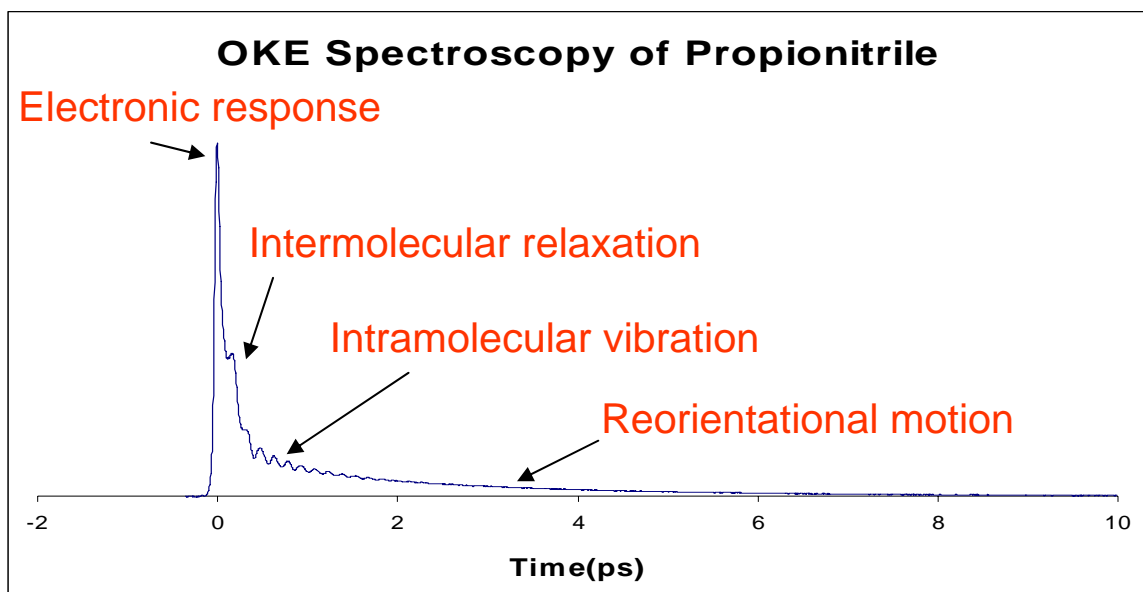


Figure 1.2 OKE data for propionitrile in 290K.

Table 1-1. Collective reorientational times (τ_R) for several liquids at 290 K. All relaxation times are measured in picoseconds. The approximate uncertainty in each time is ± 5 in the last digit.

Liquids	τ_R
Water (H ₂ O)	0.89
Acetonitrile (CH ₃ CN)	1.64
Acetonitrile-d ₃ (CD ₃ CN)	1.84
Carbon disulfide (CS ₂)	1.84
Methyl iodide (CH ₃ I)	2.51
Benzene (C ₆ H ₆)	3.19
Choloroform (CHCl ₃)	3.28
Benzene-d ₆ (C ₆ D ₆)	3.36
Sulfur monochloride (S ₂ Cl ₂)	7.25
1,3,5, trifluorobenzene (C ₆ H ₃ F ₃)	10.23
Mesitylene ((CH ₃) ₃ (C ₆ H ₃))	11.78
Hexafluorobenzene (C ₆ F ₆)	15.23

1.3 Advantages of our configuration

Although the transient response provides the same information found in frequency-domain data, OKE spectroscopy has several experimental advantages over Rayleigh-wing spectroscopy. Similarities between overdamped intermolecular modes and purely relaxational modes in the frequency domain make them almost impossible to distinguish clearly in light scattering spectra. These similarities are not as apparent in the time domain, where the resolution is limited strictly by the spectral width of the pulse and the time interval per step on the delay line. Higher resolution spectra can be obtained simply by increasing the number of data points in the time domain measurement. The OKE experiment measures the spectral response of the liquid in real time, whereas depolarized light-scattering data are weighted by the Bose-Einstein prefactor, which distorts the spectral line shape. Furthermore, reorientational dynamics can be characterized readily in the time domain by fitting the logarithm of the diffusive response over many orders of e . This decay can subsequently be subtracted off before data are converted into the frequency domain. Finally, in the light scattering experiment the high frequency “Rayleigh wing” is generally at least an order of magnitude weaker than the central Lorentzian feature (diffusive reorientation); in contrast, intense short pulses have made OKE measurements extremely sensitive in this spectral region. In general, time-domain experiments end up being better for studying slow dynamics and frequency domain experiments are better for fast dynamics. It was originally speculated that the nonlinear time-domain experiment could separate the spectroscopic effects of homogeneous and inhomogeneous broadening. However, theoretical work of Loring and

Mukamel demonstrated that current spectroscopic techniques were incapable of distinguishing among the various contributions of the spectral lines since the excitation mechanism is still formally linear.⁶² Higher-order Raman-echo experiments, which involve more than one time evolution period, are needed to unambiguously resolve the fast and slow components of the spectral lineshape.

The optically-heterodyned Kerr effect configuration also has significant advantages over the homodyned “zero-background” Kerr configuration. In addition to the enhanced sensitivity and higher signal-to-noise ratio, the optically heterodyned technique has the advantage of directly measuring $R^{(3)}$ instead of its magnitude squared. The appearance of troublesome cross terms in $|R^{(3)}|^2$ increases the dynamic complexity of the transient signal and eliminates the possibility of direct Fourier transform analysis. McMorrow and Lotshaw have shown how the in-quadrature heterodyned portion of the OKE signal can be used, along with the second harmonic generation (SHG) autocorrelation of the laser pulses, to obtain the real part of the nonlinear response function.⁶²⁻⁶⁴ This deconvolution procedure permits the clean separation of the nuclear and electronic contributions and corrects for the spectral filter effects of finite-duration optical pulses.⁶² Since the pulse itself acts as a low-pass frequency filter of the material response function, longer pulses have a tendency to filter out high frequency oscillators. These oscillators, which are not excited by the spectral bandwidth of the pulse, give rise to less destructive interference and a slower dephasing time. Spectral-filter effects accounted for the wide discrepancies in previously reported CS₂ OKE response times.

The following section briefly summarizes the formalism described by McMorro and Lottshaw.

1.4 The deconvolution procedure and heterodyne detection

If the laser pulses are transform-limited, the heterodyned portion of the signal is given by eq. 1.3, which can be rearranged into a more convenient form as:

$$T(\tau) = \int_{-\infty}^{\infty} G_0^2(\tau - t) R^{(3)}(t) dt \equiv G_0^{(2)}(\tau) \otimes R_{ijkl}(\tau) \quad (1.4)$$

where $R_{ijkl}(\tau)$ is the real part of the nonlinear response function and $G_0^{(2)}(\tau)$ is the SHG autocorrelation of the laser pulse. The Fourier transform of the convolution of two functions is equal to the product of the Fourier transforms of the functions, so $R_{ijkl}(\tau)$ can be derived from

$$R_{ijkl}(\tau) = \mathfrak{F}^{-1} \left[\frac{\mathfrak{F}(T(\tau))}{\mathfrak{F}(G_0^{(2)}(\tau))} \right] = \mathfrak{F}^{-1} [D_{ijkl}(\Delta\omega)] \quad (1.5)$$

where \mathfrak{F} and \mathfrak{F}^{-1} denote forward and reverse Fourier transforms, respectively and $D_{ijkl}(\Delta\omega)$ is the frequency-domain representation of the material response function. The nonlinear function is comprised of two parts,

$$R_{ijkl}(t) = \sigma_{ijkl}(t) + \Phi_{nuc}(t) \quad (1.6)$$

$\Phi_{nuc}(t)$ is the nuclear response and $\sigma_{ijkl}(t)$ is the response of the electron clouds of the molecules to the applied field (hyperpolarizability). Ultrashort pulses create an instantaneous electronic response, so we can write

$$\sigma_{ijkl}(t) = b\delta(t) \quad (1.7)$$

where b is an arbitrary constant. Since a delta function is completely symmetric, the electronic portion of the response is reflected only in the real part of $D_{ijkl}(\Delta\omega)$. Thus, the imaginary portion of $D_{ijkl}(\Delta\omega)$ depends only on the nuclear portion of the response function. Furthermore, since no signal is present before the pulse hits the sample, causality implies that the nuclear portion of the impulse response function is given by

$$R_{nuc}(t) = 2\Im^{-1} [\text{Im } D_{ijkl}(\Delta\omega)] H(t - t_0) \quad (1.8)$$

where $H(t)$ is the Heaviside step function (which is included to ensure causality). Therefore, the imaginary portion of $D_{ijkl}(\Delta\omega)$ provides enough information to derive the entire nuclear impulse response function. This clearly illustrates a powerful feature of the Fourier transform analysis of optically heterodyne-detected optical Kerr effect (OHD-OKE) data: its ability to separate uniquely the nuclear and electronic parts of the nonlinear optical transients.

The phase of the third-order polarization of the OKE signal is determined purely by the phase of the probe field. Referenced to the phase of the probe field, the signal field generated by the polarization can be written as:

$$E_s = (\text{Re } E_s + i \text{Im } E_s) e^{-i\omega t} \quad (1.9)$$

where $\text{Re}E_s$ and $\text{Im}E_s$ correspond respectively to the absorption and index of refraction portions of the response and ω_0 is the carrier frequency. By rotating the probe polarizer a slight amount ($<1^\circ$), a local oscillator field is generated that is $\pi/2$ out of phase with the probe beam but completely in phase with the index of refraction portion of the response:

$$E_{LO} = E_{probe} e^{-i\omega t} e^{i\pi/2} \quad (1.10)$$

The detected intensity is given by:

$$\begin{aligned} I &= |E_s + E_{LO}|^2 = |(\text{Re} E_s + i \text{Im} E_s) e^{-i\omega t} + E_p e^{-i\omega t} e^{i\pi/2}|^2 = |e^{-i\omega t}|^2 |(\text{Re} E_s + i(\text{Im} E_s + E_p))|^2 \\ &= E_p^2 + [(\text{Re} E_s)^2 + (\text{Im} E_s)^2] + 2E_p \text{Im} E_s = I_{LO} + I_s + 2E_{probe} \text{Im} E_s \end{aligned} \quad (1.11)$$

The first of these terms is the intensity of the local oscillator and its contribution is easily removed with a lock-in amplifier. The second term and third term are the homodyne and heterodyned components of the signal respectively. If the polarizer is rotated by the same amount in the opposite direction, the local-oscillator field is given by

$$E_{LO} = E_{probe} e^{-i\omega t} e^{-i\pi/2} \quad (1.12)$$

which results in a detected intensity of

$$I = I_{LO} + I_s - 2E_{probe} \text{Im} E_s \quad (1.13)$$

Thus, the difference between data sets taken with the polarizers rotated in opposite directions contains only the heterodyned contribution to the signal. Also, note that the heterodyned contribution to the signal can be made arbitrarily large compared to I_s by simply adjusting E_{probe} .

1.5 Impulsive stimulated Raman scattering⁶⁵

The development of femtosecond lasers brought entirely new possibilities into the practice of time-resolved vibrational spectroscopy. For the first time, it became possible to conduct observations on time scales that are not only shorter than vibrational lifetimes or dephasing times, but shorter than individual vibrational oscillation periods. There are two excitation mechanisms most commonly exploited for impulsive vibrational excitation, impulsive stimulated Raman scattering (ISRS), which can occur with nonresonant or resonant excitation wavelengths, and impulsive absorption, which can occur on resonance. Figure 1.4 illustrates impulsive stimulated Raman scattering when the excitation wavelength is far from any electronic absorption resonance. In this case, the ultrashort excitation pulse exerts a sudden (“impulsive”) driving force to initiate coherent vibrational motion in the ground electronic state of the molecule. The magnitude of the force, and the resulting coherent vibrational amplitude, are linearly proportional to the excitation light intensity and to the light-scattering differential polarizability for the mode being driven. This mode could be

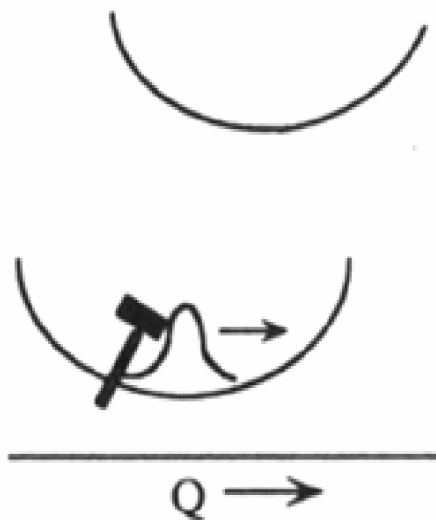


Figure 1.3 Mechanisms for impulsive stimulated scattering initiates coherent vibrations in the ground electronic state, represented in the figure by coherent wavepacket propagation. Q is vibrational displacement. an acoustic vibration of a liquid or solid, an optic phonon in a crystal lattice, a molecular vibration, or any other mode which is active in light scattering. The only requirements for ISRS excitation are that the pulse duration be short compared to the vibrational oscillation period and that the mode be Raman-active.

When the laser pulse is sufficiently short, OKE spectroscopy includes not only the partial ordering of molecules with respect to a certain polarization plane of a laser pulse, but it can also excite Raman active intramolecular vibrational modes. Ordinary Raman scattering involves a single monochromatic laser beam ω_i that is focused into the sample. Scattering off the sample results in the signal ω_s . The energy diagram is shown in Figure 1.4A. An optical heterodyned Raman-induced Kerr effect spectroscopy experiment, in contrast, involves the interaction of the sample medium with an ultrashort laser pulses having a bandwidth of several hundred cm^{-1} . The individual Fourier components of the

pump pulse ω_1 and ω_2 excite a low frequency Raman active mode of the sample. Any Raman active mode that lies within the bandwidth of the pump pulse can be excited. The state of the medium is later probed by another pulse ω_3 and the resulting signal ω_s produced. The energy diagram is shown in Figure 1.4B

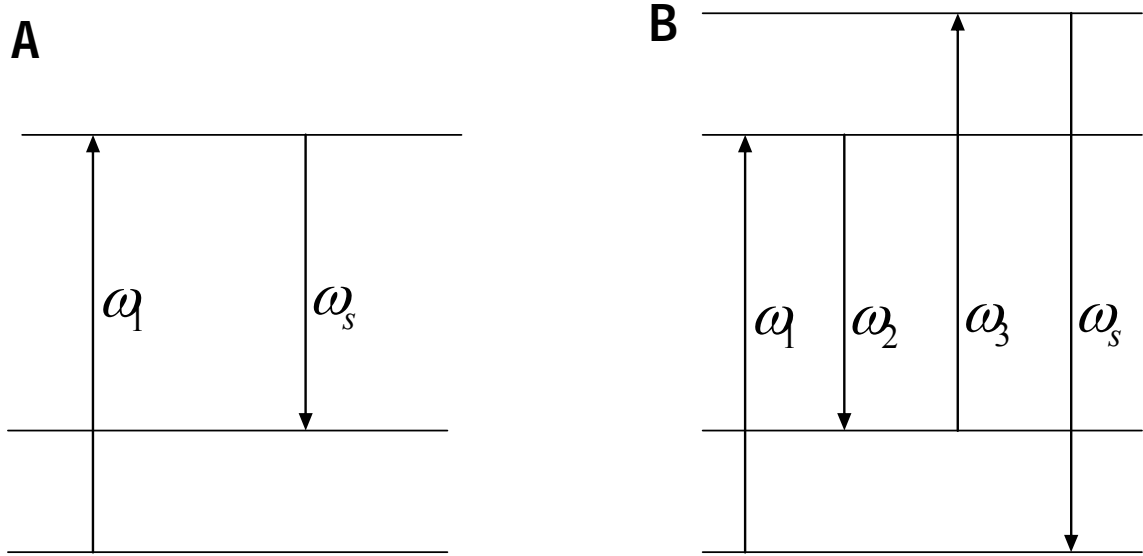


Figure 1.4 Schematic diagram illustrating the spontaneous Raman(A) and OKE experiment(B).

1.6 Surface dynamics of liquids in nanopores

The problem of the dynamical behavior of liquids in confined geometries has received considerable attention both from theoretical and experimental points of view. Understanding the role of confined geometry on dynamics of liquids is important for a variety of technological processes including catalysis, chromatography, oil recovery, and membrane separations. Despite the growing interest in the effects of confinement, little is known about the detailed mechanisms through which confinement acts on molecular relaxation processes. Therefore, it is not surprising that numerous experimental techniques have been employed to evaluate the effects of confinement on liquids, including dielectric spectroscopy,⁶⁷⁻⁶⁹ Raman scattering,⁷⁰⁻⁷² NMR spectroscopy,⁷³⁻⁷⁴ ultrafast spectroscopy,⁷⁵⁻⁷⁶ time resolved phosphorescence,⁷⁸ and dynamic light scattering.⁷⁹

On the basis of NMR experiments, Jonas and co-workers have made major contributions to the understanding of liquids in confinement. Changes in dynamics of several wetting, weakly wetting-liquids and fluorocarbon-based fluids have been observed upon confinement. The frequency of rotational or translational motion of magnetic and electric fields in the lattice nuclei is critical to the effectiveness of spin – lattice relaxation. It is common to express the frequencies of these types of molecular motion in terms of a so-called correlation time τ_c . If the angular rotation frequency is ω (in radians per second), the rotational correlation time is $\frac{1}{\omega}$, the time required for a molecule (or part of a molecule) to rotate 1 rad. Similarly, the translational correlation

time can be equated to the time required for a molecule to move a distance equal to one molecular diameter. In both cases τ_c is an average measure of how long the two nuclear magnetic dipoles remain in the appropriate relative orientation to interact. Furthermore, it can be shown that $\frac{1}{T_1} \propto \frac{\tau_c}{1 + (2\pi\nu_0\tau_c)^2}$, where ν_0 is the precessional frequency of the target nucleus. This equation tells us that for very fast molecular motion (i.e., when $1/\tau_c \gg 2\pi\nu_0$), $1/T_1$ is proportional to τ_c (T_1 is inversely proportional to τ_c). That is, as correlation time increases (molecular motion slows), relaxation time decreases (the rate of relaxation increases). Conversely, for slow molecular motion (i.e., when $1/\tau_c \ll 2\pi\nu_0$), T_1 is directly proportional to τ_c ; they both increase together. The minimum in T_1 (ca. 10^{-3} s), and hence the most efficient spin-lattice relaxation, occurs when $\tau_c = (2\pi\nu_0)^{-1}$. The ^2H spin-lattice relaxation rate ($1/T_1$) in a deuterium-labeled molecule is inversely proportional to the orientational correlation time τ_{or} . Thus, even when τ_{or} is on a picosecond time scale, T_1 may be milliseconds or longer. On this latter time scale, it is likely that each molecule samples the bulk-like and surface environments statistically. In this case, spin-lattice relaxation in a cylindrical pore is exponential with a rate given by:

$$\frac{1}{T_1} = \frac{1}{T_{1b}} + \frac{2a}{R} \left(\frac{1}{T_{1s}} - \frac{1}{T_{1b}} \right) \quad , \quad (1.14)$$

where T_{1b} is the relaxation time for the bulk liquid, T_{1s} is the relaxation time for the molecules in the surface layer, a is the thickness of the surface layer, and R is the pore radius. This is referred to as the two-state fast exchange model, since the equation is only valid when the diffusion between the surface and bulk-like phases is faster than the

experimental time scale. This model has been modified to include the effects of pure topological confinement. For instance, both methyl cyclohexane and perfluoro(methylcyclohexane) display an enhanced nuclear relaxation rate in confinement due to surface interactions and pure geometric confinement.

The basic two-state fast exchange model also has been supported by Raman measurements performed by Wallen *et al.*⁶⁶ In this study the Raman-active symmetric stretching mode, ν_1 (655 cm^{-1}), along with the first overtone bending mode ($2\nu_2$) were analyzed within the framework of the two-state fast exchange model, leading to the conclusion that the surface layer of CS_2 is approximately one monolayer thick at room temperature. Vibrational dephasing also appears to proceed more rapidly in confinement due to a collisional deactivation process with the walls of the silica glass. Furthermore, modification of the pore surfaces had no effect on either the vibrational or rotational relaxation. The decrease in the anharmonic coupling (Fermi resonance) between the ν_1 stretch and $2\nu_2$ bending mode in confinement indicates molecules become somewhat ordered within the pore.

Additional information about the role of surfaces was obtained by measurements of the non-coincidence effect in confined polar liquids. The non-coincidence effect arises when the isotropic and anisotropic Raman spectral bands have different frequencies. These differences are due to fluctuations in the intermolecular forces that are dependent on the orientation of the molecule. Several mechanism may contribute to this effect, such as hydrogen bonding and dipole-dipole interactions. In confinement the non-coincidence effect is reduced, but upon surface modification the effect returns to the bulk value.

Therefore, hydrogen bonding to the surface, rather than the dipole-dipole alignment of the polar liquid, is responsible for the reduced non-coincidence effect in the pores. This clearly demonstrates the influence of hydrogen bonds on the non-coincidence effect, which is not affected by geometrical confinement.

Using ^{13}C and ^{33}S spin lattice relaxation times of CS_2 in a variety of different pores, a theoretical model for anisotropic molecular reorientation and angular velocity for non-polar liquids was developed by Korb *et al.* The model is based on the idea that reorientation parallel to the pore surfaces is unaffected by confinement whereas reorientation perpendicular to the surface is hindered. The model predicts that the reorientational time perpendicular to the surface (τ_{\perp}) is given by:

$$\tau_{\perp} = \frac{\tau_b}{-\chi R \ln \left[1 - \frac{1}{\chi R} \left(1 - \frac{2I_1(\chi R)}{\chi R I_2(\chi R)} \right) \right]} \quad (1.15)$$

where τ_b is the bulk reorientational time, R is the pore radius, x is related to the orientational correlation length (which is assumed to be only weakly temperature dependent), and I_n is the n^{th} order modified Bessel function. It predicts the increase of the reorientational and angular velocity correlation times when the pore size is decreased. It predicts the increase of the reorientational and angular velocity correlation times when the pore size is decreased.

Investigators have used sol-gel glasses to study geometrical supercooling of liquids. The dielectric relaxation of a non-associating glass forming liquid was measured by Fischer and co-workers in 102 Å pores. The study revealed a distinct relaxation

process that was almost two orders of magnitude slower than the cooperative bulk relaxation. Upon surface modification, the peak was not observed. This feature was attributed to strong hydrogen bonding between the silanol groups on the surface and the polar N-methyl- ϵ -caprolactam molecules. The cooperativity of such an ordered structure was shown to enhance both the relaxation time and the strength of the dielectric loss peak. These results were, later, supported by optical measurements of salvation dynamics. This technique involved the use a chromophore (quinoxaline) with a long excited state lifetime, whose emission spectrum was monitored as a function of time. The chromophore represents a local probe for the orientational relaxation of permanent dipole moments revealing information complimentary to dielectric spectroscopy.

Experiments have been performed within porous glasses in order to increase the surface area probed. The relationship between liquid dynamics in this curved geometry and on a planar surface, however, is unclear. For the past decade, our group has used nanoporous glasses in concert with ultrafast OKE spectroscopy to gain a molecular level understanding of how factors such as molecular shape, chemical interactions, temperature, and the geometry and dimensions of the confining medium influence dynamics and structure of a liquid, both wetting and weakly-wetting. Most of the results described to this point have been analyzed assuming two distinct population within the pores, each having its own viscosity. However, it is equally likely that there exists a continuous range of viscosities that extend from the surface to the inner pore. Ultrafast time-domain techniques such as the OKE can monitor relaxation in real time, and can therefore probe directly the distribution of relaxation times. Furthermore, extraction of quantitative

population information from the OKE data is straightforward. For a system with multiple populations of molecules, the reorientational portion of the OKE signal is given by:

$$S(t) = \sum_n \left(\frac{p_n}{\tau_n} \right) e^{-t/\tau_n}, \quad (1.16)$$

where p_n is the relative population of molecules with reorientational time τ_n . Studying the dependence of reorientational relaxation on pore size and temperature provides a detailed picture of the microscopic dynamics that is essential to understanding the chemistry of microconfinement. Based on the results a general picture of liquids confined in nanoporous silicate glasses has emerged. The dynamics of the confined liquids are slower than those observed in the bulk. This inhibition arises from a number of different mechanisms, including geometrical constraints for reorientation at the pore surface and a change in the hydrodynamic volume for reorientation of molecules off of the pore walls in weakly wetting liquids, chemical interactions with functional groups on the pore surfaces in strongly wetting liquids, and interference with long-range cooperativity in networked liquids.

1.7 Outline

Most of the material presented in this thesis has been published in four papers. It falls into five major sections. The first section involves mode selective OKE spectroscopy. The second section involves OKE spectroscopy using time-delayed pairs of pump pulses with orthogonal polarizations. In the third section, I will discuss the orientational dynamics of benzene and benzene-d₆ confined in nanoporous sol-gel glass monoliths with a range of average pore sizes. In the fourth section, I will study the temperature-dependent orientational dynamics of a series of nitriles with n-alkyl chains ranging from one to 11 carbons in length. Finally, I will talk about a new OKE technique for microscopy.

All experimental methods are described in Chapter 2. Sample preparation techniques are discussed. A brief history of the sol-gel process is presented along with the actual synthesis used to prepare monolithic nanoporous glass samples of high optical quality. The optical set-up is illustrated and described in detail.

Chapter 1 References and Notes

- (1) Denk, W.; Strickler, J. H.; Webb, W. *Science* **1990**, 248, 73.
- (2) Cheng, J. X.; Book, L. D.; Xie, X. S. *Opt. Lett.* **2001**, 26, 1341.
- (3) Potma, E. O.; de Boeij, W. P.; Wiersma, D. A. *Biophys. J.* **2001**, 80, 3019.
- (4) Squier, J. A.; Muller, M.; Brakenhoff, G. J.; Wilson, K. R. *Opt. Express* **1998**, 3, 315.
- (5) Righini, R. *Science* **1993**, 262, 1386.
- (6) Smith, N. A.; Meech, S. R. *Int. Rev. Phys. Chem.* **2002**, 21, 75.
- (7) Kinoshita, S.; Kai, Y.; Ariyoshi, T.; Shimada, Y. *Int. J. Mod. Phys. B* **1996**, 10, 1229
- (8) Loughnane, B. J.; Scodinu, A.; Farrer, R. A.; Fourkas, J. T.; Mohanty, U. *J. Chem. Phys.* **1999**, 111, 2686.
- (9) Righini, R. *Science* **1993**, 262, 1386.
- (10) Kinoshita, S.; Kai, Y.; Ariyoshi, T.; Shimada, Y. *Int. J. Mod. Phys. B* **1996**, 10, 1229.
- (11) Fourkas, J. T. Nonresonant Intermolecular Spectroscopy of Liquids In Ultrafast Infrared and Raman Spectroscopy; Fayer, M. D., Ed.; Marcel Dekker: New York, **2001**; Vol. 26, p 473.
- (12) Smith, N. A.; Meech, S. R. *Int. Rev. Phys. Chem.* **2002**, 21, 75.
- (13) Loughnane, B. J.; Scodinu, A.; Farrer, R. A.; Fourkas, J. T.; *J. Phys. Chem. B* **2000**, 104, 5421
- (14) McMorro, D.; Lotshaw, W. T.; Kenney-Wallace, G. A. *IEEE J. Quantum Electron.* **1998**, 24, 443
- (15) McMorro, D.; Thantu, N.; Kleiman, V.; Melinger, J. S.; Lotshaw, W. T. *J. Phys. Chem. A* **2001**, 105, 7960
- (16) Castner Jr., E. W.; Maroncelli, M. *J. Mol. Liq.* **1998**, 77, 1.
- (17) Cong, P.; Deuel, H. P.; Simon, J. D. *Chem. Phys. Lett.* **1995**, 240, 72
- (18) Neelakandan, M.; Pant, D.; Quitevis, E. L. *J. Phys. Chem. A* **1997**, 101, 2936.
- (19) Bartolini, P.; Ricci, M.; Torre, R.; Righini, R.; Santa, I. *J. Chem. Phys.* **1999**, 110, 8653.
- (20) Cang, H.; Novikov, V. N.; Fayer, M. D. *Phys. Rev. Lett.* **2003**, 90, 197401
- (21) Cang, H.; Novikov, V. N.; Fayer, M. D. *J. Chem. Phys.* **2003**, 118, 2800.
- (22) Ricci, M.; Wiebel, S.; Bartolini, P.; Taschin, A.; Torre, R. *Philos. Mag. B* **2004**, 84, 1491.
- (23) Torre, R.; Bartolini, P.; Righini, R. *Nature* **2004**, 428, 296.
- (24) Cang, H.; Li, J.; Fayer, M. D. *J. Chem. Phys.* **2003**, 119, 13017.
- (25) Giraud, G.; Gordon, C. M.; Dunkin, I. R.; Wynne, K. *J. Chem. Phys.* **2003**, 119, 464.
- (26) Hyun, B. R.; Dzyuba, S. V.; Bartsch, R. A.; Quitevis, E. L. *J. Phys. Chem. A* **2002**, 106, 7579.

- (27) Loughnane, B. J.; Farrer, R. A.; Scodinu, A.; Reilly, T.; Fourkas, J. T. *J. Phys. Chem. B* **2000**, 104, 5421.
- (28) Farrer, R. A.; Fourkas, J. T. *Acc. Chem. Res.* **2003**, 36, 605.
- (29) Hunt, N. T.; Jaye, A. A.; Meech, S. R. *J. Phys. Chem. B* **2003**, 107, 3405.
- (30) Hunt, N. T.; Jaye, A. A.; Hellman, A.; Meech, S. R. *J. Phys. Chem. B* **2004**, 108, 100.
- (31) McMorro, D.; Thantu, N.; Melinger, J. S.; Kim, S. K.; Lotshaw, W. T. *J. Phys. Chem.* **1996**, 100, 10389.
- (32) Steffen, T.; Meinders, N. A. C. M.; Duppen, K. *J. Phys. Chem. A* **1998**, 102, 4213.
- (33) Idrissi, A.; Ricci, M.; Bartolini, P.; Righini, R. *J. Chem. Phys.* **2001**, 114, 6774.
- (34) Hunt, N. T.; Meech, S. R. *Chem. Phys. Lett.* **2003**, 378, 195. PAGE EST: 7.3 H J. Phys. Chem. B
- (35) Scodinu, A.; Fourkas, J. T. *J. Phys. Chem. B* **2003**, 107, 44.
- (36) Wiewior, P. P.; Shirota, H.; Castner, E. W. *J. Chem. Phys.* **2002**, 116, 4643.
- (37) Shirota, H.; Castner, E. W. *J. Am. Chem. Soc.* **2001**, 123, 12877.
- (38) Eaves, J. D.; Fecko, C. J.; Stevens, A. L.; Peng, P.; Tokmakoff, A. *Chem. Phys. Lett.* **2003**, 376, 20.
- (39) Giraud, G.; Wynne, K. *J. Am. Chem. Soc.* **2002**, 124, 12110.
- (40) Giraud, G.; Karolin, J.; Wynne, K. *Biophys. J.* **2003**, 85, 1903.
- (41) Cang, H.; Li, H.; Fayer, M. D. *Chem. Phys. Lett.* **2002**, 366, 82.
- (42) Gottke, S. D.; Cang, H.; Bagchi, B.; Fayer, M. D. *J. Chem. Phys.* **2002**, 116, 6339.
- (43) Gottke, S. D.; Brace, D. D.; Cang, H.; Bagchi, B.; Fayer, M. D. *J. Chem. Phys.* **2002**, 116, 360.
- (44) Hyun, B. R.; Quitevis, E. L. *Chem. Phys. Lett.* **2003**, 373, 526.
- (45) Hunt, N. T.; Meech, S. R. *J. Chem. Phys.* **2004**, 120, 10828.
- (46) Potma, E. O.; de Boeij, W. P.; Wiersma, D. A. *Biophys. J.* **2001**, 80, 3019
- (47) Zhu, X.; Farrer, R. A.; Gershgoren, E.; Kapteyn, H. C.; Fourkas, J. T. *J. Phys. Chem. B* **2004**, 108, 3384.
- (48) Weiner, A. M.; Leaird, D. E.; Wiederrecht, G. P.; Nelson, K. A. *Science* **1990**, 247, 1317.
- (49) Weiner, A. M.; Leaird, D. E.; Wiederrecht, G. P.; Nelson, K. A. *J. Opt. Soc. Am. B* **1991**, 8, 1264.
- (50) Wiederrecht, G. P.; Dougherty, T. P.; Dhar, L.; Nelson, K. A.; Weiner, A. M.; Leaird, D. E. *Ferroelectrics* **1993**, 144, 1.
- (51) Wefers, M. M.; Kawashima, H.; Nelson, K. A. *J. Chem. Phys.* **1998**, 108, 10248
- (52) Gershgoren, E.; Vala, J.; Kosloff, R.; Ruhman, S. *J. Phys. Chem. A* **2001**, 105, 5081.
- (53) Hecht, E. *Optics* (Addison- Wesley Publishing Reading, MA) **1987**
- (54) Mayer; Gires *Compt. Rend.* **1964**, 258, 2039.
- (55) Duguay; Hansen, *Appl. Phys. Lett.* **1969**, 15, 192.
- (56) Ippen and Shank, *Appl. Phys. Lett.* **1975**, 26, 92.
- (57) Green, B.I; Farrow, R.C. *Chem. Phys. Lett.* **1983**, 98, 273
- (58) Kalpuzos, C.; Lotshaw, W.T; McMorro, D; Kenney-Wallace, G.A. *J. Phys. Chem.* **1987**, 91, 2028.

- (59) Ruhman, S.; William,L.; Joly, A.; Kohler, B.; Nelson K.A. *J.phys.Chem* **1987**, 91,2237
- (60) Ruhman, S.; Kohler, B.; Joly, A.; Nelson, K.A. *Chem.Phys. Lett.* **1987**, 14116.
- (61) Ruhman, S.; Nelson, K.A. *J.Chem.Phys.* **1991**, 94, 859.
- (62) McMorrow, D.; Lotshaw, W.T. *Chem. Phys. Lett.* **1990**, 171(1), 85
- (63) McMorrow, D.; Lotshaw, W.T. *J. Phys. Chem.* **1991**, 95, 10395
- (64) McMorrow, D.; Lotshaw, W.T. *J. Phys. Chem.* **1996**, 100, 10389
- (65) Dhar, L.; Rogers, J. A.; Nelson, K. A. *Chem. Rev.* **1994**, 94, 157
- (66) Wallen, S.L; Nikiel, L; Yi, J.; Jonas. J. *J. Phys. Chem.* **1995**, 99, 15421
- (67) Pissis, P.; Laudat, J.; Daoukaki, D.; Kyritsis, A. *J. Non-Cryst. Solids* **1994**, 171, 201.
- (68) Schuller, J.; Richert, R.; Fisher, E. W. *Phys.Rev.B* **1995**, 52,15232
- (69) Arndt, M.; Stannarius, R.; Gorbatschow, W.; Kremer, F. *Phys. Rev. E* **1996**. 56, 5377
- (70) Nikiel, L.; Hopkins, B.; Zerda, T.W. *J. Phys.Chem.* **1995**, 99, 7458
- (71) Wallen, S.L.; Nikiel, L.; Yi, J. Jonas, *J. Phys. Chem.* **1995**, 99, 15421
- (72) Wallen, S.; Nikiel, Y.; Lee, T.; Jonas, *J. Raman Spectrosc.* **1995** 26 1019
- (73) Yi, J. Jonas, J. *J. Phys.Chem.* **1996**, 100, 16789
- (74) Liu, G.; Li, Y.; Jonas, J. *J Chem. Phys.* **1991**, 95, 6892
- (75) Warnock, J. Awschalom, D, Schafer, M. *Phys. Rev. Lett.* **1986**, 67, 1753
- (76) Schwalb, G.; Deeg, F.; Brauchle, C. *J. Non-Cryst. Solids* **1994**, 172-174, 348
- (77) Shafer, M.; Awschalom, D.; Warnock, J. *J. Appl. Phys.* **1987**, 61, 5438
- (78) Streck, C.; Mel'nichenko, Yu. B.; Richert, R. *Phys. Rev.B* **1996** 53 5341
- (79) Guo, Y.; Langley, K.H.; Kararsz, F.E. *J. Chem. Phys.* **1990**, 93, 7457

Chapter 2

Methods

2.1 The optical experimental set-up

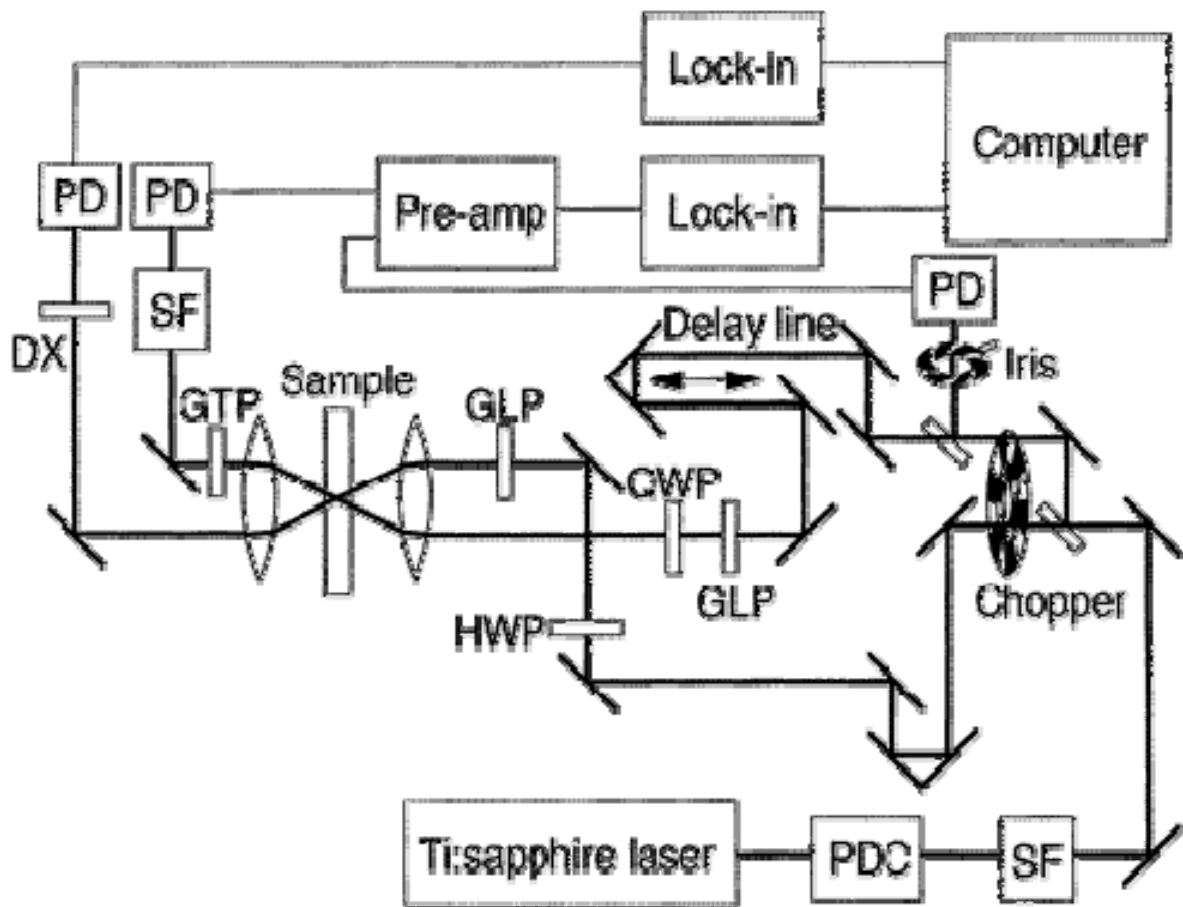


Figure 2.1. Schematic of the OKE experiment. PDC = prism dispersion compensator, SF = special filter, PD = photodiode, HWP = half-wave plate, QWP = quarter wave plate, GLP = Glan laser polarizer, DX = doubling crystal; GTP = Glan-Thompson polarizer

Our basic experiment setup for optical-heterodyne-detected OKE spectroscopy is shown in Figure 2.1. Briefly, a Ti:sapphire laser, pumped by a frequency-doubled, diode-pumped solid-state laser (Coherent Verdi 5) produces pulses at a center wavelength of 800 nm. The pulses are externally recompressed to a duration of approximately 35 fs with a pair of LaFN28 prisms (CVI) set approximately 33 inches apart. The average power is 350 mW. After recompression, the beam passes through a 90% beam splitter. Each resulting beam is chopped at a different frequency. The transmitted portion is used as the pump pulse and the reflected portion is used as the probe pulse. The pump beam passes through an achromatic half-wave plate and a Glan laser polarizer that is set vertically and is then focused into the sample using a 75-mm focal length achromatic lens. The probe beam traverses an optical delay line and passes through a Glan laser polarizer set for 45° polarization and then a quarter-wave plate. The polarizer is mounted to a high-resolution automatic rotation stage (Newport URM100 ACC with a MM 3000 DC controller). The beam is focused into the sample with the achromatic lens, is recollimated after the sample, and passes through a Glan-Thompson polarizer. To implement optical heterodyne detection, in the probe beam the first polarizer is set slightly off of 45°, the fast axis of the quarter-wave plate is set at 45°, and the analyzer is set at -45°. The polarization-analyzed light is focused onto a low-noise amplified photodiode connected to a digital lock-in amplifier referenced to the sum of the two chopping frequencies. The extinction of the polarizer pair is generally better than 5×10^5 . The signal is spatially filtered and detected by a high-bandwidth, amplified photodiode (New Focus Model 2001).

With the pump beam blocked and the quarter-wave plate removed, the angle of the analyzer polarizer is set to maximize the extinction of the probe beam. The quarter-wave plate is reinserted and adjusted to remaximize the extinction of the probe beam. The position of the quarter-wave plate then remains constant for the duration of the experiment. The “zero-background” angle is then optimized by ensuring that the intensity of the probe beam is exactly the same at opposite heterodyne angles of the probe polarizer. The orientation of the Glan laser polarizer is adjusted to provide an in-quadrature local oscillator. Alternate data sets are taken with the polarizer rotated in one direction by no more than 1° and then with it rotated by the same amount in the opposite direction so that the homodyne contribution to the signal can be removed later. The stability of the local oscillator is monitored continuously with an oscilloscope.

The pump and probe beams are chopped by the 5-slot and 7-slot rings of the same chopper (New Focus Research Model 300). After the chopper, a portion of the probe beam is picked off by a beam splitter. This beam passes through an iris and a set of polarizers (for intensity adjustment) and then is detected with another photodiode that is matched to that detecting the signal; we will refer to this as the reference diode. With the pump beam blocked the intensity of the reference beam is adjusted with the polarizers to match exactly the intensity of the local oscillator in an oscilloscope. The iris is then positioned around the beam and closed to account for any small beam distortions, which may arise from spatial filtering of the signal. The outputs of the two photodiodes are connected to the differential inputs of a low-noise preamplifier (SRS SR560). The preamplifier output is fed into a digital lock-in amplifier (Stanford Research Systems

SR810). The pump beam is then unblocked and the lock-in is referenced to the sum of the pump and probe beam chopping frequencies (7.7kHz). Not only does this scheme greatly improve the signal to noise ratio by enhancing the gain of the signal, but it also allows us to take advantage of the full dynamic range of the lock-in.

In the focal point, the average pump and probe power levels are about 20 mW and 2 mW at room temperature. The pump and probe spot sizes at the focal point are approximately 50 micron in diameter. Focusing is accomplished using an achromatic lens ($f \approx 75 \text{ mm}$), and the separation between the two beams on the lens is around 10 mm. The angle between the two beams is therefore approximately 8° . When the two pulses cross at the sample, one pulse comes before the other on the right, while the other leads on the left. This creates a range of delays across the beam size in which there is still overlap. The time resolution for the experiment is:

$$dt = \sqrt{dt_1^2 + dt_2^2} \quad (2.1)$$

where dt_1 is the real pulse length and dt_2 is the angle smear.

For the dt_2 we can calculate from the following equation:

$$dt_2 = \sqrt{2} \frac{d}{c} \tan\left(\frac{\theta}{2}\right) \quad (2.2)$$

where d is the beam diameter at the focal point, θ is the angle between pump and probe pulse, and c is the speed of light.

When we use 30 fs pulse to run the experiment, the time resolution is about 32 fs according to the above 2 equations.

After the pump beam passes through the sample it is frequency doubled in a KDP crystal. The doubled light is detected with another photodiode and lock-in amplifier.

Since the second harmonic generation (SHG) and the OHD-RIKES signal have the same nonlinearity, the OKE signal can be divided by the SHG signal to account for any small intensity fluctuations that may arise during data collection, which may take up to 24 hours.

The sample holder mounts to the cold finger of a constant-flow cryostat (Janis Research). A Model 330 Autotuning Temperature Controller (Lakeshore Electronics) controls the temperature of the cryostat. A silicon diode temperature probe is placed directly on the sample and the temperature is kept stable for at least one hour before any experiments are performed. The temperature is monitored continuously and no data are taken if the temperature changes by more than 0.5°C from the set point.

2.2 Data acquisition

Programs written in LabViewTM (National Instruments) collect data and interface with all instruments used in the experiment. For every step on the delay line both lock-in amplifiers collect data for 100 ms. The data buffers of the lock-ins are dumped into the computer and the average of the signal for each lock-in is calculated. Each point in the OHD-RIKES signal is divided by the corresponding point in the SHG signal and saved in an array. The delay line is then moved, and the instrumentation is allowed to come to equilibrium in for three time constants before data collection recommences.

To study the low-frequency intermolecular and intramolecular Raman modes, data points are recorded with a time step of 6.67 fs out to a delay time of at least 8 ps . To study slow diffusive motions, OKE scans are taken with a time step of 66.5 fs until a decay time at which the signal level is indistinguishable from the baseline. In each case

the data obtained at the negative heterodyne angle are averaged and subtracted from the average of the data obtained at the positive heterodyne angle. The baseline is then zeroed carefully, and the data are fit. Preliminary fitting of the data is done in LabView, followed by a nonlinear least-square analysis with a Levenberg-Marquardt algorithm.

2.3 Sol –gel preparation and characterization

Monolithic nanoporous glass samples of high optical quality are prepared using the two step acid-base catalyzed hydrolysis of tetraethyl orthosilicate (98% TEOS, Acros Organics).¹ Deionized water is mixed rapidly into a solution of TEOS and ethanol in a 12:1:2 molar ratio. HCl in the amount of 0.001 moles (5 ml) is added, and hydrolysis proceeds under acidic conditions. The solution is stirred in a 40°C bath for 40 minutes and eventually becomes clear and homogeneous. It is transferred to an ice bath where hydrolysis is completed under basic conditions with the addition of another 12 parts of H₂O and an amount of NH₄OH. The amount of base added is controlled carefully in order to produce samples with different average pore sizes. For instance, 0.001 moles (5 ml) of NH₄OH are added to produce the smallest pores; conditions that are more basic produce larger pores. Once the solution is well mixed, it is poured into cylindrical polystyrene containers (5X1.5 cm) that are capped tightly. Gellation occurs within 30 minutes. To create samples with the smallest pores (21 to 27 Å⁰ average pore diameter), glasses are aged for one week at room temperature and allowed to dry for a period of one month. In the drying stage, the samples are uncapped and covered with ParafilmTM in which a small

pinhole is made to allow the liquid phase to evaporate slowly. Medium-sized pore samples (28 to 60 Å average pore diameter) are aged at 55 °C for 2-4 weeks before drying. For samples with even larger pores (60 to 112 Å) it is necessary to transfer the wet gel into a 0.1 M NH₄OH bath for 24 hours after they have been aged for four weeks at 55 °C . All samples are then placed in ceramic crucibles and heated to 800 °C at a rate of 0.5 °C per minute in a Lindberg/Blue programmable muffle furnace. The samples are ground to a thickness of 2 mm with various grit sandpaper and then hand-polished to optical quality using TEXMET 100™ polishing cloth and 24, 6 and 1 μm diamond paste (Buehler) consecutively. The polished monoliths are placed in a 2 mm path length quartz optical cell, one end of which is subsequently sealed. Samples are again heated to 450 °C to remove any water and organic material that may have permeated the pores during the polishing and glass-blowing processes.

To help quantify the importance of interactions with pore surfaces, we removed the surface hydroxyl groups and rendered the pore surfaces hydrophobic by refluxing monoliths within an optical cell in a 50% solution of chlorotrimethyl silane in toluene for a period of at least 96 hours at 110 °C²⁻⁶. The samples are then washed successively in toluene, benzene, and methanol, after which they are placed in a 100 °C vacuum oven for 24 hours to remove any volatile adsorbates. This procedure converts the surface hydroxyl groups into -O-Si(CH₃)₃ moieties, which cannot donate hydrogen bonds to the liquid molecules. The success of this conversion was confirmed by infrared spectroscopy, which revealed the complete absence of surface hydroxyl groups in the treated samples.

The interaction between the liquid and the pore surfaces can also be modulated in a much less drastic manner by altering the hydrogen-bonding strength of the surface hydroxyl groups. This modulation can be effected by replacing the surface hydroxyl protons with deuterons; since an O-D bond has a lower zero-point energy than an O-H bond, O-D groups make weaker hydrogen bonds. The deuterium exchange is accomplished by immersing the samples in D₂O and then heating the samples to 450 °C to remove any excess liquid. Infrared spectra revealed no remaining surface hydroxyl protons after this procedure was applied three times.

Characterization of sol-gel samples was performed with a Brunauer, Emmett, Teller (BET) sorptometer purchased from Porous Materials Incorporated (PMI/APP).⁸⁻⁹ Gas adsorption is one of the most powerful techniques used today to measure the total surface area, pore volume and size distribution of porous solids. In adsorption-desorption processes, a gas is condensed and evaporated from a pore.

The PMI Automated BET Sorptometer is a precision volumetric sorption instrument in which grade 5.0 dry nitrogen gas is used as the adsorbate. The porous solid is placed in a U-tube whose total volume has been previously determined. The U-tube is heated to 200 °C for at least six hours and evacuated to remove any residual vapor or gas that may have collected within the pores. The bottom portion of the tube, which includes the sample, is immersed in liquid nitrogen and the liquid nitrogen is automatically kept at a constant level throughout the entire measurement by periodically raising the dewar flask. Adsorption isotherms are determined by means of a vacuum system that makes pressure measurements before and after the nitrogen gas is admitted into the sample. The

equilibrium amount of gas adsorbed on the sample is calculated from four quantities: the measured pressure drop at P_1 , the known quantity of nitrogen gas and the reference (V_A) and sample chamber ($V_{it}+V_{ln}$) volumes (V_{it} is the volume of the stem of the glass U tube, V_{ln} is the volume of the base of the U tube). Valves are open and the system comes to equilibrium in the sample chamber at three temperatures and volumes:

1. The reference volume V_A at instrument temperature
2. The stem volume of the sample V_{it} at room temperature
3. The bulb volume of the sample V_{ln} at the temperature of liquid nitrogen.

A final pressure P_f is recorded when the pressure becomes stable. The sample chamber is once again isolated and a new P_i is measured. More gas is allowed to expand into the sample chamber and the process continues until the isotherm is complete. The saturation pressure (P_o) is monitored continuously throughout the experiment through a separate pressure gauge (P_2).

In 1938, Brunauer, Deming, and Teller classified five types of isotherms to describe the uptake of gas on most solid materials.¹⁰ Numerous kinetic models have been developed to explain the various experimental isotherms. The differences in each of the proposed models arise from the degree of importance each model attributes to capillary condensation as opposed to a multi-layered adsorption process. They extended Langmuir's treatment¹¹ of gases to arrive at a general equation that works fairly well with both porous and non-porous solids.¹⁰ Although created 50 years ago, the BET equation is still used today in most applications because of its simplicity.



Figure 2.2 Sol-Gel nanoporous glass monoliths

Chapter 2 References and Notes

- (1) Oogaz, F.; Rawson, H. *J. Non-Crystalline Solids* **1986**, 82, 57.
- (2) Ballard, C.C.; Broge, E.C.; Iler, R.K.; St. John; McWhorther; J.R. *J. Am. Chem. Soc.* **1960**, 60, 20
- (3) Hair, M.L.; Hertl, W.; *J. Phys. Chem.* **1969**, 73, 2372
- (4) Armistead, C.G.; Hockey, J.A. *Trans. Faraday Soc.* **1967**, 63, 2549
- (5) Sindorf, D.W.; Maciel, G.E. *J. Phys. Chem.* **1983**, 87, 5516
- (6) Majors, R.E.J. *Chroma. Sci.* **1974**, 12, 767.
- (7) Brinker, C.J.; Scherer, G.W. *Sol-gel Science: The Physics and Chemistry of Sol-Gel processing* Academic Press: San Diego, CA, **1990**
- (8) Iler, R.K. *The Chemistry of Silica*; (Wiley, New York) **1979**
- (9) Gregg, S. J.; Sing, K.S.W. *Adsorption, Surface Area, and Porosity* (Academic Press, London) **1967**
- (10) Brunauer, S; Emmett, P.H; Teller, E. *J. Am. Chem. Soc* **1938**, 60, 309
- (11) Langmuir, I *J. Am. Chem. Soc.* **1918**, 40, 1961

Chapter 3

Mode-Selective OKE Spectroscopy

3.1 Introduction

Nelson, Weiner and co-workers showed that by using phase masks to create trains of appropriately-timed, evenly-spaced pulses for excitation in an impulsive stimulated scattering¹ (transient grating²) geometry, they could strongly enhance the OKE signal from selected vibrational modes of a crystal.^{3,4} Recent work demonstrated that for OKE spectroscopy such pulse trains can be generated using a combination of a dispersive delay line and an interferometer.⁵ However, all this past work used pulse trains of constant linear polarization.

In principle, excitation pulse trains can be used to control the contributions to the OKE signal in liquids. However, if all of the pulses have the same polarization, the contribution from collective reorientational diffusion will be enhanced roughly as strongly as that from any intramolecular vibrational mode of interest. We have developed a new mode-selective OKE technique that is based on the use of two pump pulses.⁶ Here we demonstrate that, similar to what has been demonstrated for lattice vibrations in crystalline quartz,⁷ intramolecular vibrational contributions to the OKE signal in liquids can be controlled using two pump pulses with independently controlled

polarization, intensity and timing in an optical-heterodyne-detected polarization-spectroscopy geometry.⁸ We further demonstrate that by using a pair of perpendicularly-polarized pump pulses it is possible to enhance a desired vibration while eliminating the reorientational component of the signal.

3.2 Experimental section

To implement the two-pump scheme we have modified the pump-beam portion of the setup (Figure 2.1) as shown in Figure 3.1 to allow the timing, intensity and polarization of each pump beam to be adjusted independently. The pump beam is split by a 50% beam splitter. The two halves of the pump beam each traverse an adjustable delay line, a half-wave plate, and a Polarcor polarizer before being recombined at a second beam splitter and sent on to the sample.

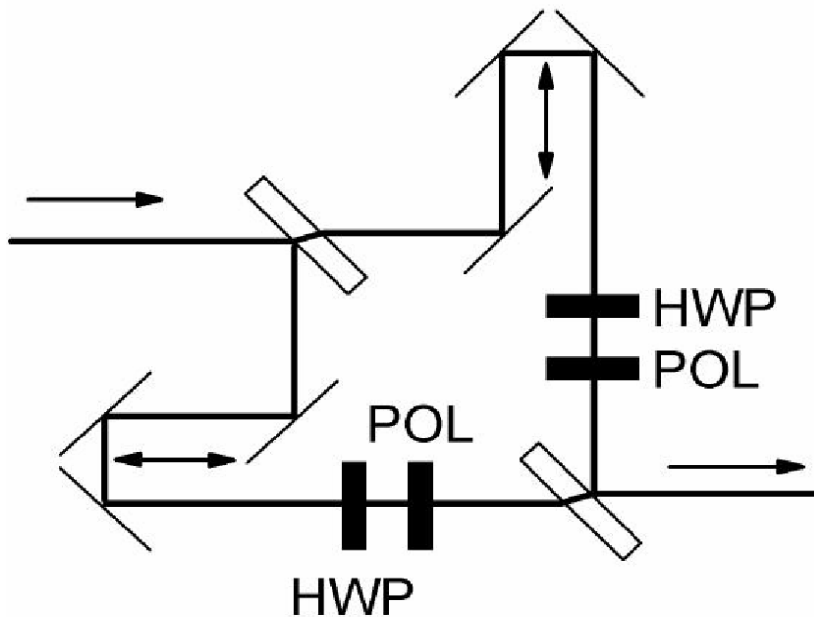


Figure 3.1. Schematic of the optics for creation of dual pump pulses. HWP = half-wave plate, POL = polarizer.

3.3 Theory

We begin by considering a conventional OKE experiment performed in an isotropic medium using a polarization-spectroscopy configuration. Excitation is accomplished with a single linearly polarized pump pulse, the polarization of which we will call x . The probe pulse, which arrives at some time τ later, is polarized at 45° to the pump $((x + y)/\sqrt{2})$ and the signal at -45° to the pump $((x - y)/\sqrt{2})$. The only nonzero tensor elements of the third-order response function in an isotropic medium are those in which each spatial index appears an even number of times. The response function measured in the polarization-spectroscopy geometry is therefore

$$R_{PS}^{(3)}(\tau) = \frac{1}{2} R_{xxxx}^{(3)}(\tau) - \frac{1}{2} R_{yyxx}^{(3)}(\tau) \quad (3.1)$$

where the subscript indices refer to the polarizations of the interactions in reverse temporal order. Furthermore, in an isotropic medium the relationships among the different tensor elements of the third-order response are such that^{9,10}

$$\frac{1}{2} R_{xxxx}^{(3)}(\tau) - \frac{1}{2} R_{yyxx}^{(3)}(\tau) = R_{xyxy}^{(3)}(\tau) \quad (3.2)$$

This latter quantity is known as the depolarized response, and it arises solely from modes that affect the polarizability of the liquid anisotropically.

Now consider the use of two orthogonally polarized pump pulses that are not time coincident (Figure 3.1). We will assume that the first pulse is x -polarized and arrives at time zero and that the second pulse is y -polarized and arrives at time t_p . The intensity of the second pump pulse is a times that of the first. The probe pulse is again polarized at

45° and arrives at time τ , and detection is performed at -45°. We will constrain ourselves to the case in which none of the pulses overlap in time and $\tau > t_p$. Under these circumstances, the most possible contribution to the signal is the sum of the independent third-order responses from each of the pump beams with the probe beam. The response function in the case of two orthogonally polarized pump pulses is given by:

$$R_{-ddyx}^{(3+3)}(t_p, \tau) = R_{xyxy}^{(3)}(\tau) - aR_{xyxy}^{(3)}(\tau - t_p) \quad (3.3)$$

where we have taken advantage of the fact that $R_{xyxy}^{(3)} = R_{yxyx}^{(3)}$ in an isotropic medium. Here the superscript of the response denotes that it is the sum of two third-order responses, and the subscript gives the polarizations of the pump beams, the probe beam, and the signal beam in reverse temporal order; d denotes a polarization of 45°, and $-d$ denotes a polarization of -45°.

From eq 3.3, it is straightforward to see how mode selectivity might be achieved. We consider in particular two contributions to the depolarized response, that from orientational diffusion and that from coherently excited intramolecular vibrations. For symmetric top molecules,¹¹ the former contribution is given by:

$$R_{xyxy, reor}^{(3)}(\tau) \propto \exp(-\tau / \tau_r) \quad (3.4)$$

where τ_r is the collective orientational correlation time. Inspection of eqs (3.3) and (3.4) shows that if a is chosen to be $\exp(-t_p / \tau_r)$, then

$$R_{-ddyx, reor}^{(3+3)}(t_p, \tau) \propto \exp(-\tau / \tau_r) - \exp(-t_p / \tau_r) \exp(-(\tau - t_p) / \tau_r) = 0 \quad (3.5)$$

and so the reorientational contribution to the signal can be canceled. In a similar vein, the

contribution to the depolarized response from a coherently excited intramolecular vibration, in the limit of exponential damping, is given by:

$$R_{xyxy,vib}^{(3)}(\tau) \propto \exp(-\tau / \tau_v) \sin(\omega\tau) \quad (3.6)$$

where ω is the frequency of the vibration and τ_v is its damping time. Combining eqs (3.3) and (3.6) and choosing a to be equal to $\exp(-t_p/\tau_v)$, we find that

$$\begin{aligned} R_{-ddyx,vib}^{(3+3)}(t_p, \tau) &\propto \exp(-\tau / \tau_v) \sin(\omega\tau) - \exp(-t_p / \tau_v) \exp(-(\tau - t_p) / \tau_v) \sin(\omega(\tau - t_p)) \\ &= \exp(-\tau / \tau_v) [\sin(\omega\tau) - \sin e(\omega\tau - \varphi)] \end{aligned} \quad (3.7)$$

where $\varphi = \omega t_p$. If the phase is chosen to be $2n\pi$, where n is an integer, then the contribution from an intramolecular vibration can be canceled completely, and so long as τ_r is not equal to τ_v , there will still be a reorientational signal. Conversely, if the phase is chosen to be $(2n + 1)\pi$, then the vibrational signal will instead be enhanced, regardless of the choice of a .

In a similar way, the response function in the case of two parallel-polarized pump pulses is given by

$$R_{-ddyx}^{(3+3)}(t_p, \tau) = R_{xyxy}^{(3)}(\tau) + aR_{xyxy}^{(3)}(\tau - t_p) \quad (3.8)$$

As discussed above, in this situation the response function from each pump pulse is of the same sign. For the intramolecular vibrations, this reversal of sign is equivalent to a 180° shift in the sine-wave portion of their contribution to the response. Thus, parallel polarized pulses separated by a full period of a vibration lead to a constructive interference of the response function, whereas pulses separated by half a period lead to a destructive interference; this is exactly the opposite of what happens with perpendicularly

polarized pump pulses. However, it is impossible to suppress the reorientational contribution to the signal, because the sum of exponentials is always bigger than 0.

The strategy for controlling the relative contribution of an intramolecular vibration to the OKE signal is straightforward when we represent it by wavepacket propagation. We depict the strategy in Figure 3.2. In the case of two perpendicularly polarized pumps, if the two pump pulses are separated by half a period of the vibration, then the vibration will be enhanced. On the contrary, if the two parallelly polarized pump pulses are separated by a half period of the vibration, then by choosing the appropriate relative pump intensities it should be possible to suppress the contribution of the vibration entirely.

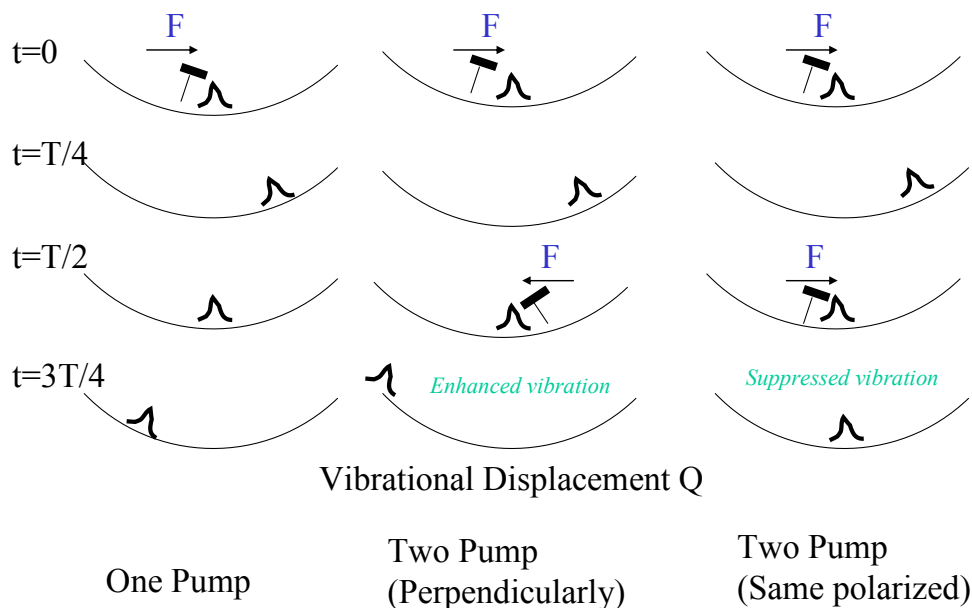


Figure 3.2 Mechanisms for mode selective excitation of coherent vibrational motion, represented in the figure by coherent wavepacket propagation. The left column describes the wavepacket propagation in one vibrational cycle from only one pump; the middle column describes the wavepacket propagation induced by two perpendicularly polarized pumps; the right column describes the wavepacket propagation induced by two parallel polarized pumps.

3.4 Results

We demonstrate that by using two pump pulses with independently-controllable polarizations, intensity and timing, different contributions to the optical Kerr effect signal in liquids can be enhanced and suppressed. When both pump pulses have the same polarization, intramolecular vibrations can be enhanced or suppressed without affecting the reorientational diffusion contribution to the signal significantly. Similar control can be exerted over intramolecular vibrations when the pump pulses are perpendicularly polarized, and under these conditions it is also possible to suppress the reorientational diffusion component of the signal completely. When two intramolecular vibrational modes are present in the signal, it is possible to enhance one while completely suppressing the other if the pump polarizations and timing are chosen appropriately. This technique should be a useful means for enhancing contrast in OKE microscopy.

The strategy for controlling the relative contribution of an intramolecular vibration to the OKE signal is straightforward. In the case of two parallel-polarized pumps, if the pump pulses are separated by a full period of the vibration, then the vibration will be enhanced. If the pump pulses are separated by a half period of the vibration, then by choosing the appropriate relative pump intensities it should be possible to suppress the contribution of the vibration entirely. We illustrate the implementation of this concept in Figure 3.3 for the case of propionitrile. Figure 3.3a shows the OKE decay for propionitrile when only a single pump pulse is employed. Following the electronic response at zero delay time, there is a contribution from coherently-excited intermolecular modes that decays away over ~ 2 picoseconds, a contribution from

collective reorientation that decays exponentially over many picoseconds, and a decaying oscillatory contribution from an intramolecular vibrational mode with a frequency of 220 cm^{-1} (corresponding to a period of 152 fs).¹² Figure 3.3b shows the propionitrile OKE decay for two pump pulses that are separated by 76 fs. The ratio of pump pulse intensities has been adjusted to eliminate the contribution of the intramolecular vibration completely while retaining the reorientational decay. Figure 3.3c shows the propionitrile OKE decay for two pump pulses that are separated by 150 fs. In this case the amplitude of the vibrational and reorientational portions of the signal remain comparable, as both of them are enhanced similarly by the second pump pulse.

Consider now the effect of perpendicularly polarized pump pulses on intramolecular modes. The modes observed in the polarization spectroscopy geometry are necessarily depolarized,¹⁰ which is to say coherent pumping of these modes induces an oscillating birefringence as opposed to an oscillating isotropic change in the index of refraction. Thus, along the direction of the polarization vector of the first pump pulse, the contribution of a given intramolecular mode to the bulk polarizability starts at its equilibrium value, grows to a maximum, goes back to and then below its equilibrium value, and then returns to its equilibrium value over the course of one vibrational cycle. However, perpendicular to the polarization of the pump pulse, the contribution of this mode to the polarizability oscillates 180° out of phase with the contribution along the polarization vector. Therefore, after half of a vibrational cycle the polarizability along the polarization vector is at its equilibrium value and decreasing whereas the polarizability perpendicular to this vector is at its equilibrium value and increasing. This

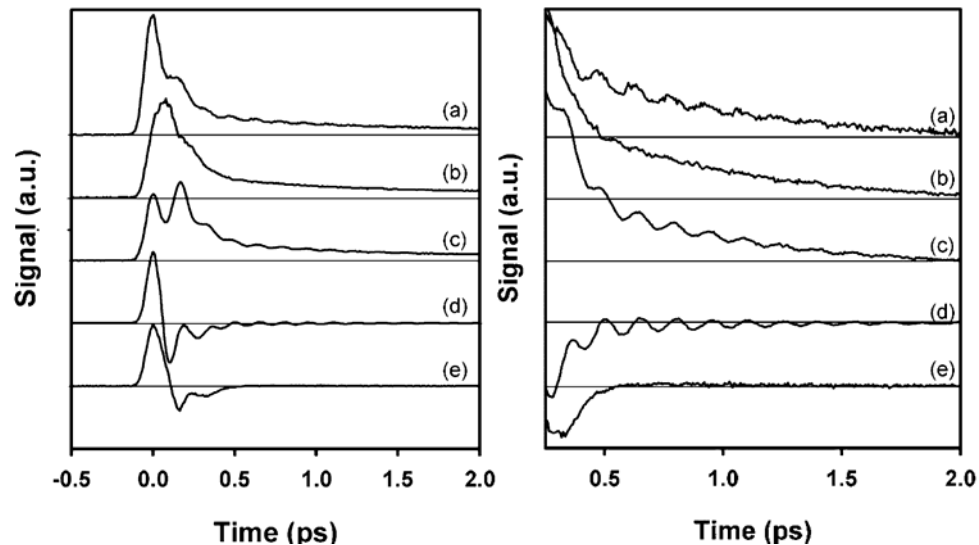


Fig 3.3 OKE decays for room-temperature propionitrile with: (a) a single pump pulse; (b) parallel-polarized pump pulses separated by one half period of the intramolecular vibration; (c) parallel-polarized pump pulses separated by one period of the intramolecular vibration; (d) perpendicularly-polarized pump pulses separated by one half period of the intramolecular vibration; and (e) perpendicularly-polarized pump pulses separated by one period of the intramolecular vibration.

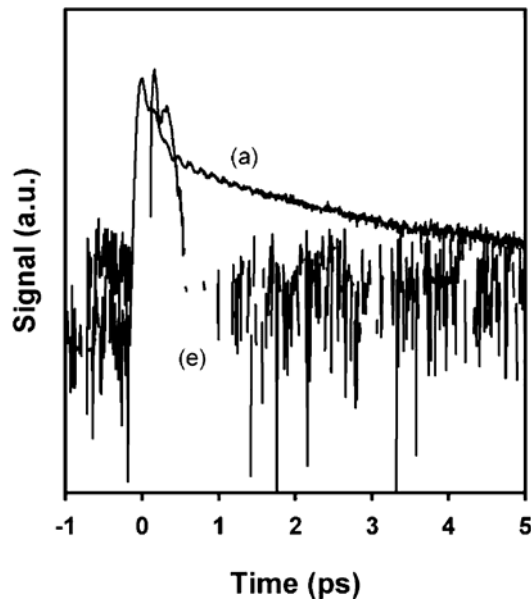


Figure 3.4 Semilog plots of trace (a) and the negative of trace (e), demonstrating the complete suppression of the reorientational signal.

means that a second, perpendicularly-polarized pump pulse that arrives a half cycle after the first pump pulse can enhance the signal from the vibration while cancelling the reorientational signal, so long as the molecules do not reorient significantly during this half cycle. Similarly, if a second, perpendicularly-polarized pump pulse arrives a full cycle after the first pump pulse, both the vibrational and reorientational signal can be suppressed. These two situations are illustrated for propionitrile in Figs. 3.3d and 3.3e, respectively. Note that the second pulse reverses the birefringence in the sample, and so generates a negative-going signal. The reorientational component is absent in both of these decays. The intramolecular vibrational mode contributes strongly to the decay in Fig. 3.3d, but only the intermolecular and electronic responses are evident in Fig. 3.3 e. Semilog plots of trace (a) and negative of trace (e), demonstrate the complete suppression of the reorientational signal in Fig. 3.4.

When more than one intramolecular vibration contributes to the OKE signal, paired pump pulses can also be used to select among them. Shown in Figure 3.5a is the room-temperature OKE decay for S_2Cl_2 with a single pump pulse. Two strong vibrational modes are evident, one¹⁰ at 105 cm^{-1} (with a corresponding period of 318 fs) and another¹⁰ at 242 cm^{-1} (with a corresponding period of 138 fs). By using two parallel-polarized pump pulses separated by 159 fs with appropriate relative intensities, it is possible to suppress the lower-frequency mode nearly completely (Fig. 3.5b). However, since the higher-frequency mode is at nearly twice the frequency of the other mode, it is not possible to enhance the lower-frequency mode selectively with parallel-polarized

pump pulses. This can be accomplished instead with perpendicularly-polarized pump pulses separated by 138 fs, as shown in Fig. 3.5c.

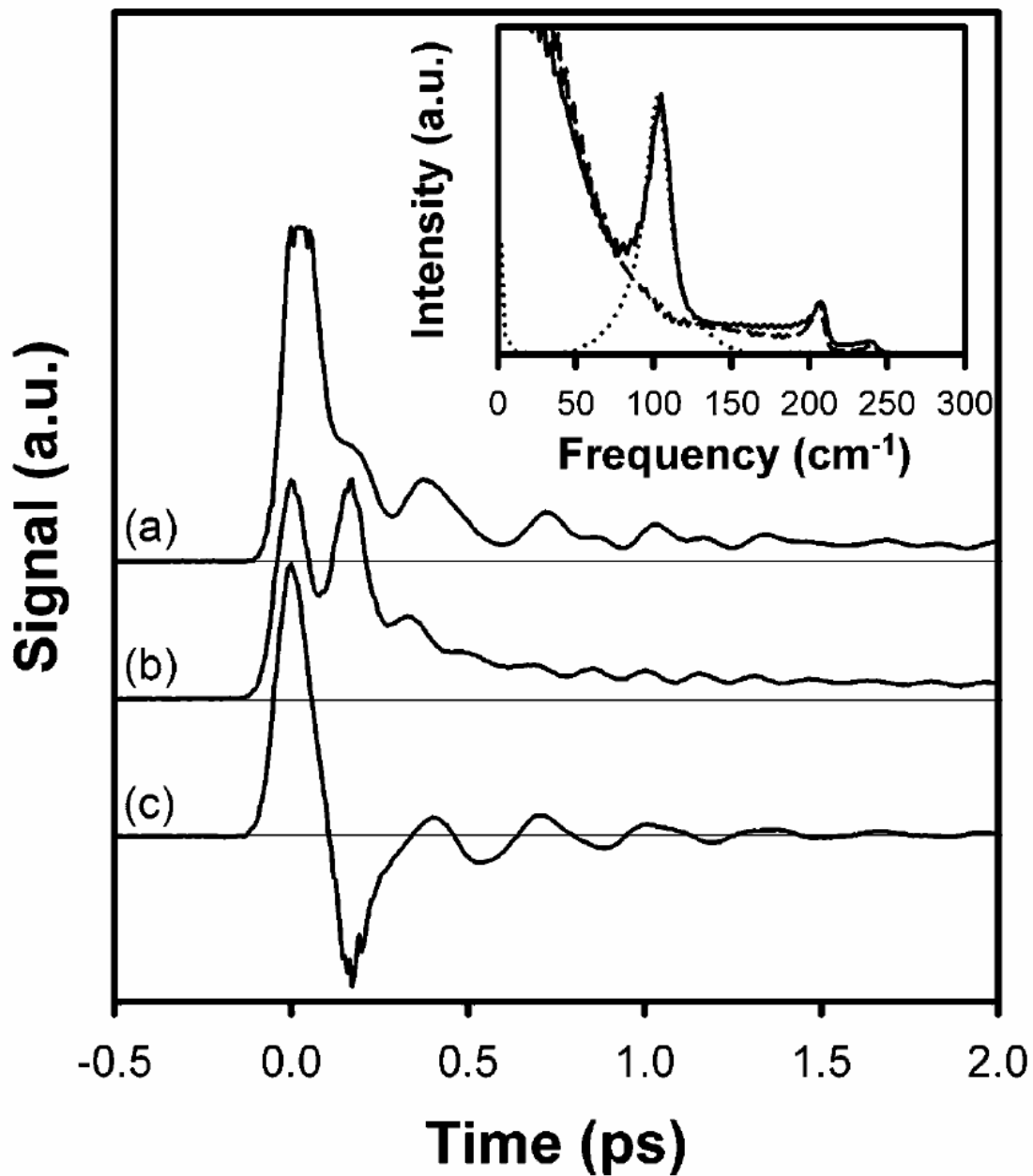


Figure 3.5. OKE decays for room-temperature S_2Cl_2 with (a) a single pump pulse; (b) parallel-polarized pump pulses separated by one cycle of the higher-frequency intramolecular vibration; and (c) perpendicularly-polarized pump pulses separated by one cycle of the higher-frequency intramolecular vibration.

3.5 Conclusions

Nonlinear optical techniques are finding increasing use in optical microscopy,¹⁶⁻¹⁸ in part because they can provide both three-dimensional resolution and unique types of contrast. OKE spectroscopy is only just beginning to be added to the arsenal of nonlinear optical techniques used in microscopy, however.¹⁹ OKE spectroscopy has the potential to generate contrast based on a number of different mechanisms, including Raman-active intramolecular vibrations and collective reorientation. To attain maximal contrast in OKE microscopy it would be useful to be able to suppress any unwanted contributions to the signal. For instance, for imaging of biological samples it would be desirable to suppress the reorientational contribution to the signal in order to focus on low-frequency vibrational modes of proteins, which appear at frequencies of 600 cm^{-1} and higher.²⁰ This can be accomplished using the technique described here, which can be implemented readily in an OKE microscopy setup.

Although the experiments described here employ two pulses, effecting control over n contributions to the OKE signal will generally require the use of n pulses. Our work underscores the utility of using polarization as a factor in the control scheme. Ultimately the use of pulse-shaping technology with amplitude and polarization control²¹ should provide the means for inducing a strong enhancement of any desired OKE contribution with the simultaneous suppression of all other modes.

Chapter 3 References and Notes

- (1) Dhar, L.; Rogers, J. A.; Nelson, K. A. *Chem. Rev.* **1994**, *94*, 157
- (2) Fourkas, J. T.; Fayer, M. D. *Acc. Chem. Res.* **1992**, *25*, 227.
- (3) Weiner, A. M.; Leaird, D. E.; Wiederrecht, G. P.; Nelson, K. A. *Science* **1990**, *247*, 1317
- (4) Weiner, A. M.; Leaird, D. E.; Wiederrecht, G. P.; Nelson, K. A. *J. Opt. Soc. Amer. B* **1991**, *8*, 1264.
- (5) Gershgoren, E.; Bartels, R. A.; Fourkas, J. T.; Tobey, R.; Murnane, M. M.; Kapteyn, H. C. *Opt. Lett.* **2003**, *28*, 361.
- (6) Zhu, X.; Farrer, R. A.; Gershgoren, E.; Kapteyn, H. C.; Fourkas, J. T. *J. Phys. Chem. B* **2004**, *108*, 3384
- (7) Wefers, M. M.; Kawashima, H.; Nelson, K. A. *J. Chem. Phys.* **1998**, *108*, 10248
- (8) McMorrow, D.; Lotshaw, W. T. *J. Phys. Chem.* **1991**, *95*, 10395.
- (9) Hellwarth, R. W. *Prog. Quantum Electron.* **1977**, *5*, 1
- (10) Murry, R. L.; Fourkas, J. T. *J. Chem. Phys.* **1997**, *107*, 9726
- (11) Berne, B. J.; Pecora, R. *Dynamic Light Scattering*; Wiley: New York, **1976**.
- (12) Wurrey, C. J.; Bucy, W. E.; Durig, J. R. *J. Phys. Chem.* **1976**, *80*, 1129.
- (13) Frankiss, S. G. *J. Mol. Struct.* **1968**, *2*, 271.
- (14) So, P. T. C.; Dong, C. Y.; Masters, B. R.; Berland, K. M. *Annu. Rev. Biomed. Eng.* **2000**, *2*, 399.
- (15) Millard, A. C.; Fittinghoff, D. N.; Wiseman, P. W.; Muller, M.; Brakenhoff, G. J.; Squier, J. A.; Wilson, K. R. *Biophys. J.* **2000**, *78*, 800Plat.
- (16) Volkmer, A.; Cheng, J. X.; Xie, X. S. *Phys. Rev. Lett.* **2001**, *87*02, 023901.
- (17) Potma, E. O.; de Boeij, W. P.; Wiersma, D. A. *J. Opt. Soc. Amer. B* **2000**, *17*, 1678.
- (18) Klar, T. A.; Jakobs, S.; Dyba, M.; Egner, A.; Hell, S. W. *Proc. Nat. Acad. Sci. USA* **2000**, *97*, 8206.
- (19) Potma, E. O.; de Boeij, W. P.; Wiersma, D. A. *Biophys. J.* **2001**, *80*, 3019.
- (20) Eaves, J. D.; Fecko, C. J.; Stevens, A. L.; Peng, P.; Tokmakoff, A. *Chem. Phys. Lett.* **2003**, *376*, 20.
- (21) Brixner, T.; Gerber, G. *Opt. Lett.* **2001**, *26*, 557.

Chapter 4

OKE spectroscopy using time-delayed pairs of pump pulses with orthogonal polarization

4.1 Introduction

In last chapter I demonstrated that with two pump pulses with independently controllable timing, intensity, and polarization it is possible to suppress or enhance the contribution of a specific intramolecular vibrational mode or of reorientation to the OKE signal. While it is possible to exert a considerable amount of control over the contributions to the OKE signal with just two pump pulses, for microscopy and other applications ultimately it will be desirable to employ trains of pulses with arbitrary time delays, intensities, and polarizations to isolate the contributions of individual modes. To be able to design appropriate excitation pulse sequences, it is first necessary to develop a detailed understanding of the dual-pulse-excitation scheme. With that goal in mind, here we present a detailed study of the OKE spectroscopy of liquids using two perpendicularly polarized excitation pulses.

I examine the ratio of pump pulse intensities required to cancel the contribution of reorientational diffusion or of a Raman-active intramolecular vibration to the signal as a function of the delay time between excitation pulses. These results indicate that the signal can be described well as arising from the sum of independent third-order responses

initiated by each pump pulse. This conclusion is further supported by using data obtained with a single pump pulse to model decays obtained with two pump pulses.

4.2 Experimental section

The experimental setup is similar to the one used in the last chapter but differs in some details. A commercial Ti:sapphire laser (KMLabs TS) pumped by a frequency-doubled, diode-pumped solid-state laser (Coherent Verdi 5) produces 30 fs pulses with a center wavelength of 800 nm and a repetition rate of 90 MHz. The output of the laser is sent through a prism dispersion compensator and a spatial filter, after which it is split into a pump beam and a weaker probe beam. The two pump pulses are then created by the optical setup shown in Figure 4.1. A half-wave plate is used to rotate the polarization of the beam, after which it is split into beams of orthogonal polarization by a polarizing beam cube. The timing of one beam is adjusted with an optical delay line, and the beams are recombined at a second polarizing beam cube and focused into the sample. The input wave plate can be used to adjust the relative intensities of the pump beams, and if beams of the same polarization are desired, then a half-wave plate and a polarizer can be placed between the second polarizing beam cube and the sample.

All of the liquids were filtered before use and, if necessary, were distilled. Samples were placed in cuvettes with a 1 mm path length and mounted to a three-axis translation stage. The lab temperature was constant to within $\pm 1^\circ$ F for all experiments, so no additional temperature control for the samples was deemed necessary.

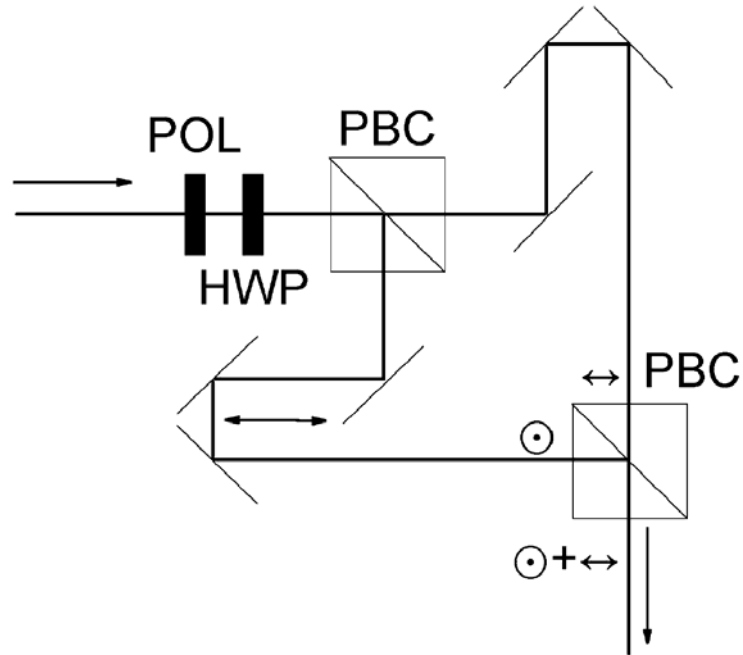


Figure 4.1. Experimental setup for creating perpendicularly polarized pump pulses with independently adjustable intensities and timing. POL = polarizer, HWP = half-wave plate, and PBC = polarizing beam cube. The symbols near the second PBC denote the polarizations in each leg and at the output of the interferometer.

4.3 Theory

We begin by considering a conventional OKE experiment performed in an isotropic medium using a polarization-spectroscopy configuration, the interactions of which are shown schematically as a ladder diagram in Figure 4.2a. Excitation is accomplished with a single linearly polarized pump pulse, the polarization of which we will call x . The probe pulse, which arrives at some time τ later, is polarized at 45° to the pump $((x + y)/\sqrt{2})$ and the signal at -45° to the pump $((x - y)/\sqrt{2})$. The only nonzero tensor elements of the third-order response function in an isotropic medium are those in

which each spatial index appears an even number of times. The quantity R_{xyxy} is known as the depolarized response, and it arises solely from modes that affect the polarizability of the liquid anisotropically.

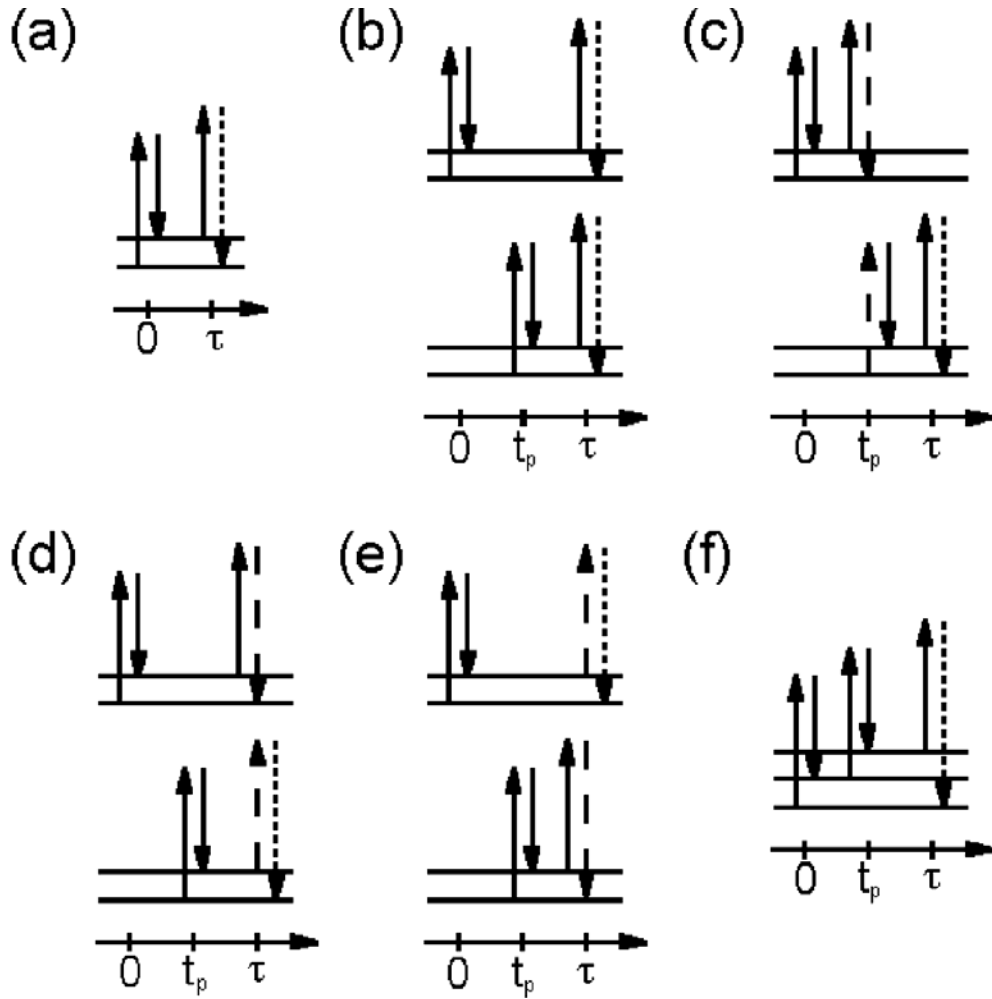


Figure 4.2 Ladder diagram representations of processes that contribute to the OKE decay with (a) one and (b-f) two pump pulses. Horizontal lines denote energy levels of Raman-active intermolecular and intramolecular modes of the liquid. In parts b-e, the pair of horizontal lines is involved in an independent third-order response. Solid vertical arrows indicate laser interactions, dotted arrows indicate signal fields, and dashed arrows indicate intermediate fields arising from a third-order response that act as one of the source fields for another third-order response. The diagram in part b illustrates the case of two independent third-order responses, part c shows a serial cascade, parts d and e are parallel cascades, and part f is a representative pathway in the fifth-order nonresonant response.

Now consider the use of two orthogonally polarized pump pulses that are not time coincident (Figure 4.2b). We will assume that the first pulse is x -polarized and arrives at time zero and that the second pulse is y -polarized and arrives at time t_p . The intensity of the second pump pulse is a times that of the first. The probe pulse is again polarized at 45° and arrives at time τ , and detection is performed at -45° . We will constrain ourselves to the case in which none of the pulses overlap in time and $\tau > t_p$. Under these circumstances, there are three possible contributions to the signal, all of which are phase-matched.

The first type of contribution is the sum of the independent third-order responses from each of the pump beams with the probe beam. The response function in the case of independent responses is given by:

$$R_{-ddyx}^{(3+3)}(t_p, \tau) = R_{xyxy}^{(3)}(\tau) - aR_{xyxy}^{(3)}(\tau - t_p) \quad (4.1)$$

where we have taken advantage of the fact that $R_{xyxy}^{(3)} = R_{yxyx}^{(3)}$ in an isotropic medium. Here the superscript of the response denotes that it is the sum of two third-order responses, and the subscript gives the polarizations of the pump beams, the probe beam, and the signal beam in reverse temporal order; d denotes a polarization of 45° , and $-d$ denotes a polarization of -45° . From eq 4.1, it is straightforward to see how mode selectivity might be achieved.

The second potential contribution to the signal arises from cascaded third-order processes,^{1,2} of which there are two possible cases, serial and parallel. In the former case (Figure 4.2c), the second pump pulse acts as a probe pulse for the coherence created by the first pump pulse. The resultant third-order signal field then acts as one pump field for

an ensuing third-order process. Within the polarization scheme used here, the response arising from the serial cascade follows

$$R_{-ddyx}^{(3,3,s)}(t_p, \tau) \propto \frac{a}{2} R_{yyxx}^{(3)}(t_p) \left(R_{xxyy}^{(3)}(\tau - t_p) - R_{yyxy}^{(3)}(\tau - t_p) \right) = a R_{yyxx}^{(3)}(t_p) R_{xxyy}^{(3)}(\tau - t_p) \quad (4.2)$$

where the superscript on the response function denotes that it arises from a serial cascade of two third-order responses. In the latter case, the signal electric field generated from one pump pulse and the probe pulse acts as a pump field for the coherence generated by the other pump pulse. There are two ways in which such a parallel cascaded signal can be generated (Figure 4.2, parts d and e), and here both pathways yield an identical response.

The total response from the parallel cascade is given by

$$R_{-ddyx}^{(3,3,P)}(t_p, \tau) \propto 2a \left(R_{xxxx}^{(3)}(\tau) R_{xxyy}^{(3)}(\tau - t_p) - R_{yyxx}^{(3)}(\tau) R_{yyxy}^{(3)}(\tau - t_p) \right) = 2a \left(R_{xxxx}^{(3)}(\tau) R_{xxyy}^{(3)}(\tau - t_p) - R_{xxyy}^{(3)}(\tau) R_{xxxx}^{(3)}(\tau - t_p) \right) \quad (4.3)$$

where the superscript on the response function denotes that it arises from a parallel cascade of two third-order responses.

The final potential contribution to the signal arises from a direct fifth-order response.⁴ A number of different pathways contribute to this response, and one representative such pathway is shown in Figure 4.2f. The relevant fifth-order response in this case is given by

$$R_{-ddyx}^{(5)}(t_p, \tau) = R_{xxyyxx}^{(5)}(t_p, \tau - t_p) - R_{yyxyxx}^{(5)}(t_p, \tau - t_p) \quad (4.4)$$

The total response function, which is measured directly when optical heterodyne detection is employed, is given by the sum of the individual contributions

$$R_{-ddy}^{(total)}(t_p, \tau) = R_{-ddy}^{(3+3)}(t_p, \tau) + R_{-ddy}^{(3,3,s)}(t_p, \tau) + R_{-ddy}^{(3,3,p)}(t_p, \tau) + R_{-ddy}^{(5)}(t_p, \tau) \quad (4.5)$$

Thus, in general the total response could be quite complex. However, the fifth-order response is known to be many orders of magnitude smaller than the cascaded third-order responses² and so can safely be ignored. It is further expected that the cascaded third-order responses should be significantly weaker than the sum of individual third-order responses, since the electric field from any individual third-order response would normally be much weaker than the electric field of any of the laser pulses. It is still possible that the cascaded response could be appreciable, however. To distinguish the sum of individual third-order responses from that of cascaded third-order responses, we note that in the former case the temporal behavior of the signal depends explicitly on the relative intensities of the pump pulses, whereas in the latter case it does not. Furthermore, in the case of serial cascades the response function is the product of two third-order response functions, so it is not possible to cancel vibrational or reorientational contributions to this response by adjusting the delay and amplitudes of the pump pulses. The response from parallel cascades is necessarily zero when $\tau = 2t_p$, but it is otherwise not generally possible to cancel the vibrational or reorientational contributions to this response by adjusting the delay and amplitudes of the pump pulses.

4.4 Results

We begin by considering the suppression of the contribution of reorientational diffusion in the OKE decay of a simple liquid. Shown in Figure 4.3 (black line) is the

OKE decay of benzene at room temperature after a single pump pulse. As can be seen in the semilogarithmic plot in the inset of this figure, the OKE decay features a long exponential tail. This tail, which has a time constant τ_r of 3.03 ps,³ arises from the diffusive decay of the orientational anisotropy created by the probe pulse.

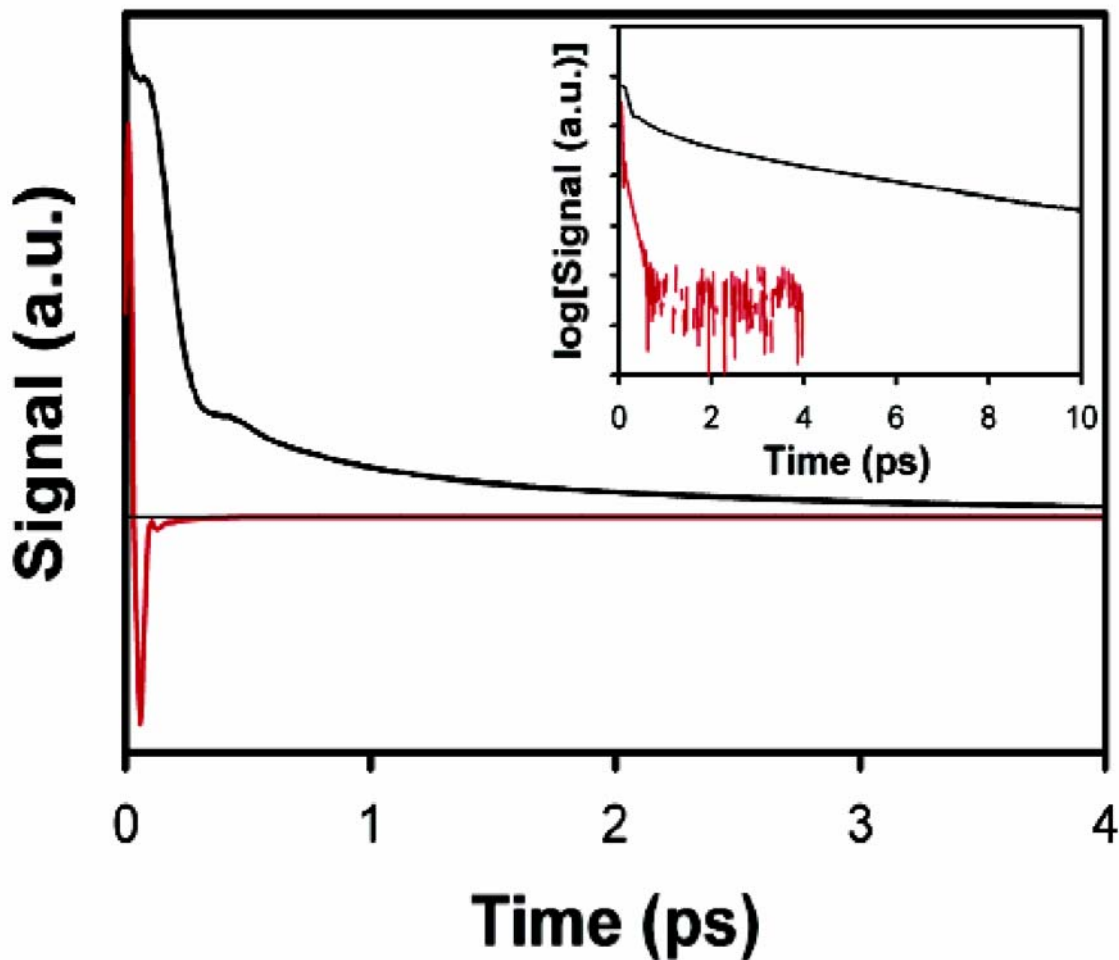


Figure 4.3. OKE decays for room-temperature benzene with one pump pulse (black line) and two perpendicularly polarized pump pulses separated by 133 fs (red line). The horizontal line demarcates the zero level of the signal. Shown in the inset is a semilogarithmic plot of the data with single-pulse excitation (black line) and the negative of the data two-pulse excitation (red line). The tick marks on the ordinate are factors of 10. The bottom of the inset is the approximate zero level of the spectra.

The red line in Figure 4.3 shows a benzene OKE decay in which perpendicularly polarized pump pulses have been employed. For this particular set of data, the delay between the pump pulses was 133 fs. Note that the decay becomes negative in sign around the time of arrival of the second pump pulse and remains so for all subsequent delay times, as is predicted by eq. 4.1 so long as the intensity of the second pump pulse is great enough relative to that of the first pump pulse. If desired, the sign of the decay can be flipped by using a negative value of t_p . For these data, the intensity ratio of the pump pulses was chosen to optimize the suppression of the contribution of reorientational diffusion. As can be seen in the inset of this figure, the diffusive contribution to the decay is smaller than the noise in the signal and so has been suppressed by more than three and a half orders of magnitude. If the ratio of the intensities of the pump pulses is made either larger or smaller than the optimal value, then the diffusive decay becomes visible again. The greater the deviation of the ratio from the optimal value, the greater is the amplitude of diffusive decay.

According to eq. 4.1, the ratio of pump pulse intensities needed to suppress the reorientational contribution to the data completely should scale as $\exp(-t_p/\tau_r)$. To test this prediction, we measured the ratio of intensities needed to suppress this contribution for values of t_p ranging from 133 fs to 4.5 ps. The results of these experiments are plotted in semilogarithmic form in Figure 4.4. The intensity ratio is clearly an exponential function of t_p . A linear least-squares fit of the data yields a slope of -0.33 ps^{-1} , which is identical to the value of $-1/\tau_r$.

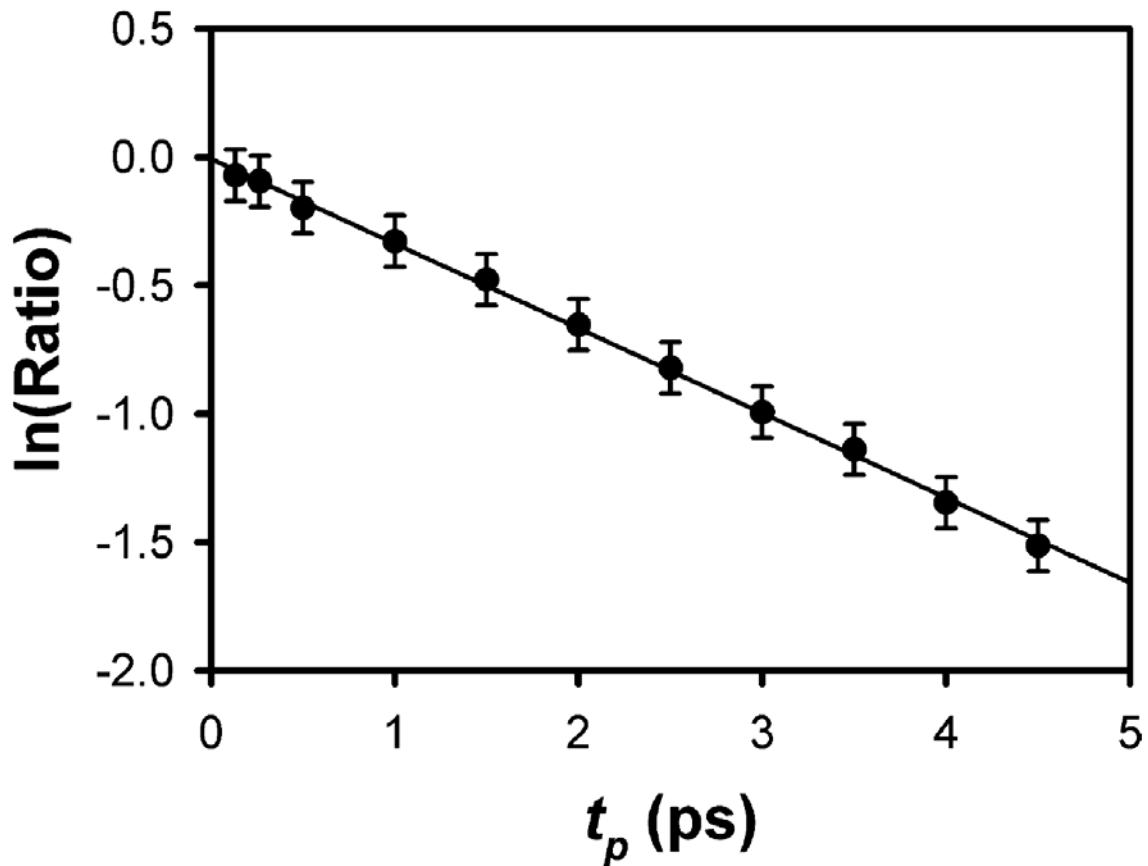


Figure 4.4. Ratio of pump beam intensities required to cancel the orientational diffusion component of the benzene OKE decay as a function of t_p . The solid line is a linear least-squares fit to the data.

These results are consistent with the signal being dominated by the sum of two third-order responses. The shape of the decay changes with the ratio of pump pulse intensities, and the ratio of intensities required to suppress the orientational contribution to the signal follows the behavior predicted for the sum of responses. It is also worth note that the predicted behavior is followed even when the separation between the pump

pulses is so short as to lie within the portion of the response that is dominated by intermolecular modes, as in Figure 4.3.

We now turn to the suppression of the contributions of specific intramolecular vibrational modes. Shown in Figure 4.5 is the OKE decay for iodobenzene at room temperature (black line). The inset shows the imaginary portion of the Fourier transform of these data from 100-300 cm^{-1} . There are two depolarized, Raman-active intramolecular vibrations within the bandwidth of the laser, one at 167 cm^{-1} and one at 273 cm^{-1} .

Also shown in Figure 4.5 are OKE decays for iodobenzene that have been excited with perpendicularly polarized pump pulses. In the red decay, the delay between pump pulses was set to 122 fs, one period of the higher-frequency vibration. In the blue decay, t_p was set to 200 fs, one period of the lower-frequency mode. For each data set, the relative intensities of the pump pulses were adjusted to optimize the suppression of the mode of interest. It can be seen in the inset of Figure 4.5 that in both cases the contribution of the suppressed vibrations is greatly reduced.

To examine the intensity ratio of the pump pulses that is needed to suppress an intramolecular vibrational mode, we turn to the case of chloroform. Shown as a black line in Figure 4.6 is the OKE decay for chloroform at room temperature for a single pump pulse. As can be seen in the inset spectrum, two Raman-active intramolecular modes contribute to the decay, a strong one at 262 cm^{-1} and a weaker one at 365 cm^{-1} . The red line in Figure 4.6 is the OKE decay resulting from the use of two perpendicularly polarized pump pulses separated by one period of the 262 cm^{-1} vibration (127 fs). As can

be seen in the inset, under these conditions the contribution from this vibration is strongly suppressed.

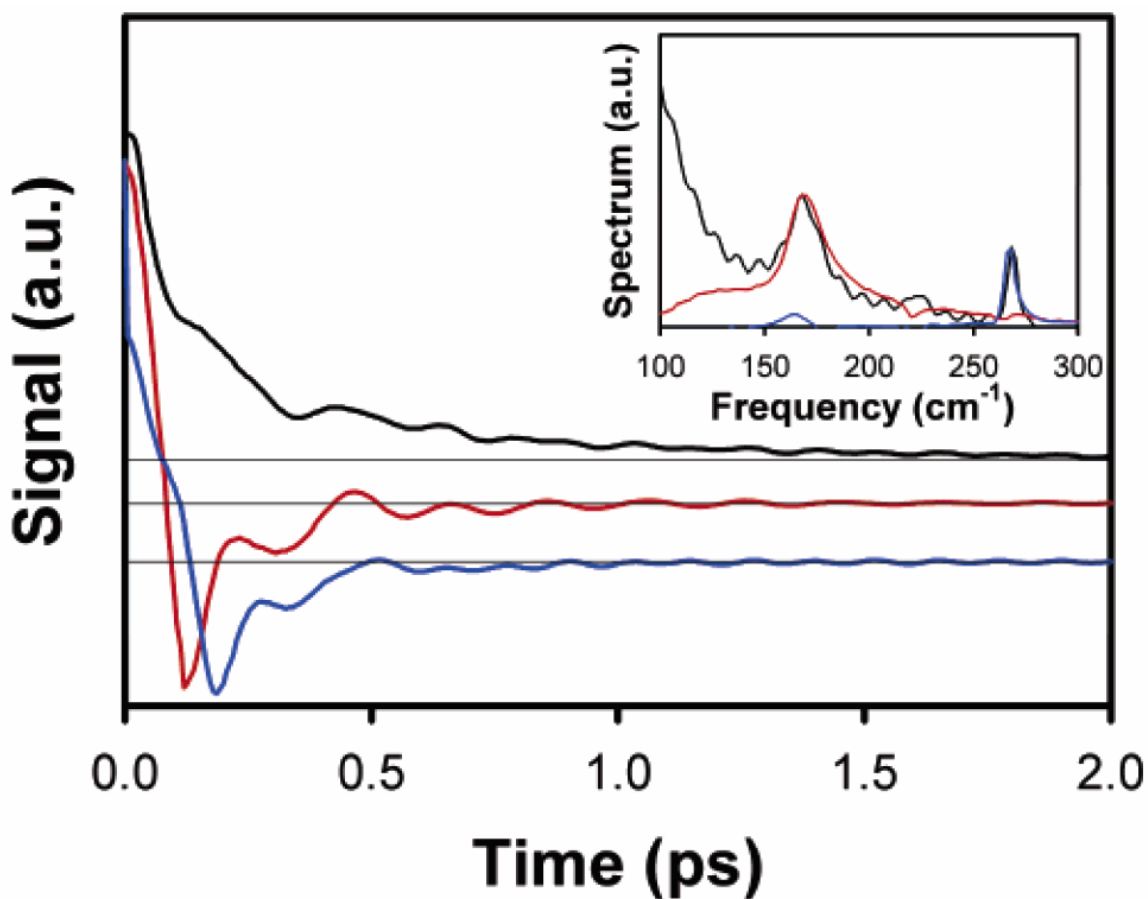


Figure 4.5 OKE decays for iodobenzene at room temperature. The black line is the data for a single pump pulse, the red line is the data for pump pulses separated by one period of the higher-frequency vibration (122 fs), and the blue line is the data for pump pulses separated by one period of the lower-frequency vibration (200 fs). The horizontal lines demarcate the zero level of the signal. The inset shows part of the imaginary portion of the Fourier transform of each decay, demonstrating the excellent mode suppression when dual pump pulses are employed.

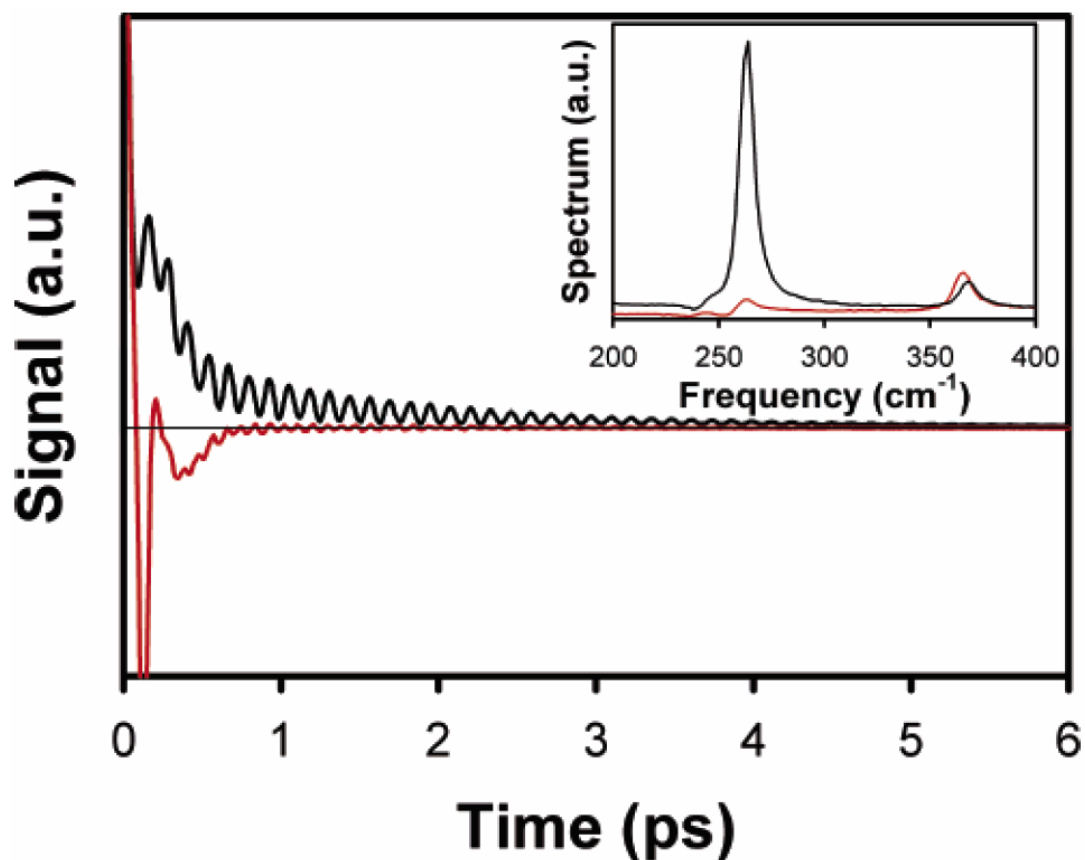


Figure 4.6 Room-temperature OKE decays for chloroform with a single pump pulse (black line) and with two perpendicularly polarized pump pulses separated by one period (127 fs) of the lower-frequency vibrational mode (red line). The horizontal line demarcates the zero level of the signal. Shown in the inset are part of the imaginary portions of the Fourier transforms of the two decays. The bottom of the inset is the approximate zero level of the spectra.

According to eq. (3.7), the intensity ratio needed to cancel the contribution of a vibration when t_p is an integral number of periods of the vibration should scale as $\exp(-t_p/\tau_r)$. To test this prediction, we first obtained an OKE decay in which the mode at 365 cm^{-1} was suppressed. The portion of this decay after the intermolecular modes had damped out was then fit to the equation:

$$S(\tau) = A \exp(-\tau / \tau_r) + B \exp(-\tau / \tau_v) \sin(\omega_v \tau) \quad (4.6)$$

where A and B are amplitudes, τ_r is the collective orientational correlation time (which we have previously measured³ to be 3.28 ps at room temperature), and ω_v and τ_v are the angular frequency and dephasing time of the 262 cm⁻¹ vibration. On the basis of this fit, the vibrational dephasing time was determined to be 1.6 ps. We next measured the ratio of pump intensities required to suppress this mode for values of t_p that were integer multiples of the period of the vibration. These data are plotted in semilogarithmic form in Figure 4.7. The solid line is the result of a linear least-squares fit in which the slope has been constrained to be the negative inverse of τ_v . The fit is in good agreement with the data, which further supports the sum of independent third-order responses model for the signal.

As an additional check of the sum of independent responses model, we can test eq. 4.3 directly by using the OKE decay with a single pump pulse to model the decay from perpendicular pump pulses. The signal from a single pump pulse is time shifted by t_p , multiplied by the ratio of the intensity of the second pump pulse to the first, and then subtracted from the signal from a single pump pulse. Shown in Figure 4.8 is the result of this procedure for the perpendicularly polarized pump OKE decays for iodobenzene from Figure 4.5. As can be seen from the time-domain data and from the imaginary portion of their Fourier transforms in the inset, the model gives a good fit to the data. The fit is particularly good for the case in which the 167 cm⁻¹ mode is suppressed, but both data sets offer strong support for the signal arising predominantly from the sum of independent third-order responses. We have obtained equally good results in using eq 4.3

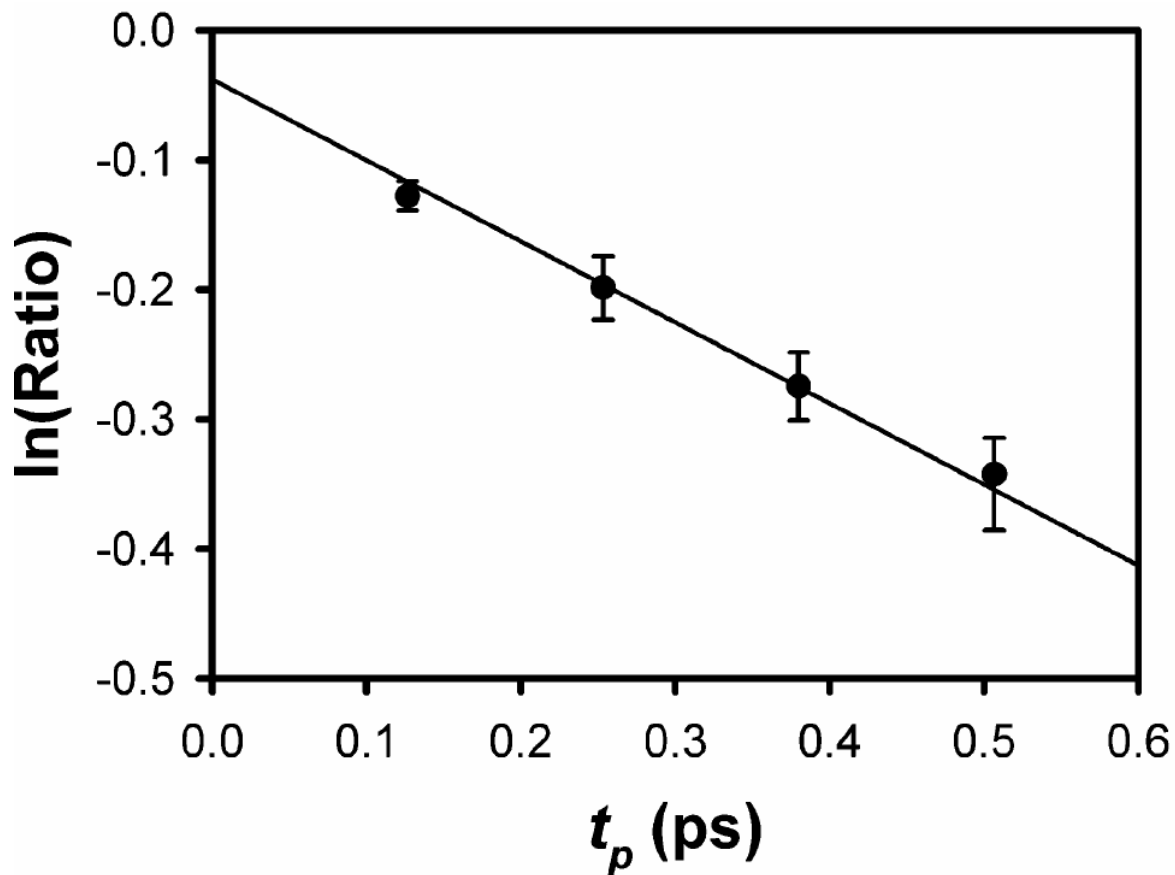


Figure 4.7 Ratio of pump beam intensities required to suppress the contribution of the 262 cm^{-1} mode in the OKE decay of chloroform as a function of t_p . The line is a linear least-squares fit to the data in which the slope has been constrained to be the logarithm of the dephasing rate of the vibration.

to simulate the perpendicularly polarized pump pulse OKE decays for all of the other liquids studied here.

A potentially important application of mode-selective OKE spectroscopy is the isolation of the signal of a single component in a mixture. With this thought in mind, we used perpendicularly polarized pump pulses to study the OKE response of a 1:1 (V/V) mixture of chloroform and chlorobenzene. As discussed above, chloroform has an

intramolecular vibration at 262 cm^{-1} that contributes strongly to its OKE signal. Chlorobenzene, however, has a strong depolarized Raman-active mode at 199 cm^{-1} . As shown in the decays and the inset spectra in Figure 4.9, when the separation between the pump pulses is one period of the chloroform mode (128 fs), its contribution is strongly suppressed. The same is true for the chlorobenzene mode when the pump pulses are separated by 172 fs. Even when the liquids are in volume ratios as large as 20:1, we have found that it is possible to suppress the vibrational contribution of the major component so that it is significantly smaller than that of the minor component.

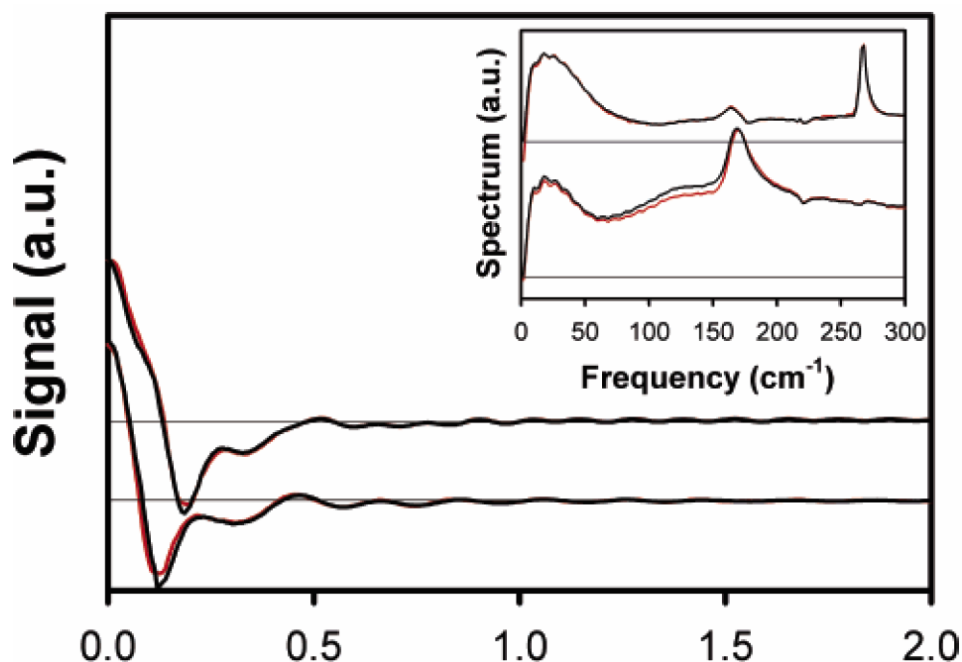


Figure 4.8. The black lines are OKE decays for room-temperature iodobenzene. In the upper data set, the lower-frequency vibration has been suppressed ($t_p = 122\text{ fs}$), and in the lower data set, the higher-frequency vibration has been suppressed ($t_p = 200\text{ fs}$). The red lines are simulations of the decays that are derived from the single-pulse excitation data. The horizontal lines demarcate the zero level of the signal and the approximate zero levels of the spectra. As can be seen from the decays and from the inset with the corresponding spectra, the agreement between the data and the simulation is excellent.

In the results presented up to now, we have suppressed the contributions of a vibrational mode by separating the two pump pulses by a single period of the vibration. However, if one wishes to suppress one mode while maximally enhancing another, then it may be desirable to separate the pump pulses by some other judiciously chosen integer multiple of the period. The mixture of chloroform and chlorobenzene is a case in point. Two periods of the 262 cm^{-1} chloroform mode is 256 fs, whereas 1.5 periods of the

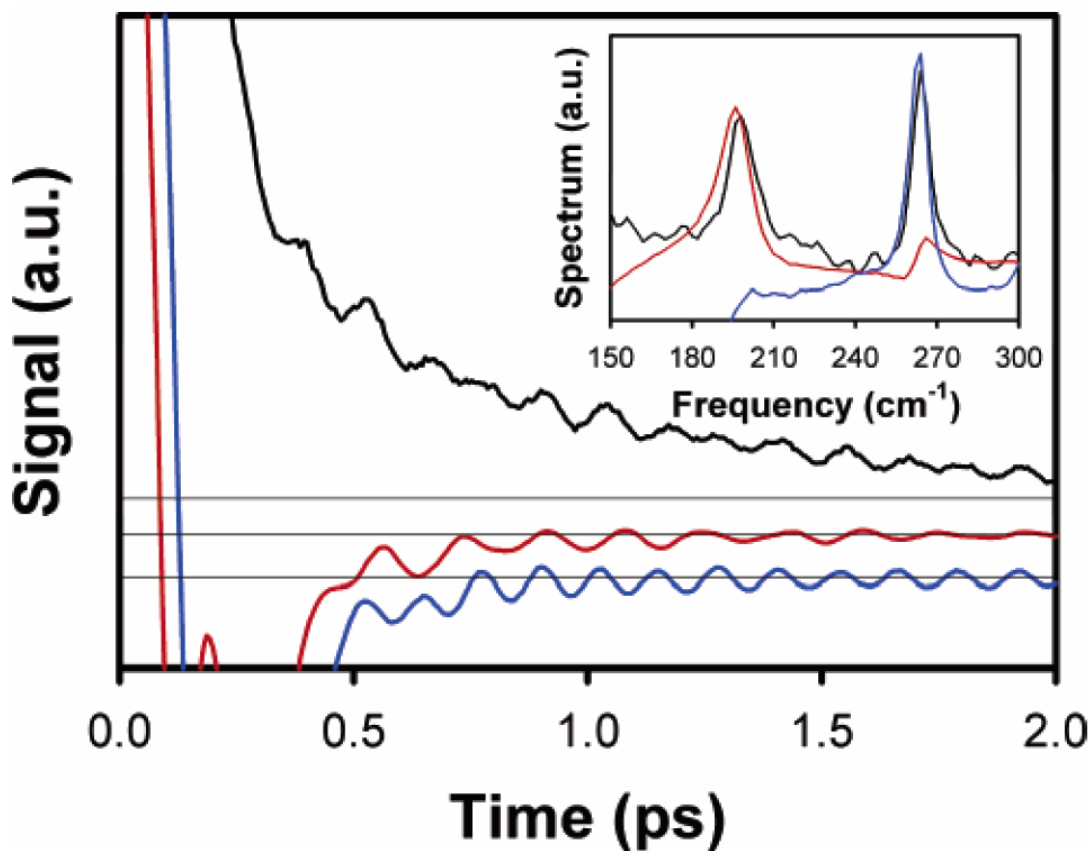


Figure 4.9. OKE decays for a 1:1 v/v mixture of chloroform and chlorobenzene. The black line is the decay for a single pump pulse. Two pump pulses have been used to suppress the chlorobenzene mode at 199 cm^{-1} in the red decay ($t_p = 128\text{ fs}$) and to suppress the chloroform mode at 262 cm^{-1} in the blue decay ($t_p = 172\text{ fs}$). The horizontal lines demarcate the zero level of the signal. The inset spectra demonstrate the quality of the mode suppression. The bottom of the inset is the approximate zero level of the spectra.

chlorobenzene mode is 258 fs. Thus, separating the pump pulses by 256 fs not only serves to cancel the chloroform mode but is nearly optimal for enhancing the chlorobenzene mode as well. Shown in Figure 4.10 is a comparison of the imaginary portion of the Fourier transform of OKE data in a 1:1 mixture of chloroform and chlorobenzene with a single pump pulse, with two pump pulses separated by 128 fs and with two pump pulses separated by 256 fs. As expected, the spectral discrimination is strongest for the 256 fs separation between the pump pulses.

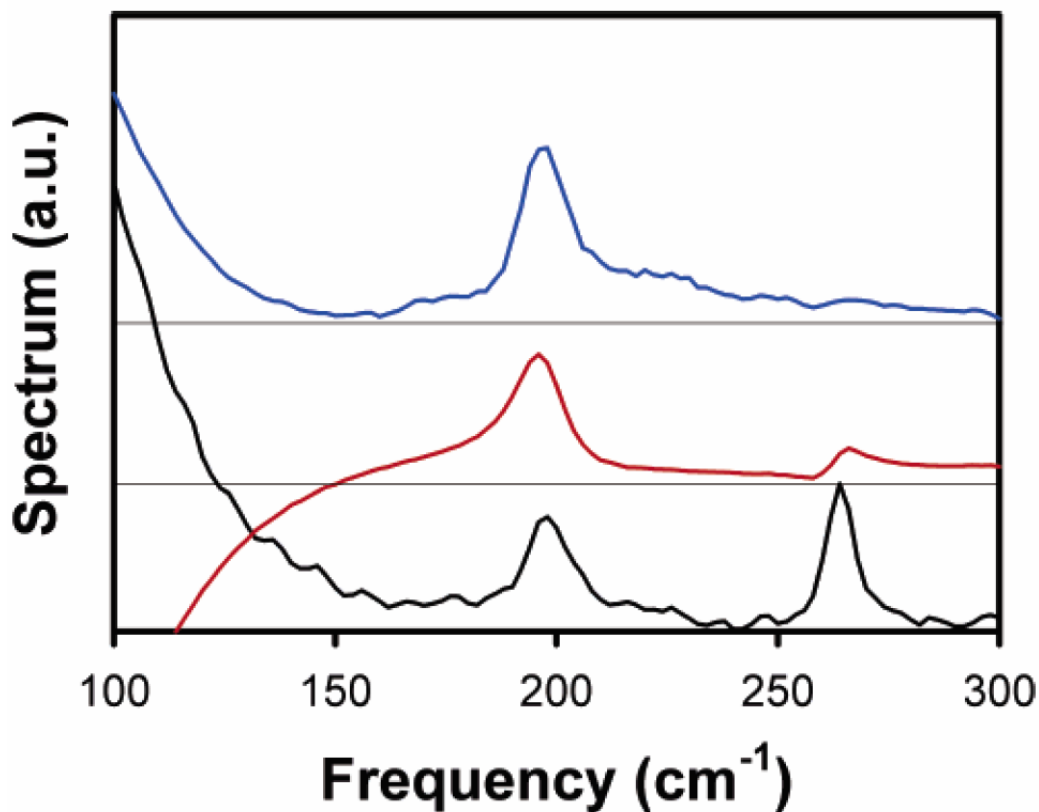


Figure 4.10. Imaginary portion of the Fourier transform of OKE decays in a 1:1 mixture of chloroform and chlorobenzene. The black spectrum is for a single pump pulse, the red spectrum is for pump pulses separated by 128 fs, and blue spectrum is for pump pulses separated by 256 fs. The spectra have been offset for clarity, and the horizontal lines denote the approximate zero levels.

4.5 Discussion

In symmetric top liquids, we have shown that it is possible to suppress the reorientational contribution to the signal completely by selecting appropriate intensities for the pump pulses at a given value of t_p . Since the use of perpendicularly polarized pump pulses will always tend to suppress the reorientational contribution to the signal, this latter contribution is also weakened considerably in all of the examples above in which we manipulate the strength of intramolecular vibrational contributions.

The complete suppression of reorientation becomes more difficult when molecules that are not symmetric tops are employed, however, since the reorientational decay is no longer described by a single exponential. However, the fact that the signal can be modeled to a high degree of accuracy by the sum of independent third-order responses from each pump pulse suggests that it will be straightforward to accomplish complete suppression of the reorientational contribution in more complex situations with the use of a larger number of pump pulses. Consider, for instance, a liquid composed of molecules with a polarizability tensor that has the same principal axes as its diffusion tensor but that has different diffusion constants about the principal axes of the latter tensor. In this case, the reorientational portion of the OKE decay is expected to be described by the sum of two exponentials⁵ with amplitudes a_1 and a_2 and time constants τ_1 and τ_2 . We can use three pump pulses, with intensities A_1 , A_2 , and A_3 , to prepare this system. Pulse 1 is vertically polarized and arrives at time zero, pulse 2 is horizontally polarized and arrives at time t_{p1} , and pulse 3 is vertically polarized and arrives at time t_{p2} . Within the sum of

independent responses model, the reorientational portion of the OKE response at probe delay $\tau > t_{p2}$ is then given by

$$R_{xy,xy,reor}^{(3)}(\tau) \propto A_1 (a_1 e^{-\tau/\tau_{r1}} + a_2 e^{-\tau/\tau_{r2}}) - A_2 (a_1 e^{-(\tau-t_{p1})/\tau_{r1}} + a_2 e^{-(\tau-t_{p2})/\tau_{r2}}) + A_3 (a_1 e^{-(\tau-t_{p2})/\tau_{r1}} + a_2 e^{-(\tau-t_{p2})/\tau_{r2}}) \quad (4.7)$$

The only way for this response to be zero for all times $\tau > t_{p2}$ is for the contribution from each reorientational component to be zero. Collecting the terms for each component, we find that

$$1 - B_2 e^{t_{p1}/\tau_{r1}} + B_3 e^{t_{p2}/\tau_{r1}} = 0 \quad (4.8)$$

and

$$1 - B_2 e^{t_{p1}/\tau_{r2}} + B_3 e^{t_{p2}/\tau_{r2}} = 0 \quad (4.9)$$

where $B_n = A_n/A_1$. These two equations are satisfied when

$$B_2 = \frac{e^{t_{p2}/\tau_{r1}} - e^{t_{p2}/\tau_{r2}}}{e^{t_{p2}/\tau_{r1}} e^{t_{p1}/\tau_{r2}} - e^{t_{p1}/\tau_{r1}} e^{t_{p2}/\tau_{r2}}} \quad (4.10)$$

and

$$B_3 = \frac{e^{t_{p1}/\tau_{r1}} - e^{t_{p1}/\tau_{r2}}}{e^{t_{p2}/\tau_{r1}} e^{t_{p1}/\tau_{r2}} - e^{t_{p1}/\tau_{r1}} e^{t_{p2}/\tau_{r2}}} \quad (4.11)$$

Note that these intensities are independent of the amplitudes of the two exponential decays, a_1 and a_2 . The generalization of this result is that an orientational decay composed of n exponentials can be canceled completely by $n + 1$ pulses of appropriate intensities.

A parallel argument can be made for the suppression of vibrational modes, i.e., in general it should be possible to suppress the contributions of n vibrational modes completely with a sequence of $n + 1$ pulses. This strategy differs somewhat from that of Weiner, Nelson, and co-workers, who used trains of evenly spaced pulses of a single polarization to enhance a particular vibrational mode selectively, without the need to design the sequences to suppress other modes at the same time.⁶⁻⁷ Given a tractable number of vibrational modes, employing a strategy that combines both enhancement and suppression would be desirable. However, when a large number of depolarized modes are present, focusing solely on enhancement of the mode of interest is the preferable approach. One key issue in this regard is that pulse trains that are significantly longer than the dephasing time of a vibration offer diminishing returns in enhancement. This situation can be improved upon by incorporating perpendicular polarizations into the excitation scheme. Rather than exciting with n pulses of the same polarization that are spaced by the period of the vibration, $n/2$ pulses of one polarization could be alternated with $n/2$ pulses of the orthogonal polarization. The pulses of each polarization would still be spaced by the vibrational period, but there would be a half-period offset between the two polarizations. In this manner, the total duration of the pulse sequence would be halved, which should lead to a significant improvement in excitation efficiency given the same integrated excitation intensity. Techniques for the simultaneous temporal and polarization shaping of ultrafast pulses should make such pulse sequences straightforward to implement.⁸

It is also worthwhile to compare our technique with other OKE techniques that take advantage of noncollinear pump beams with controllable polarizations to generate selective responses.⁹⁻¹¹ The other type of technique takes advantage of the symmetry properties of the third-order response tensor to suppress different contributions to the OKE signal. However, this type of technique relies on creating linear combinations of different tensor elements of the response at the same delay time. In contrast, our technique creates linear combinations of the same tensor element of the response at different delay times. Thus, while our technique can suppress the contribution of specific modes, the other type of technique necessarily suppresses every contribution that has the same tensor symmetry, e.g., all depolarized modes, all isotropic modes, or the electronic hyperpolarizability.

The technique that we have described here allows for the selective enhancement and suppression of particular contributions to the OKE signal. However, some of the remaining contributions to the signal, particularly those from intermolecular vibrational modes, may be distorted as compared to what is seen with a single pump pulse. As a result, using multiple pump pulses is not desirable in all circumstances. For instance, when two pump pulses are used, Fourier transform deconvolution¹² cannot be employed to derive the intermolecular spectrum.

One situation in which this new technique is useful is when oscillations from intramolecular vibrations overwhelm a reorientational decay. One application of particular interest to us is OKE microscopy. OKE spectroscopy shares many of the advantages of other nonlinear optical techniques that have been used for microscopy

recently, including high spatial and temporal resolution and the ability to image in three dimensions. However, the potentially large number of contributions to the OKE signal can have a deleterious effect on contrast. By enhancement of the strength of a chosen contribution while others are suppressed, our technique may provide the means for increasing the contrast and the signal-to-noise ratio of OKE microscopy considerably, and this is an application that we will be pursuing soon.

4.6 Conclusion

In this chapter, we have further explored a technique that we introduced recently in which a pair of perpendicularly polarized pump pulses is used in the excitation step of an OKE experiment in a polarization-spectroscopy geometry. We have shown that this scheme allows for the essentially complete suppression of the contribution of reorientational diffusion or of a selected vibrational mode to the OKE signal. Studies of the ratio of intensities of pump pulses required to cancel the contribution of reorientation or a specific vibration as a function of the delay time between the pump pulses are in good agreement with the signal arising from the sum of an independent third-order response originating with each pump pulse. Simulations of the signal from two pump pulses based on the signal with a single pump pulse further supports this picture. These experiments pave the way for using sequences of multiple pump pulses with controllable polarization, timing, and intensity to single out the contribution of a single mode of interest in a complex OKE decay. Such a technique would be of great interest for performing mode-selective OKE microscopy, among other applications.

Chapter 4 References and Notes

- (1) Ulness, D. J.; Kirkwood, J. C.; Albrecht, A. C. *J. Chem. Phys.* **1998**, 108, 3897.
- (2) Blank, D. A.; Kaufman, L. J.; Fleming, G. R. *J. Chem. Phys.* **1999**, 111, 3105.
- (3) Loughnane, B. J.; Scodinu, A.; Farrer, R. A.; Fourkas, J. T.; Mohanty, U. *J. Chem. Phys.* **1999**, 111, 2686.
- (4) Tanimura, Y.; Mukamel, S. *J. Chem. Phys.* **1993**, 99, 9496.
- (5) Berne, B. J.; Pecora, R. *Dynamic Light Scattering*; Wiley: New York, **1976**.
- (6) Weiner, A. M.; Leaird, D. E.; Wiederrecht, G. P.; Nelson, K. A. *Science* **1990**, 247, 1317
- (7) Weiner, A. M.; Leaird, D. E.; Wiederrecht, G. P.; Nelson, K. A. *J. Opt. Soc. Amer. B* **1991**, 8, 1264.
- (8) Brixner, T.; Gerber, G. *Opt. Lett.* **2001**, 26, 557.
- (9) Etchepare, J.; Kenney-Wallace, G. A.; Grillon, G.; Migus, A.; Chambaret, J. P. *IEEE J. Quantum Electron.* **1982**, QE-18, 1826.
- (10) Etchepare, J.; Grillon, G.; Chambaret, J. P.; Hamoniaux, G.; Orszag, A. *Opt. Commun.* **1987**, 63, 329.
- (11) Deeg, F. W.; Fayer, M. D. *J. Chem. Phys.* **1989**, 91, 2269.
- (12) McMorro, D.; Lotshaw, W. T. *J. Phys. Chem.* **1991**, 95, 10395.
- (13) Zhu, X.; Farrer, R.A.; Fourkas, J. T. *J. Phys. Chem. B* **2005**, 109, 8481

Chapter 5

Dynamics of nanoconfined benzene

5.1. Introduction

Nanoconfinement can have a profound influence on the behavior of liquids.¹⁻⁵ The prevalence of liquids confined on molecular distance scales in science and technology has resulted in considerable effort being devoted to studying this problem. While significant progress has been made in understanding how nanoconfinement affects the structure and dynamics of liquids, there also remains much to be learned.

Our efforts in studying nanoconfined liquids have focused on using ultrafast spectroscopy to study the dynamics of liquids confined in sol-gel silicate glasses.⁶⁻¹⁷ These materials are ideally suited for optical spectroscopy of nanoconfined liquids. Monoliths with high optical quality and high porosity can be fabricated readily in the laboratory.¹⁸ The average pore size can be controlled synthetically, and the pore diameters are relatively monodisperse. In addition, the interactions between the pore surfaces and the confined liquid can be controlled via well-known surface-modification chemistry.¹⁹ Our method of choice for studying dynamics of liquids confined in sol-gel monoliths is optical Kerr effect spectroscopy.²⁰⁻³⁰ While a number of different factors contribute to the decay of the birefringence of the sample following excitation,²⁰⁻³⁰ in studies of nanoconfined liquids we are most interested in the slowest relaxation, which

results from the orientational diffusion of molecules to return the liquid to an isotropic orientational state.

In previous studies we have found that even when the confined liquid only weakly wets the surfaces of the nanopores, its reorientational dynamics are still affected significantly.^{6,7,9,11,17} In weakly-wetting liquids composed of rod-like molecules, such as CS₂ and 2-butyne, multiexponential decays are observed.^{6,7,11,17} The fastest of these exponentials has a decay constant that matches that of the bulk liquid, whereas the other exponentials can decay significantly more slowly. In the case of 2-butyne, we have observed a second exponential with a decay time that is exactly twice that of the bulk liquid, regardless of pore size, and a third, even slower decay that does depend on pore size.¹⁷ Our interpretation of such data is that there is a population of molecules in the centers of the pores that is not affected by confinement and a second population at the pore surfaces that is affected in two ways. First, for reorientation off of the pore surfaces there is necessarily a factor of two increase in hydrodynamic volume, which accounts for the intermediate decay component. Second, reorientation along the pore surfaces is inhibited by geometric constraints, accounting for the pore-size dependent decay component observed. Furthermore, the thickness of the surface layer of molecules that have retarded orientational dynamics is less than a monolayer, which we believe is indicative of the fact that the orientational dynamics of molecules that lie normal to the pore surfaces are not influenced by their proximity to the pore walls.^{11,16} These proposed mechanisms for dynamic inhibition of weakly-wetting liquids at pore surfaces rely upon the molecules being rod-like in nature. If the molecules are instead disk-shaped, it is not

obvious that the same phenomena should be observed. For instance, reorientation about the axis of the disk should not necessarily be inhibited at pore surfaces, and so the geometric confinement effect might not be expected to exist for such liquids. Furthermore, the increase in hydrodynamic volume for reorientation should be smaller for disks rotating off of the surface of a pore than for cylinders. Here we investigate whether the same phenomena observed for weakly-wetting liquids composed of rod-like molecules hold for benzene or benzene-d₆, both of which are composed of disk-shaped molecules that cannot hydrogen bond to silicate surfaces.

5.2. Experimental Section

Nanoporous sol-gel monoliths were prepared as described in chapter 2, and pore size distributions were measured with nitrogen adsorption and desorption isotherms.¹⁸ The monoliths were disks of approximately 6 mm in diameter that were polished on both sides to a thickness of slightly less than 1 mm. Monoliths of different average pore sizes were placed in a cuvette with a 1 mm path length and immersed in liquid. Once the sol-gel samples had filled completely with liquid, enough additional liquid was added to ensure that the samples would remain submerged. The cell was then sealed. Surface modification was accomplished by refluxing the monoliths for 24 hours in a 50% solution of trimethylchlorosilane in dry toluene.¹⁹ The OKE setup employed was similar to one we have described previously in chapter 2, and so I will give only a brief description here. A solid-state laser (Coherent Verdi 5) was used to pump a commercial Ti:sapphire laser (KMLabs TS), producing 50-fs pulses with a center wavelength of about 800 nm at a

repetition rate of 90 MHz. The laser output was divided into pump and probe beams, each of which passed through a different ring of a chopper wheel. The pump beam was polarized vertically and was focused into the sample using an achromatic lens. When taking data on a sol-gel sample, we ensure that the beams overlap only within the monolith so that there is no signal from the surrounding bulk liquid. All data reported here were collected at a temperature of 293 K. All data sets were averages of at least eight scans. Since the OKE signal is the negative time derivative of the orientational correlation function,³¹ the negative integral of the averaged data sets was taken, which served to smooth out any high-frequency noise. The constant of integration for each data set was determined by ensuring that the decay was exponential at long times. Fits were made to data at decay times greater than 5 ps, at which point the signal is dominated by orientational diffusion. Fitting was performed using a commercial software package (Systat SigmaPlot 9.0). In all cases, a biexponential function was found to provide an excellent fit to the data.

5.3. Results

The collective orientational correlation functions ($C_{\text{coll}}(\tau)$) derived from the OKE decays for benzene in the bulk and in nanoconfinement in unmodified sol-gel monoliths are shown in Fig. 5.1, and the corresponding correlation functions for benzene- d_6 are shown in Fig. 5.2. In all cases the decays in confinement are considerably slower than those in the bulk liquid. The average decay time becomes longer as the average pore diameter decreases.

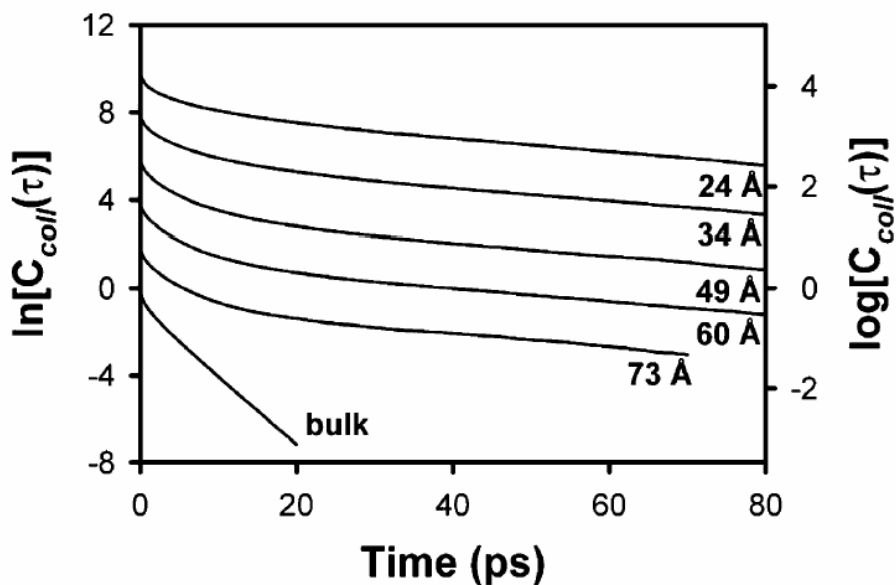


Figure 5.1. Collective orientational correlation functions for benzene in the bulk (bottom trace) and, from top to bottom, confined in 24 Å, 34 Å, 49 Å, 60 Å and 73 Å pores. All data were obtained at 293K and the correlation functions have been offset for clarity.

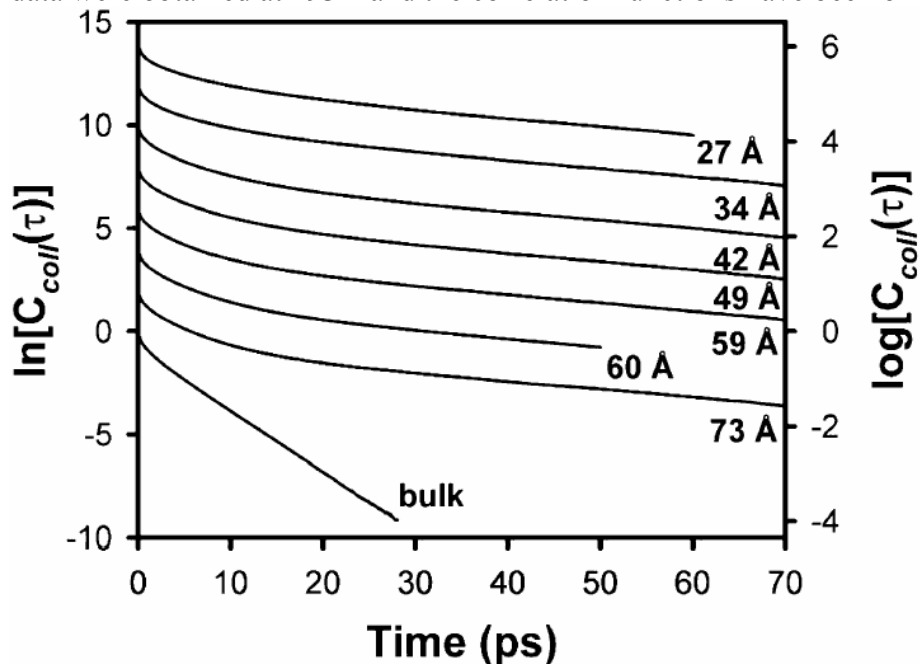


Figure 5.2. Collective orientational correlation functions for benzene- d_6 in the bulk (bottom trace) and, from top to bottom, confined in 27 Å, 34 Å, 42 Å, 49 Å, 50 Å, 60 Å, and 73 Å pores. All data were obtained at 293 K and the correlation functions have been offset for clarity.

In nanoconfined weakly-wetting liquids that we have studied previously, our OKE data could be fit to a sum of exponentials.^{6,7,9,11,17} In all cases, the time constant of the fastest of these exponentials matched well to the diffusive orientational decay of the bulk liquid. This decay has been ascribed to molecules in the centers of the pores that are not influenced by confinement. The slower portions of the decays were assigned to molecules at the pore surfaces with retarded orientational dynamics.

In analogy with these previous results, the correlation functions in Figs. 5.1 and 5.2 can be described well by the sum of two exponentials. In unconstrained fits, the time constant of the faster exponential (τ_1) was found to depend on pore size, becoming larger as the pore size decreases for both liquids. However, the time constants for the slower decay (τ_2) were similar for all pore sizes for a given liquid, although they differed between the two liquids. There was no trend observed in the variation of this decay constant with pore size. We therefore took the average value of this decay time in all the different pore sizes for each liquid, and then refit the data with the longer decay time constrained to this value but with the constant of integration allowed to float in the nonlinear least-squares fit. In all cases the constant of integration did not change significantly when the slower decay time was constrained. The decay constants and corresponding normalized amplitudes (A_1 and A_2) for these fits are given in Tables 5.1 and 5.2, and the dependence of τ_1 on pore curvature is plotted for both liquids in Fig. 5.3.

If we assume that τ_2 arises from reorientation of molecules at the pore surfaces and τ_1 from molecules in the centers of the pores, then the amplitudes of these two exponentials reflect the relative populations of molecules with these dynamics. We can

TABLE 5-1: Fit Parameters and Surface Layer Thickness for Benzene in Unmodified Pores^a

pore diameter (Å)	A_1	τ_1 (ps)	A_2	τ_2 (ps)	R_s (Å)
24	0.64	6.2	0.36	33.3	2.4
34	0.74	5.5	0.26	33.3	2.4
49	0.82	4.9	0.18	33.3	2.3
60	0.84	4.3	0.16	33.3	2.5
73	0.86	4.0	0.14	33.3	2.6
bulk	1	3.19			

^a Uncertainties are approximately $\pm 5\%$ for A_1 and A_2 , $\pm 5\%$ for τ_1 , $\pm 10\%$ for τ_2 , and $\pm 20\%$ for R_s .

TABLE 5-2: Fit Parameters and Surface Layer Thickness for Benzene-d₆ in Unmodified Pores^a

pore diameter (Å)	A_1	τ_1 (ps)	A_2	τ_2 (ps)	R_s (Å)
27	0.67	5.2	0.33	24.8	2.4
34	0.71	4.7	0.29	24.8	2.7
42	0.81	4.6	0.19	24.8	2.1
49	0.81	4.5	0.19	24.8	2.4
59	0.81	4.4	0.19	24.8	3.0
60	0.84	4.2	0.16	24.8	2.5
73	0.86	4.0	0.14	24.8	2.7
bulk	1	3.36			

^a Uncertainties are approximately $\pm 5\%$ for A_1 and A_2 , $\pm 5\%$ for τ_1 , $\pm 10\%$ for τ_2 , and $\pm 20\%$ for R_s .

TABLE 5-3: Fit Parameters and Surface Layer Thickness for Benzene in Modified Pores^a

pore diameter (Å)	A_1	τ_1 (ps)	A_2	τ_2 (ps)	R_s (Å)
24	0.69	5.0	0.31	20.6	2.3
34	0.79	4.5	0.21	20.6	1.9
42	0.85	4.0	0.15	20.6	1.6
59	0.85	4.0	0.15	20.6	2.3
60	0.87	3.8	0.13	20.6	1.9
73	0.91	3.8	0.09	20.6	1.6
bulk	1	3.19			

^a Uncertainties are approximately $\pm 5\%$ for A_1 and A_2 , $\pm 5\%$ for τ_1 , $\pm 10\%$ for τ_2 , and $\pm 20\%$ for R_s .

TABLE 5-4: Fit Parameters and Surface Layer Thickness for Benzene-d₆ in Modified Pores^a

pore diameter (Å)	A_1	τ_1 (ps)	A_2	τ_2 (ps)	R_s (Å)
27	0.72	4.8	0.28	19.6	2.0
34	0.76	4.2	0.24	19.6	2.2
42	0.87	4.3	0.13	19.6	1.5
49	0.85	4.0	0.15	19.6	1.9
59	0.85	4.0	0.15	19.6	2.2
60	0.89	4.0	0.11	19.6	1.7
73	0.91	3.8	0.09	19.6	1.7
bulk	1	3.36			

^a Uncertainties are approximately $\pm 5\%$ for A_1 and A_2 , $\pm 5\%$ for τ_1 , $\pm 10\%$ for τ_2 , and $\pm 20\%$ for R_s .

then estimate the thickness of the surface layer with retarded reorientational dynamics using the equation

$$R_s = R(1 - \sqrt{A_1}) \quad (5.1)$$

where R is the pore radius and R_s is the surface layer thickness. The derivation of this equation is in appendix 1. The values of R_s determined from this equation are given in Tables 5.1 and 5.2 and are plotted in Fig. 5.4 as a function of pore diameter for both liquids. Within the margin of error in determining R_s , it takes on the same value for both liquids regardless of pore size. The average value of these measurements is 2.5 Å, or about the thickness of one benzene molecule.

In Fig. 5.5 we illustrate typical effects of silanization of the pore surfaces on the dynamics of confined benzene and benzene-d₆ by comparing the OKE decays for the former liquid in unmodified and silanized pores with 34 Å diameters. Silanization does not lead to qualitative differences in the OKE decays beyond a modest rate enhancement. The decays can still be described well by the sum of two exponentials, one that with a decay time (τ_1) that is slightly larger than the bulk relaxation time and that increases with decreasing pore size and one with a decay time (τ_2) that is significantly larger than the bulk decay time and does not depend on pore size. The decay constants and normalized amplitudes for these fits are given in Tables 5.3 and 5.4. The values of τ_1 as a function of pore curvature are plotted for both liquids in Fig. 5.6. As in the case of the unmodified pores, this decay time depends roughly linearly on pore curvature. It is also worth noting that due to silanization, the true pore diameters must be somewhat smaller than the values

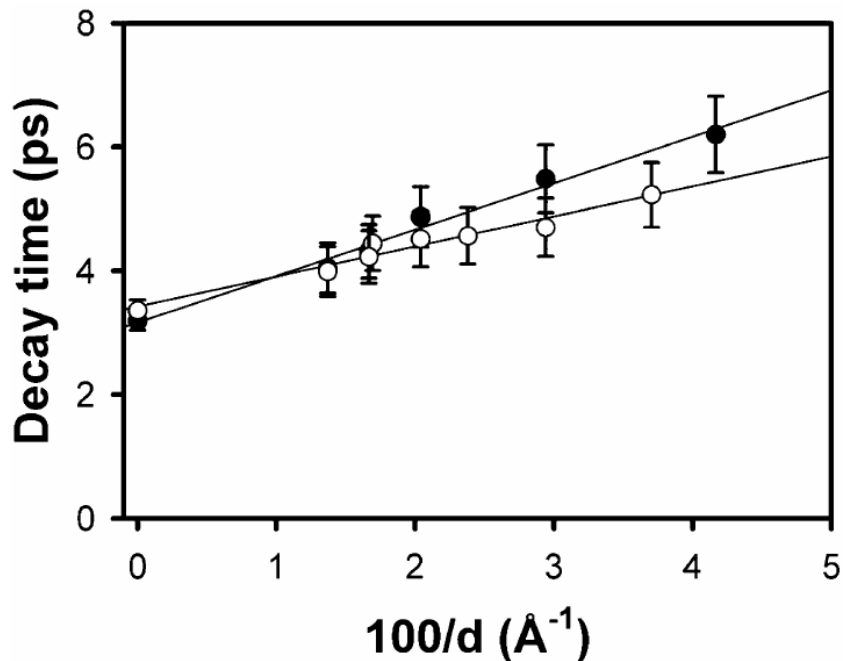


Figure 5.3. Fastest decay time (τ_1) as a function of the pore curvature (inverse of the pore diameter) for benzene (solid circles) and benzene- d_6 (open circles). The data points at zero curvature are for the bulk liquids, and the lines are linear least-squares fits to the data.

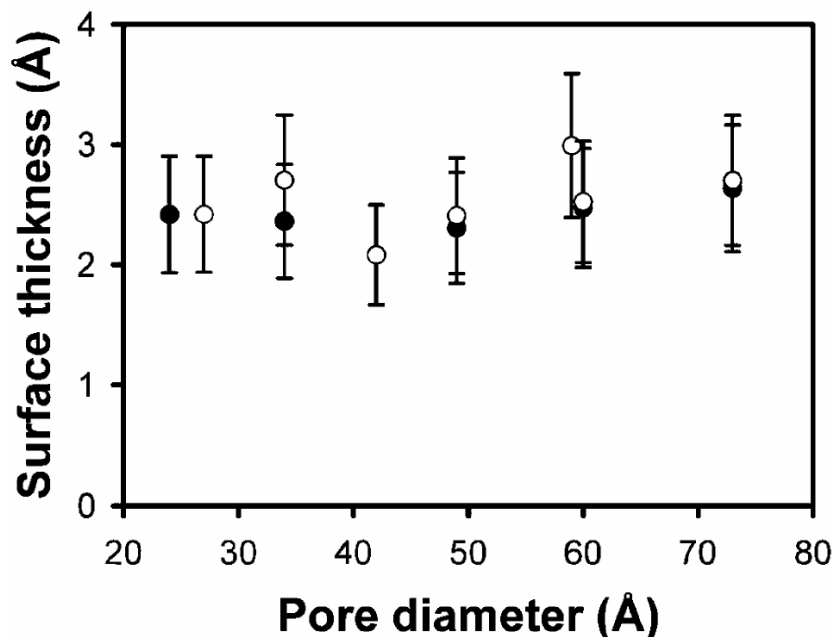


Figure 5.4. Calculated surface-layer thickness for benzene (solid circles) and benzene- d_6 (open circles) as a function of pore diameter.

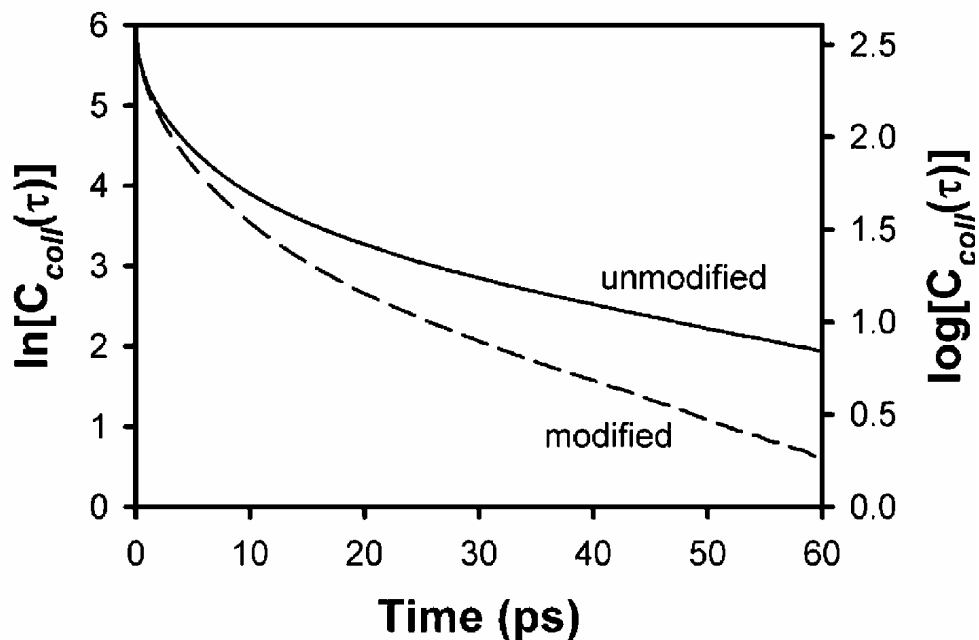


Figure 5.5. Representative OKE decays for benzene in 34-Å pores that are untreated (solid line) and that have surface methyl groups (dashed line).

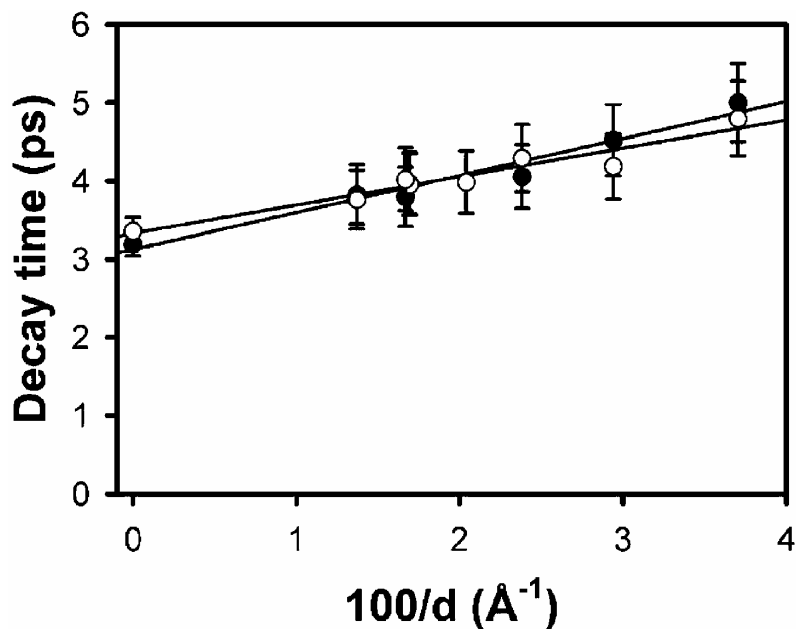


Figure 5.6. Fastest decay time (τ_1) as a function of the pore curvature (inverse of the pore diameter) for benzene (solid circles) and benzene- d_6 (open circles) in silanized pores. The data points at zero curvature are for the bulk liquids, and the lines are linear least-squares fits to the data.

given, which were measured in the untreated samples. Finally, the surface layer thickness is plotted as a function of pore size for both liquids in Fig. 5.7; in each case, the average value of the thickness is about 1.9 Å.

5.4. Discussion

The behavior of these liquids in unmodified pores differs from what we have observed previously for weakly-wetting liquids composed of rod-like molecules^{6,7,11,17} in at least two significant aspects. First, while there is a clear bulk-like component in the orientational dynamics of weakly-wetting confined liquids such as CS₂ and 2-butyne, no bulk-like component is observed in benzene or benzene-d₆. However, as can be seen in Fig. 5.3, τ_1 for benzene and benzene-d₆ varies linearly with pore curvature and is equal to the bulk relaxation time in the limit of zero curvature. Second, the surface relaxation of benzene and benzene-d₆ is, within the accuracy of our measurements, independent of pore size. This observation rules out any significant influence of the geometric effects that inhibit surface reorientation in weakly-wetting liquids such as CS₂ and 2-butyne. On the other hand, τ_2 is up to an order of magnitude greater than τ_1 , which is too large for an increase in the hydrodynamic volume for reorientation to be responsible for the retardation of orientational dynamics at pore surfaces. Undoubtedly much of the explanation for the differences between the dynamics of confined benzene and those of liquids such as CS₂ and 2-butyne lies in the fact that while benzene neither has a dipole moment nor can accept hydrogen bonds, it nevertheless wets silica surfaces strongly.

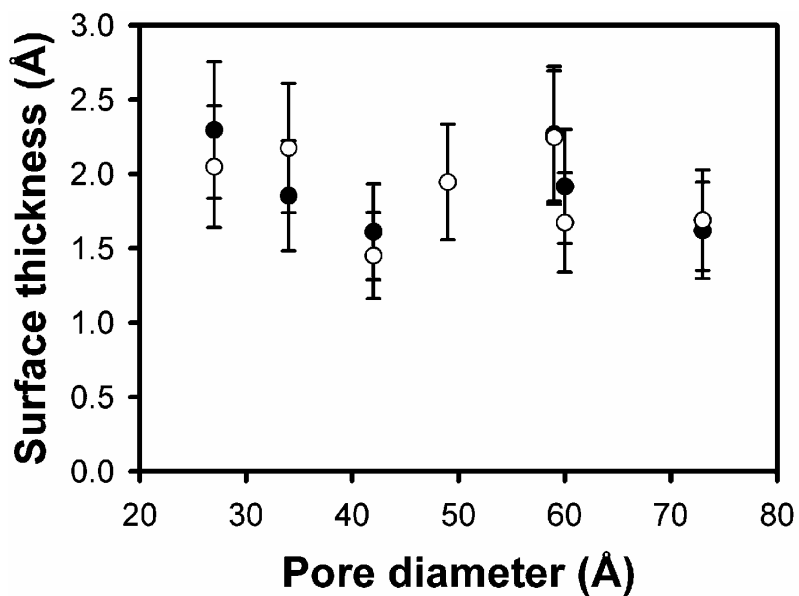


Figure 5.7. Calculated surface-layer thickness for benzene (solid circles) and benzene-*d*6 (open circles) as a function of pore diameter in silanized pores.

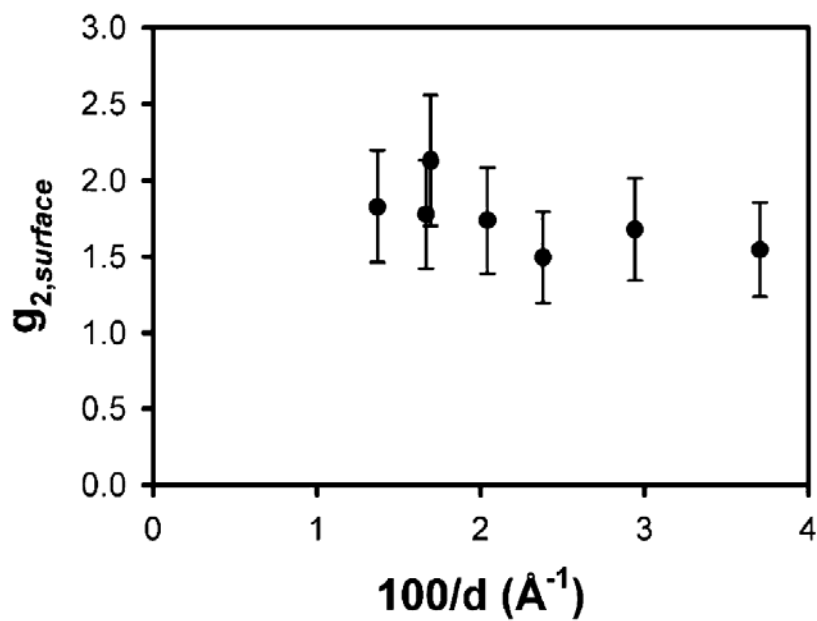


Figure 5.8. Estimated values of $g_{2,surface}$ as a function of pore curvature.

Indeed, the contact angle of benzene on glass is approximately 6° .³² The interactions between benzene and silica surfaces arise through a combination of electrostatic interactions (via the substantial quadrupole moment of benzene³³), dispersion interactions and cation- π interactions³⁴ with the protons of the surface hydroxyl groups (both of which rely on the sizable polarizability of benzene), all of which are likely to favor benzene lying flat on the pore surfaces. Thus, the relatively large surface reorientation times in all likelihood can be ascribed to the significant energy required to pull benzene off of the surfaces, rather than to geometric or hydrodynamic volume effects. This interpretation is further supported by the fact that the surface layer thickness is on the order of the thickness of a benzene molecule but is substantially less than its diameter.

Given that benzene wets silica strongly, it is appropriate to compare its dynamics in confinement to those of other strongly-wetting liquids. We have previously used OKE spectroscopy to study the orientational dynamics of acetonitrile and acetonitrile- d_3 confined in nanoporous glasses.^{8,12} The molecules of these liquids are able to accept hydrogen bonds from the surface hydroxyl groups of silica, and so wet the pore surfaces strongly. The OKE decays for these liquids are triexponential. The fastest of the three time constants matches that of the bulk liquid. The other two time constants are independent of pore size at a given temperature, although the relative amplitudes of the three exponentials do change with pore size. We have interpreted these results in terms of a bulk-like population of molecules in the pore centers and a population that experiences dynamic inhibition at the pore surfaces.^{8,12} We have been able to explain the data with a model in which exchange of molecules off of the pore surfaces into the bulk-like

population is an additional channel for surface relaxation. Roughly half of the molecules at the pore surfaces undergo orientational relaxation without exchanging, whereas the remaining surface molecules do exchange into the bulk. Deuterium exchange on the surface hydroxyl groups does not change the observed dynamics,¹² suggesting that the non-exchanging surface molecules are tethered by hydrogen bonds whereas the exchanging molecules are not.

There are two important differences between the dynamics of confined benzene and those of confined acetonitrile. First, benzene has no bulk-like relaxation component. Second, there is no sign of exchange of molecules off of the surface in the benzene data. The second of these differences can be explained by the differences in surface interactions between the two liquids. We believe that the orientational dynamics of acetonitrile molecules that are near, but not bound to, the pore surfaces are constrained by the dynamics of their neighbors that are bound to the surfaces. However, these unbound molecules are capable of exchanging into the bulk-like component of the liquid. The molecules that are bound to the surface, on the other hand, relax while remaining tethered to the surface. In the case of benzene, molecules that are lying flat on the surface cannot reorient about an axis in the plane of the disk (the only type of motion to which OKE spectroscopy is sensitive) without coming off of the surface. In this sense, reorientation and exchange of surface-bound molecules are essentially the same process.

The only liquid that we have studied previously that has not exhibited a bulk-like relaxation component in confinement is water.¹⁵ Even in pores with a diameter of 100 Å, there is no sign of bulklike relaxation in confined water. We believe that

nanoconfinement has such a profound effect on the orientational dynamics of water because this liquid is so highly networked. While a highly hydrogen bonded liquid such as water would not seem to be a good point of comparison for the data presented here, simulations and scattering data suggest that benzene is in fact a relatively highly ordered liquid.^{35,36} Due to the sizable quadrupole moment of the benzene molecules, they tend to form local T shaped structures.^{35,36} This motif is also observed in benzene crystals,³⁷ which feature a herring bone like pattern of molecules. Because molecules will tend to lie flat on the pore surfaces, the liquid structure may be disrupted significantly. Furthermore, the slow orientational dynamics of these surface molecules can exert an effect over large distances via this networked T structuring.

It is also worthy of note that the surface relaxation times of benzene and benzene-d₆ differ from one another significantly. Although benzene relaxes somewhat more quickly than does benzene-d₆ in the bulk (3.19 ps versus 3.36 ps at 293 K), the surface relaxation time for benzene is approximately 33 ps, while that of benzene-d₆ is approximately 25 ps. While the uncertainty in each surface relaxation time is on the order of $\pm 10\%$, it proved to be impossible to fit both the benzene and benzene-d₆ data with the same surface relaxation time, and so we are confident that this difference in surface relaxation times is real. We note also that the pore-size dependence of τ_1 for benzene-d₆ is somewhat milder than that for benzene.

The differences in the surface relaxation times of these two liquids are probably related to differences in surface energies on silica. Since C-D bonds are somewhat shorter than C-H bonds, both the polarizability and the quadrupole moment of benzene-d₆ are

slightly smaller than those of benzene. This leads to benzene-d₆ having a somewhat smaller surface tension than benzene,³⁸ and presumably also leads to benzene-d₆ having weaker interactions with the pore surfaces (it is difficult to measure any difference between the contact angles of the two liquids on silica as these angle are so small). The faster surface relaxation of benzene-d₆ can in turn lead to faster relaxation in the pore centers as compared to benzene as well.

We now turn to the dynamics of these liquids in modified pores. Benzene wets solid, saturated hydrocarbons well, and so could have interactions with the silanized surfaces that are comparable to those with unmodified silica surfaces. Indeed, contact angle measurements of benzene and benzene-d₆ on silanized cover slips revealed contact angles in the range of 13°, which is larger than the 6° contact angle on unmodified cover slips. This corresponds to enough of a difference in surface energy that the surface relaxation in modified pores is still much slower than in the bulk, although it is significantly faster than that in unmodified pores. As a result, the relaxation of the remaining confined molecules is faster than in unmodified pores as well. Furthermore, as shown by Fig. 5.7 the apparent surface layer thickness is markedly smaller after the pores have been modified. In addition, because modification makes the pore diameters smaller to some extent, the difference in surface layer thickness is probably even greater than what we have estimated. We can draw an analogy here to weakly-wetting liquids, in which we have also observed sub-monolayer populations of dynamically inhibited molecules. Our interpretation in these weakly-wetting systems is that only molecules that lie flat on the pore surfaces exhibit additional dynamic inhibition. This model would

suggest that benzene has less of a tendency to lie flat on silanized surfaces than on unmodified silica. In other words, the face of a benzene molecule is more “hydrophilic” and the edges are more “hydrophobic.” This idea could be tested with surface sum-frequency generation experiments.

It is also interesting to compare our results to those of Yi and Jonas,³⁹ who used Raman spectroscopy to study the dynamics of orientational diffusion of benzene-d₆ in the same type of monolithic porous glasses. The orientational correlation time measured in these experiments, τ_{Raman} , was also found to vary linearly with pore curvature.³⁹ Based on this linear fit, we have tabulated in Table 5.5 the values of τ_{Raman} that would be expected for the pore diameters used in our benzene-d₆ OKE experiments.

TABLE 5-5: Comparison of Raman and OKE Data for Benzene-d₆ in Unmodified Pores^a

pore diameter (Å)	τ_{Raman} (ps)	$\tau_{\text{Raman,corr}}$ (ps)	$\langle\tau_{\text{OKE}}\rangle$ (ps)	$\langle g_2 \rangle$	$g_{2,\text{surface}}$
27	4.9	8.7	11.6	1.3	1.5
34	4.3	7.6	10.6	1.4	1.7
42	3.9	6.8	8.4	1.2	1.5
49	3.6	6.3	8.3	1.3	1.7
59	3.3	5.8	8.4	1.4	2.1
60	3.3	5.8	7.5	1.3	1.8
73	3.0	5.4	6.9	1.3	1.8
bulk	1.9	3.36	3.36	1.0	

^a Uncertainties are approximately $\pm 5\%$ for τ_{Raman} and $\tau_{\text{Raman,corr}}$, $\pm 10\%$ for $\langle\tau_{\text{OKE}}\rangle$, $\pm 10\%$ for $\langle g_2 \rangle$, and $\pm 10\%$ for $g_{2,\text{surface}}$.

There are two important differences between the OKE and Raman measurements in this system. First, the Raman experiments were used to measure average orientational correlation times rather than the orientational correlation function, and so τ_{Raman} effectively averages over all of the dynamic environments in the pores. Second, while OKE experiments measure a collective orientational correlation time, Raman experiments measure a single-molecule orientational correlation time. Given a single dynamic population of molecules, these two times are related by⁴⁰

$$\tau_{\text{OKE}} = \frac{g_2}{j_2} \tau_{\text{Raman}} \quad (5.2)$$

where g_2 and j_2 are, respectively, the static and dynamic pair orientational correlation parameters. In liquids j_2 is generally believed to be unity,⁴⁰ and so g_2 is assumed to be the constant of proportionality between the OKE and Raman orientational correlation times. The static pair orientational correlation parameter can take on values of unity or greater, with larger values corresponding to a greater degree of parallel ordering among molecules in the liquid.

In benzene, g_2 takes on a value of approximately unity,^{23,41} which is presumably in part a result of the propensity of this liquid to form T-shaped structures.³⁶ Benzene-d₆ should have a value of g_2 that is similar to that of benzene, and yet the values of τ_{Raman} and τ_{OKE} for the bulk liquid differ considerably. If we assume that there is a systematic difference between the two, then we can calculate a corrected Raman correlation time $\tau_{\text{Raman,corr}}$ by multiplying τ_{Raman} by the ratio of τ_{OKE} to τ_{Raman} in the bulk liquid. The values of $\tau_{\text{Raman,corr}}$ for the different pore sizes are also listed in Table 5.5.

To compare our OKE data to the corrected Raman data, we compute an average OKE relaxation time $\langle\tau_{OKE}\rangle$ using

$$\langle\tau_{OKE}\rangle = A_1\tau_1 + A_2\tau_2 \quad (5.3)$$

This average value can in turn be used in conjunction with $\tau_{Raman,corr}$ to estimate the average value of the static pair orientational correlation parameter, $\langle g_2 \rangle$, for each pore size. Both $\langle\tau_{OKE}\rangle$ and $\langle g_2 \rangle$ are tabulated in Table 5.5. It can be seen from these results that $\langle g_2 \rangle$ takes on a value near 1.3 in confinement, which points to an increased degree of parallel alignment in the pores. However, there is little reason to believe that in the centers of the pores g_2 should differ significantly from its bulk value, particularly when the pore diameter is large. If we assume that g_2 can take on different values for the surface and bulk-like populations of confined molecules, then the corrected Raman correlation time can be written as:

$$\tau_{Raman,corr} = \frac{A_1\tau_1}{g_{2,bulklike}} + \frac{A_2\tau_2}{g_{2,surface}} \quad (5.4)$$

If we further assume that $g_{2,bulklike}$ is unity, then we find that

$$g_{2,surface} = \frac{A_2\tau_2}{\tau_{Raman,corr} - A_1\tau_1} \quad (5.5)$$

Values of $g_{2,surface}$ estimated in this manner are tabulated in Table 5.5.

The values of $g_{2,surface}$ suggest that there is significant parallel ordering of benzene-d₆ on the pore surfaces, which is consistent with the idea that the molecules tend to lie flat on the pore walls. This result is also in line with the results of previous experiments on confined acetonitrile.¹² It is apparent from these data that the degree of

surface ordering increases with increasing pore size, which at first might seem surprising. It is possible that the surface relaxation time does depend somewhat on pore curvature, but that the dependence is too subtle for us to detect without data of even higher quality. Any such dependence of τ_2 on pore curvature could not be great enough to account for the observed variation of $g_{2,surface}$, however. On the other hand, while the molecules may lie flat on the pore surfaces, since the surfaces themselves are not flat the surface molecules are not necessarily parallel to one another. Indeed, in more tightly curved pores it would be expected that there would be less parallel surface ordering. In Fig. 5.8 we plot the estimated value of $g_{2,surface}$ as a function of pore curvature. The dependence on pore curvature is roughly linear, and if we extend a linear fit out to zero curvature we find a value near 2. This extrapolation suggests that there is nearly perfect parallel alignment at a flat surface, which is consistent with benzene molecules lying flat on silica.

5.5. Conclusions

We have presented a detailed study of the orientational dynamics of benzene and benzene-d₆ confined in nanoporous glasses, both with silica surface and with silanized surfaces. In all cases the observed dynamics can be described well by the sum of two exponentials, one with a time constant that is somewhat longer than that for the bulk liquid and that depends on the pore size and the other with a much longer time constant that does not depend on pore size. We have assigned these two exponentials to bulk-like molecules in the pore centers and surface molecules, respectively. The slow surface relaxation is indicative of strong interactions between the liquid and the pore surfaces, which is consistent with the results of contact angle measurements. In the unmodified

pores, the surface layer has the thickness of about one benzene molecule, which suggests that the benzene molecules lie flat on the pore surfaces. Comparison with Raman data supports this picture. Although benzene is not a networked liquid, in the centers of the pores its reorientational dynamics are still strongly influenced by confinement, which is reminiscent of what we have seen in confined water and suggests that benzene retains strong ordering in the nanopores. It will be of great interest to extend these studies to other confined aromatic systems and to make further comparisons with single-molecule orientational data.

Chapter 5 References and Notes

- (1) Drake, J. M.; Klafter, J., Eds.; *Molecular Dynamics in Restricted Geometries*; Wiley: New York, **1989**.
- (2) Drake, J. M.; Klafter, J.; Kopelman, R.; Awschalom, D.D., Eds.; *Dynamics in Small Confining Systems*; Materials Research Society: Pittsburgh, **1993**; Vol. 290, pp 377.
- (3) Drake, J. M.; Klafter, J.; Kopelman, R.; Troian, S. M., Eds.; *Dynamics in Small Confining Systems II*; Materials Research Society: Pittsburgh, **1995**; Vol. 366, pp 466.
- (4) Drake, J. M.; Klafter, J.; Kopelman, R., Eds. *Dynamics in Small Confining Systems III*; Materials Research Society: Pittsburgh, **1997**; Vol. 464, pp 388.
- (5) Drake, J. M.; Grest, G. S.; Klafter, J.; Kopelman, R., Eds.; *Dynamics in Small Confining Systems IV*; Materials Research Society: Warrendale, PA, **1999**; Vol. 543, pp 372.
- (6) Farrer, R. A.; Loughnane, B. J.; Fourkas, J. T. *J. Phys. Chem. A* **1997**, 101, 4005.
- (7) Drake, J. M., Klafter, J., Kopelman, R., Eds.; Temperature-Dependent Dynamics of Microconfined CS₂. In *Dynamics in Small Confining Systems III*; Materials Research Society: Pittsburgh, **1997**; Vol. 464; pp 263.
- (8) Loughnane, B. J.; Farrer, R. A.; Fourkas, J. T. *J. Phys. Chem. B* 1998, 102, 5409.
- (9) Loughnane, B. J.; Fourkas, J. T. *J. Phys. Chem. B* **1998**, 102, 10288.
- (10) Loughnane, B. J.; Farrer, R. A.; Fourkas, J. T. Rotational Diffusion of Microconfined Liquids. In *Dynamics in Small Confining Systems IV*; Materials Research Society: Pittsburgh, **1999**; pp 33.
- (11) Loughnane, B. J.; Scodinu, A.; Fourkas, J. T. *J. Phys. Chem. B* **1999**, 103, 6061.
- (12) Loughnane, B. J.; Farrer, R. A.; Scodinu, A.; Fourkas, J. T. *J. Chem. Phys.* **1999**, 111, 5116.
- (13) Loughnane, B. J.; Scodinu, A.; Fourkas, J. T. *Chem. Phys.* **2000**, 253, 323.
- (14) Loughnane, B. J.; Farrer, R. A.; Scodinu, A.; Reilly, T.; Fourkas, J. T. *J. Phys. Chem. B* **2000**, 104, 5421.
- (15) Scodinu, A.; Fourkas, J. T. *J. Phys. Chem. B* **2002**, 106, 10292.
- (16) Farrer, R. A.; Fourkas, J. T. *Acc. Chem. Res.* **2003**, 36, 605.
- (17) Scodinu, A.; Farrer, R. A.; Fourkas, J. T. *J. Phys. Chem. B* **2002**, 106, 12863.
- (18) Brinker, C. J.; Scherer, G. W. *Sol-Gel Science: The Physics and Chemistry of Sol-Gel Processing*; Academic Press: San Diego, CA, **1990**.
- (19) Majors, R. E.; Hopper, M. J. *J. Chromat. Sci.* **1974**, 12, 767.
- (20) Righini, R. *Science* **1993**, 262, 1386.
- (21) Fourkas, J. T. Nonresonant Intermolecular Spectroscopy of Liquids. In *Ultrafast Infrared and Raman Spectroscopy*; Fayer, M. D., Ed.; Marcel Dekker: New York, **2001**; Vol. 26; pp 473.
- (22) Kinoshita, S.; Kai, Y.; Ariyoshi, T.; Shimada, Y. *Int. J. Mod. Phys. B* **1996**, 10, 1229.
- (23) Loughnane, B. J.; Scodinu, A.; Farrer, R. A.; Fourkas, J. T.; Mohanty, U. *J. Chem. Phys.* **1999**, 111, 2686.

- (24) McMorow, D.; Lotshaw, W. T. *J. Phys. Chem.* **1991**, 95, 10395.
- (25) Chang, Y. J.; Castner Jr., E. W. *J. Phys. Chem.* **1996**, 100, 3330.
- (26) Neelakandan, M.; Pant, D.; Quitevis, E. L. *Chem. Phys. Lett.* **1997**, 265, 283.
- (27) Ricci, M.; Bartolini, P.; Chelli, R.; Cardini, G.; Califano, S.; Righini, R. *Phys. Chem. Chem. Phys.* **2001**, 3, 2795.
- (28) Chelli, R.; Cardini, G.; Ricci, M.; Bartolini, P.; Righini, R.; Califano, S. *Phys. Chem. Chem. Phys.* **2001**, 3, 2803.
- (29) Ratajska-Gadomska, B.; Gadomski, W.; Wiewior, P.; Radzewicz, C. *J. Chem. Phys.* **1998**, 108, 8489.
- (30) Ricci, M.; Wiebel, S.; Bartolini, P.; Taschin, A.; Torre, R. *Philosoph. Mag.* **2004**, 84, 1491.
- (31) Berne, B. J.; Pecora, R. *Dynamic Light Scattering*; Wiley: New York, **1976**.
- (32) Irons, E. *J. Philosoph. Mag.* **1943**, 34, 614.
- (33) Battaglia, M. R.; Buckingham, A. D.; Williams, J. H. *Chem. Phys. Lett.* **1981**, 78, 421.
- (34) Ma, J. C.; Dougherty, D. A. *Chem. Rev.* **1997**, 97, 1303.
- (35) Narten, A. H. *J. Chem. Phys.* **1977**, 67, 2102.
- (36) Cabaco, M. I.; Danten, Y.; Besnard, M.; Guissani, Y.; Guillot, B. *J. Phys. Chem. B* **1997**, 101, 6977.
- (37) Bacon, G. E.; Curry, N. A.; Wilson, S. A. *Proceeding of the Royal Society (London) Series A* **1964**, 279, 98.
- (38) Gaines, G. L., Jr.; Le Grand, D. G. *Colloids and Surfaces, A: Physicochemical and Engineering Aspects* **1994**, 82, 299.
- (39) Yi, J.; Jonas, J. *J. Phys. Chem.* **1996**, 100, 16789.
- (40) Kivelson, D.; Madden, P. A. *Annu. Rev. Phys. Chem.* **1980**, 31, 523.
- (41) Madden, P. A.; Battaglia, M. R.; Cox, T. I.; Pierens, R. K.; Champion, J. *Chem. Phys. Lett.* **1980**, 76, 604.
- (42) Zhu, X.; Farrer, R.A.; Fourkas, J. T. *J. Phys. Chem. B* **2005**, 109, 12724

Chapter 6

Orientalional diffusion of *n*-alkyl cyanides

6.1. Introduction

Ultrafast optical Kerr effect spectroscopy has been used to study the temperature-dependent orientational dynamics of a series of nitriles with *n*-alkyl chains ranging from one to 11 carbons in length. In all cases the orientational diffusion is found to be described by a single-exponential decay. Analysis of the orientational correlation times using the Debye–Stokes–Einstein equation suggests that the molecules adopt extended configurations and reorient as rigid rods. The liquids with shorter alkyl chains undergo an apparent ordering transition as they are cooled.

The determination of diffusion constants is a powerful means of gaining microscopic information about the structure and dynamics of liquids. Both translational and orientational diffusion constants are capable of providing detailed insights into microscopic properties such as local viscosity, molecular association, local structure, and even molecular structure. Here we present detailed studies of orientational diffusion in liquid *n*-alkyl cyanides. Linear alkyl cyanides have been used widely in the study of dynamics in solution, due to the smooth variation of their physical properties with chain length.^{1–7} Despite the ubiquity of these solvents, little is known regarding their microscopic structure in the liquid phase. Tools such as neutron scattering, x-ray scattering, and molecular dynamics simulation, which are commonly used to study such

microscopic structure, have not been applied to *n*-alkyl cyanides to a significant extent. Indeed, while methyl cyanide (acetonitrile), ethyl cyanide (propionitrile) and propyl cyanide (butyronitrile) have been studied using x-ray scattering,⁸ to our knowledge no experiments have been performed to determine the liquid structure of any of the *n*-alkyl cyanides with longer alkane chains. Linear alkanes are well known to display a relatively high degree of ordering in the liquid phase.^{9–11} While short-chain alkanes show little ordering, as the chain length increases there is a tendency for molecules to adopt an extended conformation and to exhibit local parallel ordering, with some differences being observed between alkanes with odd and even numbers of carbon atoms.^{9–11} As the chains grow longer still, the molecular conformations become less extended, and local ordering decreases.^{9–11} Our goal here is to address these same microscopic structural issues in *n*-alkyl cyanides. These liquids are not subject to the hydrogen-bonding interactions that contribute to the structure of liquids such as straight-chain alcohols and straight-chain carboxylic acids. However, cyanide groups are highly polar, and so dipole–dipole interactions would be expected to contribute significantly to local structuring in *n*-alkyl cyanides. For short-chain alkyl cyanides these interactions would be expected to dominate the local structure, but as the alkyl chain lengthens the microscopic structure might be expected to approach that of *n*-alkanes. Our technique for studying these issues is ultrafast optical Kerr effect spectroscopy.^{12–15} We present the results of OKE experiments on *n*-alkyl cyanides over a broad range of temperatures; these experiments have allowed us to develop a microscopic picture of the structure of these liquids and

have revealed the possibility of an ordering transition in the alkyl cyanides with shorter alkyl chains at the lower end of their liquid temperature range.

6.2. Experiment

Our experimental apparatus and data collection procedure for optical heterodyne detected OKE spectroscopy have been described in detail in chapter 2. Our results for methyl cyanide are taken from a previous publication.¹⁸ Samples of all of the other n-alkyl cyanides (ethyl cyanide to undecyl cyanide) were used as received. A complete list of the liquids studied and relevant physical parameters is given in table 6-1. Each liquid was placed in a 2 mm path-length cuvette, which was subsequently capped and sealed with vacuum epoxy. The cell was mounted on the cold finger of a nitrogen-flow vacuum cryostat. A temperature probe was placed directly on the face of the cuvette, near the point where data were obtained, so that the temperature could be measured and maintained accurately at this position. Data were obtained for each liquid over a broad range of temperatures, and the temperature of each sample was allowed to equilibrate for at least 30 min before any data were collected. Typically, at least ten OKE decays were recorded for each liquid, half at a small positive heterodyne angle and half at the equivalent negative heterodyne angle. The data for each angle were averaged, and then the averaged data for the opposite angles were subtracted from one another to obtain the pure heterodyne contribution to the signal. The final data sets were then integrated with respect to time to obtain the collective orientational correlation function, $C_{\text{coll}}(\tau)$,¹⁹ the constant of integration was set by ensuring that the long-time decay was exponential, in

good agreement with the unintegrated data. The integrated data were fitted to the sum of two exponentials using a nonlinear least-squares fitting routine.²⁰ The fits began at a time (typically on the order of 5 ps) great enough that the peak from the intermolecular response had decayed to a negligible value. Viscosities were obtained from.²¹

Table 6-1. Melting points, boiling points, and slopes of Debye–Stokes–Einstein plots for the liquids studied here.

Liquid	T_m (K)	T_b (K)	Slope 1 (ns K cP ⁻¹)	Slope 2 (ns K cP ⁻¹)
Methyl cyanide	225	354	1.13(6)	
Ethyl cyanide	180	370	1.66(9)	0.81(8)
Propyl cyanide	161	388	2.1(1)	1.2(1)
Butyl cyanide	177	412	3.0(2)	1.6(2)
Pentyl cyanide	193	437	5.9(3)	2.8(3)
Hexyl cyanide	209	459	6.3(6)	
Heptyl cyanide	228	471	7.1(6)	4.4(4)
Octyl cyanide	239	497	8.9(8)	5.4(6)
Nonyl cyanide	255	517	12(1)	
Decyl cyanide		538	16(1)	
Undecyl cyanide		543	19(2)	

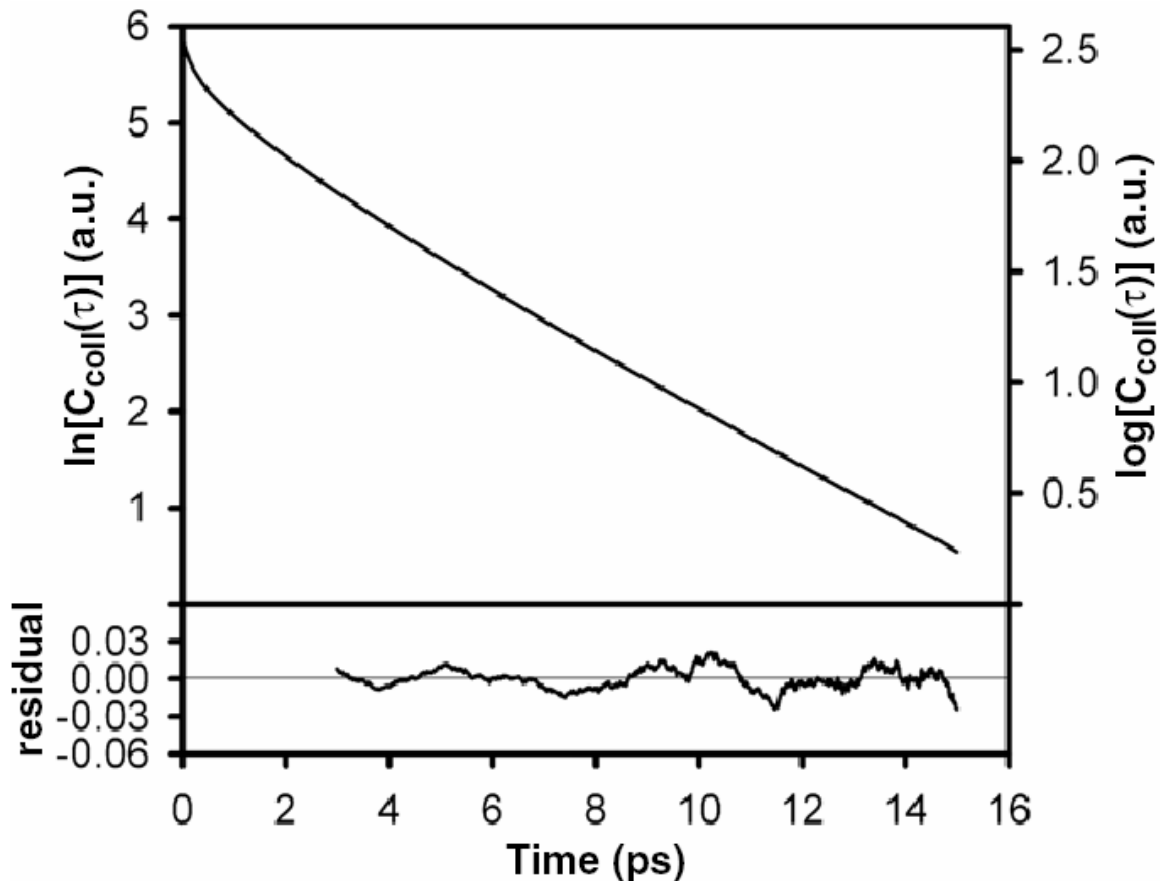


Figure 6.1. Collective orientational correlation function (solid line) and biexponential fit (dotted line) for butyl cyanide at 366.5 K. The lower panel shows the residual derived by subtracting the fit from the data.

6.3. Results

Shown in figure 6.1 is the logarithm of a typical $C_{\text{coll}}(\tau)$ derived from an OKE decay, in this case for n-butyl cyanide at a temperature of 366.5K, along with a fit to the sum of two exponentials. The quality of the fit is excellent, as can be seen from the flatness of the residual plot. The time constant of the more slowly decaying exponential, τ_1 , is 3.48 ps. The time constant of the other exponential, τ_2 , is 1.74 ps. The collective

orientational correlation functions for this liquid at other temperatures, shown in figure 6.2, are fitted equally well by the sum of two exponentials. As would be expected, the time constants of these exponentials increase as the temperature is lowered. These results are representative of those observed for each liquid studied here; in every case the collective orientational correlation function is fitted well by the sum of two exponentials. The fit parameters for all of the liquids are summarized in tables 6-2 to 6-11.

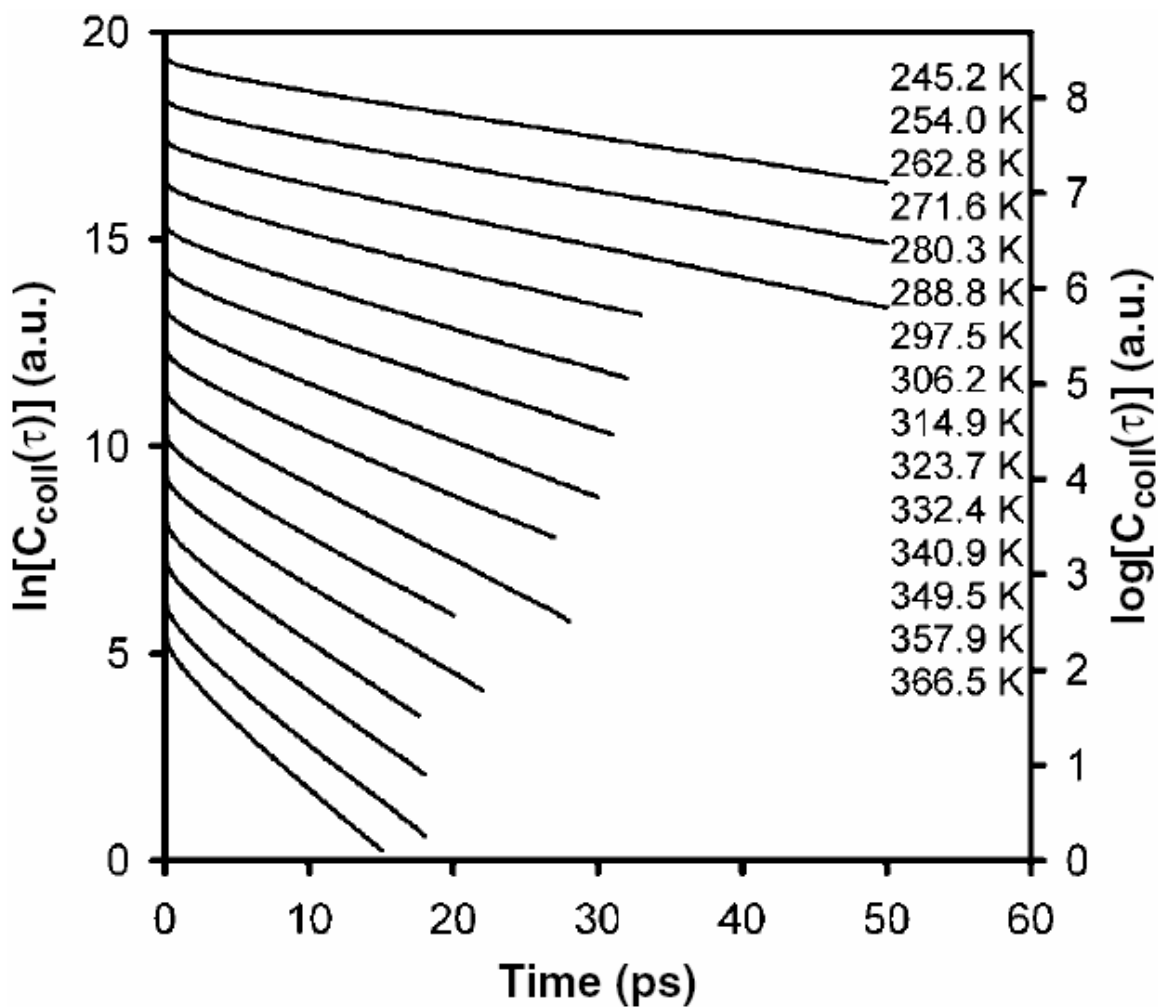


Figure 6.2. Collective orientational correlation functions for butyl cyanide as a function of temperature.

Table 6-2. Normalized amplitudes and decay times for biexponential fits to $C_{\text{coll}}(\tau)$ for ethylcyanide as a function of temperature.

T (K)	A_1	τ_1 (ps)	A_2	τ_2 (ps)
174.3	0.67(7)	45(2)	0.33(7)	15(6)
179.8	0.78(4)	33(2)	0.22(4)	11(3)
186.1	0.84(3)	21.6(7)	0.16(3)	5.6(9)
193.3	0.84(2)	16.9(3)	0.16(2)	4.3(4)
200.6	0.82(2)	14.3(3)	0.18(2)	4.5(4)
209.3	0.80(1)	11.6(2)	0.20(1)	4.3(3)
220.8	0.78(2)	10.3(2)	0.22(2)	3.9(4)
221.4	0.75(2)	10.4(2)	0.25(2)	4.4(5)
237.3	0.78(2)	7.2(1)	0.22(2)	2.8(2)
255.4	0.77(2)	5.1(1)	0.23(2)	2.0(2)
272.4	0.70(2)	4.05(7)	0.30(2)	2.0(2)
289.0	0.71(1)	3.16(5)	0.29(1)	1.6(1)
304.9	0.77(3)	2.48(8)	0.23(3)	1.1(2)
321.2	0.57(8)	2.24(3)	0.43(8)	1.4(1)
337.4	0.57(2)	1.90(7)	0.43(2)	1.2(2)
357.4	0.65(3)	1.49(6)	0.35(3)	0.9(2)

6.4. Discussion

Alkyl cyanides are composed of two portions with quite distinct properties. Although the cyanide groups do not hydrogen bond with one another, they are highly polar and

Table 6-3. Normalized amplitudes and decay times for biexponential fits to $C_{\text{coll}}(\tau)$ for propyl cyanide as a function of temperature.

T (K)	A_1	τ_1 (ps)	A_2	τ_2 (ps)
175.7	0.83(11)	85(9)	0.17(11)	19(10)
182.4	0.83(7)	60(4)	0.17(7)	14(4)
196.4	0.81(5)	35(2)	0.19(5)	10(2)
209.5	0.83(4)	23(1)	0.17(4)	5(1)
219.6	0.81(3)	17.8(7)	0.19(3)	5.1(7)
242.1	0.73(4)	11.8(9)	0.27(4)	4.5(9)
258.1	0.59(3)	8.9(9)	0.41(3)	4.7(9)
273.9	0.77(2)	6.0(3)	0.23(2)	2.1(3)
289.2	0.76(2)	4.8(2)	0.24(2)	1.8(2)
296.7	0.71(2)	4.5(2)	0.29(2)	1.9(2)
313.3	0.71(2)	3.7(2)	0.29(2)	1.7(2)
330.0	0.71(2)	3.0(2)	0.29(2)	1.5(2)
346.0	0.70(2)	2.5(1)	0.30(2)	1.0(1)
362.0	0.62(1)	2.23(8)	0.38(1)	1.14(8)
368.0	0.68(1)	2.05(7)	0.32(1)	1.00(7)

Table 6-4. Normalized amplitudes and decay times for biexponential fits to $C_{\text{coll}}(\tau)$ for butyl cyanide as a function of temperature.

T (K)	A_1	τ_1 (ps)	A_2	τ_2 (ps)
245.2	0.86(6)	18(1)	0.14(6)	4(1)
254.0	0.83(2)	16.0(3)	0.17(2)	4.4(4)
262.8	0.79(3)	13.7(6)	0.21(3)	4.5(6)
271.6	0.63(2)	12.8(8)	0.37(2)	5.7(8)
280.3	0.67(2)	10.4(7)	0.33(2)	5.0(7)
288.8	0.73(2)	8.8(4)	0.27(2)	3.8(4)
297.5	0.75(3)	7.4(5)	0.25(3)	3.4(5)
306.2	0.65(1)	7.0(2)	0.35(1)	3.6(3)
314.9	0.76(2)	5.5(2)	0.24(2)	1.8(6)
323.7	0.65(2)	5.5(3)	0.35(2)	2.8(5)
332.4	0.68(2)	4.8(2)	0.32(2)	2.1(2)
340.9	0.68(1)	4.3(2)	0.32(1)	1.9(2)
349.5	0.57(2)	4.1(3)	0.43(2)	2.1(3)
357.9	0.57(2)	3.8(2)	0.43(2)	1.9(2)
366.5	0.57(2)	3.5(3)	0.43(2)	2.0(3)

Table 6-5. Normalized amplitudes and decay times for biexponential fits to $C_{\text{coll}}(\tau)$ for pentyl cyanide as a function of temperature.

T (K)	A_1	τ_1 (ps)	A_2	τ_2 (ps)
231.5	0.77(7)	64(5)	0.23(7)	16(6)
253.3	0.66(4)	41(2)	0.34(4)	14(4)
271.1	0.76(3)	22.1(7)	0.24(3)	6(1)
288.9	0.78(2)	16.6(4)	0.22(2)	4.2(5)
297.3	0.65(6)	16(1)	0.35(6)	6(2)
305.7	0.64(4)	13.5(7)	0.36(4)	5(1)
314.1	0.70(2)	10.9(2)	0.30(2)	3.5(4)
323.8	0.73(3)	8.8(3)	0.27(3)	3.5(7)
341.3	0.73(3)	6.8(2)	0.27(3)	2.5(4)

Table 6-6. Normalized amplitudes and decay times for biexponential fits to $C_{\text{coll}}(\tau)$ for hexyl cyanide as a function of temperature.

T (K)	A_1	τ_1 (ps)	A_2	τ_2 (ps)
262.4	0.76(14)	57(9)	0.24(14)	11(5)
271.3	0.80(11)	39(5)	0.20(11)	9(5)
280.2	0.70(6)	36(2)	0.30(6)	10(3)
289.2	0.65(4)	31(2)	0.35(4)	10(3)
297.4	0.75(7)	22(2)	0.25(7)	6(2)
305.8	0.74(6)	19(1)	0.26(6)	5(2)
314.3	0.75(6)	16(1)	0.25(6)	4(1)
322.9	0.73(8)	14(1)	0.27(8)	4(1)
331.5	0.75(7)	11.4(9)	0.25(7)	3(1)
340.0	0.73(6)	10.5(7)	0.27(6)	2.7(9)
348.4	0.70(6)	9.3(6)	0.30(6)	2.6(8)
356.9	0.68(6)	8.7(6)	0.32(6)	2.6(9)

Table 6-7. Normalized amplitudes and decay times for biexponential fits to $C_{\text{coll}}(\tau)$ for heptyl cyanide as a function of temperature.

T (K)	A_1	τ_1 (ps)	A_2	τ_2 (ps)
249.3	0.87(10)	97(10)	0.13(10)	16(8)
254.7	0.84(10)	84(8)	0.16(10)	12(6)
272.0	0.83(15)	56(6)	0.17(15)	11(6)
280.4	0.79(6)	47(3)	0.21(6)	10(3)
289.3	0.72(6)	42(3)	0.28(6)	11(4)
296.6	0.73(4)	36(2)	0.27(4)	8(2)
304.2	0.75(9)	29(3)	0.25(9)	7(3)
311.6	0.77(10)	24(2)	0.23(10)	5(2)
319.3	0.74(7)	21(2)	0.26(7)	5(2)
326.8	0.73(6)	18(1)	0.27(6)	4(1)
341.7	0.72(5)	14.2(8)	0.28(5)	4(1)
349.0	0.70(7)	13(1)	0.30(7)	3(1)

Table 6-8. Normalized amplitudes and decay times for biexponential fits to $C_{\text{coll}}(\tau)$ for octyl cyanide as a function of temperature.

T (K)	A_1	τ_1 (ps)	A_2	τ_2 (ps)
243.2	0.83(16)	220(48)	0.17(16)	33(16)
250.8	0.82(12)	184(31)	0.18(12)	29(12)
266.6	0.74(12)	118(14)	0.26(12)	20(12)
278.1	0.72(12)	97(12)	0.28(12)	19(12)
289.3	0.76(8)	67(6)	0.24(8)	14(6)
304.1	0.74(5)	55(4)	0.26(5)	11(3)
321.5	0.79(5)	31(2)	0.21(5)	6(2)
337.3	0.71(3)	26.7(7)	0.29(3)	8(1)
352.1	0.73(4)	21(1)	0.27(4)	5(1)
367.1	0.72(5)	18(1)	0.28(5)	4(1)
382.0	0.66(3)	17.2(6)	0.34(3)	4.9(8)

Table 6-9. Normalized amplitudes and decay times for biexponential fits to $C_{\text{coll}}(\tau)$ for nonylcyanide as a function of temperature.

T (K)	A_1	τ_1 (ps)	A_2	τ_2 (ps)
297.1	0.78(9)	110(11)	0.22(9)	16(8)
311.0	0.68(8)	84(8)	0.32(8)	19(9)
314.0	0.73(11)	70(19)	0.27(11)	11(6)
319.7	0.72(10)	63(7)	0.28(10)	14(7)
322.7	0.74(5)	55(3)	0.26(5)	12(3)
331.3	0.71(9)	48(5)	0.29(9)	9(3)
341.6	0.72(8)	39(4)	0.28(8)	9(4)
348.5	0.73(11)	34(7)	0.27(11)	7(3)
350.1	0.71(4)	36(2)	0.29(4)	8(2)
358.6	0.76(8)	26(3)	0.24(8)	5(2)

Table 6-10. Normalized amplitudes and decay times for biexponential fits to $C_{\text{coll}}(\tau)$ for decylcyanide as a function of temperature.

T (K)	A_1	τ_1 (ps)	A_2	τ_2 (ps)
288.9	0.74(6)	191(13)	0.26(6)	30(10)
297.0	0.73(11)	152(19)	0.27(11)	26(10)
305.4	0.77(5)	112(6)	0.23(5)	16(4)
313.7	0.76(5)	92(5)	0.24(5)	17(4)
322.2	0.75(2)	74(2)	0.25(2)	15(2)
330.7	0.78(3)	61(2)	0.22(3)	11(2)
339.2	0.75(4)	51(2)	0.25(4)	9(2)
347.8	0.75(5)	45(2)	0.25(5)	8(2)
356.3	0.74(8)	39(5)	0.26(8)	7(3)
364.6	0.76(6)	32(2)	0.24(6)	7(2)

Table 6-11. Normalized amplitudes and decay times for biexponential fits to $C_{\text{coll}}(\tau)$ for undecyl cyanide as a function of temperature.

T (K)	A_1	τ_1 (ps)	A_2	τ_2 (ps)
314.1	0.75(8)	140(12)	0.25(8)	23(10)
322.5	0.77(4)	106(5)	0.23(4)	18(4)
331.0	0.77(5)	87(5)	0.23(5)	13(4)
339.4	0.76(8)	71(7)	0.24(8)	12(5)
347.8	0.78(4)	59(3)	0.22(4)	10(2)
356.3	0.77(4)	46(2)	0.23(4)	7(1)
372.7	0.77(4)	36(1)	0.23(4)	7(1)

interact relatively strongly with one another. The alkyl tails interact with one another through weak dispersion interactions, but as the chain length is increased these interactions become increasingly important in the liquid. The relative importance of these two types of interactions, as well as the cross interactions between the two moieties, is crucial in determining how the alkyl chain length influences the microscopic properties of the liquid. We begin by considering the origin of the two exponentials used to fit the collective orientational correlation functions in these liquids. For a liquid composed of linear or symmetric-top molecules, orientational diffusion is expected to result in a single-exponential decay in the OKE signal.²² This is indeed what is generally observed

in such liquids. However, a second, faster exponential decay is also commonly observed in these liquids,^{16, 18, 23–29} even though only a single orientational diffusion time should exist. We have previously performed detailed, temperature-dependent OKE studies of a number of linear and symmetric-top liquids, including methyl cyanide, to study the behaviour of this component of the relaxation (which is often called the intermediate decay in the OKE literature).¹⁸ We have found that the intermediate decay time in these liquids generally scales with viscosity over temperature, suggesting a hydrodynamic origin, and is a factor of three to six faster than the contribution from orientational diffusion.¹⁸ The physical origin of the intermediate decay remains a topic of debate, but this relaxation component is a ubiquitous feature of the OKE decay in simple liquids.

The biexponential nature of all of the OKE decays presented here is highly reminiscent of the behaviour of linear and symmetric-top liquids, suggesting that τ_1 is the time constant for collective orientational diffusion and τ_2 is the time constant for the intermediate decay. Before making such an assignment, however, we must note that the OKE spectroscopy of the liquids studied here has the potential to be considerably more complex than that of linear molecules or symmetric tops. While n-alkyl cyanides are roughly linear, the majority of the polarizability of these molecules is associated with the cyanide moieties, which are not collinear with the alkyl chains (except in the case of methyl cyanide). As a result, even if the molecules were to reorient as rigid rods, the diffusion tensor and the polarizability tensor do not share the same principal axis system, which could lead to decays that are described by as many as five exponentials.²² Given the conformational freedom of these molecules, the decays could be more complex still.

There is no direct experimental evidence from previous studies that these molecules adopt a fully extended conformation in the liquid phase, although this is a reasonable hypothesis based upon analogies with straight chain alkanes and related molecules.⁹⁻¹¹ Even if the molecules are fully extended it is not clear that they would reorient in a rod-like manner. Given long enough alkyl chains, the local orientational dynamics of a cyanide group should differ from the overall orientational dynamics of its parent molecule, with the limiting case being a cyanide group at the end of a long polyethylene molecule. Based on these considerations, it is therefore possible that both τ_1 and τ_2 reflect diffusive orientational dynamics.

While there is no absolute means of determining from our OKE data whether τ_2 arises from orientational diffusion or is a manifestation of the intermediate decay, the relationship between τ_1 and τ_2 can give us a basis for favouring one of these two possibilities. When multiple exponentials appear in the collective orientational correlation function, individual exponentials generally cannot be assigned to diffusion about particular axes.²² Nevertheless, the relationships among the time constants of these exponentials should be connected to the aspect ratio of the liquid molecules. Thus, if both exponentials arise from orientational diffusion, we would expect their relationship to be very different in going from ethyl cyanide to undecyl cyanide. On the other hand, we have found for liquids composed of linear molecules or symmetric tops that the collective orientational correlation time and the intermediate decay time generally scale with one another.¹⁸ In figure 6.3 we plot τ_2 versus τ_1 for all of the OKE decays for all of the liquids studied here, as well as for methyl cyanide. Within the uncertainty of our measurements,

all of these data fall on a single straight line, which strongly suggests that τ_2 does reflect the same intermediate decay as observed in liquids composed of simpler molecules.

While it is somewhat surprising that even long-chain alkyl cyanides should exhibit single exponential orientational diffusion in OKE data, this behavior has significant precedent in other types of molecules. For instance, single-exponential OKE decays have also been observed in liquids composed of disk-like molecules with single substituents that should break the symmetry of the diffusion tensor and lead to multiple exponentials in the OKE decays.^{23, 29, 30} In addition, as mentioned above, the polarizability of the molecules studied here is highly localized on the cyanide groups. For the molecules with short alkyl chains, the OKE decays must reflect the orientational dynamics of the entire molecules. On the other hand, for longer alkyl chains the OKE decays may reflect only the cyanide orientational dynamics rather than the overall orientational dynamics of the molecules. The fact that similar behavior is seen for all of the liquids studied here suggests that we are observing the dynamics of the entire molecules in all of the liquids studied here, but this argument on its own is not conclusive.

Orientalional diffusion of molecules in simple liquids generally follows the Debye–Stokes–Einstein (DSE) relation:

$$\tau \propto \frac{\eta V_H}{k_B T} \quad (6.1)$$

where τ is the orientational correlation time, η is the viscosity, V_H is the hydrodynamic

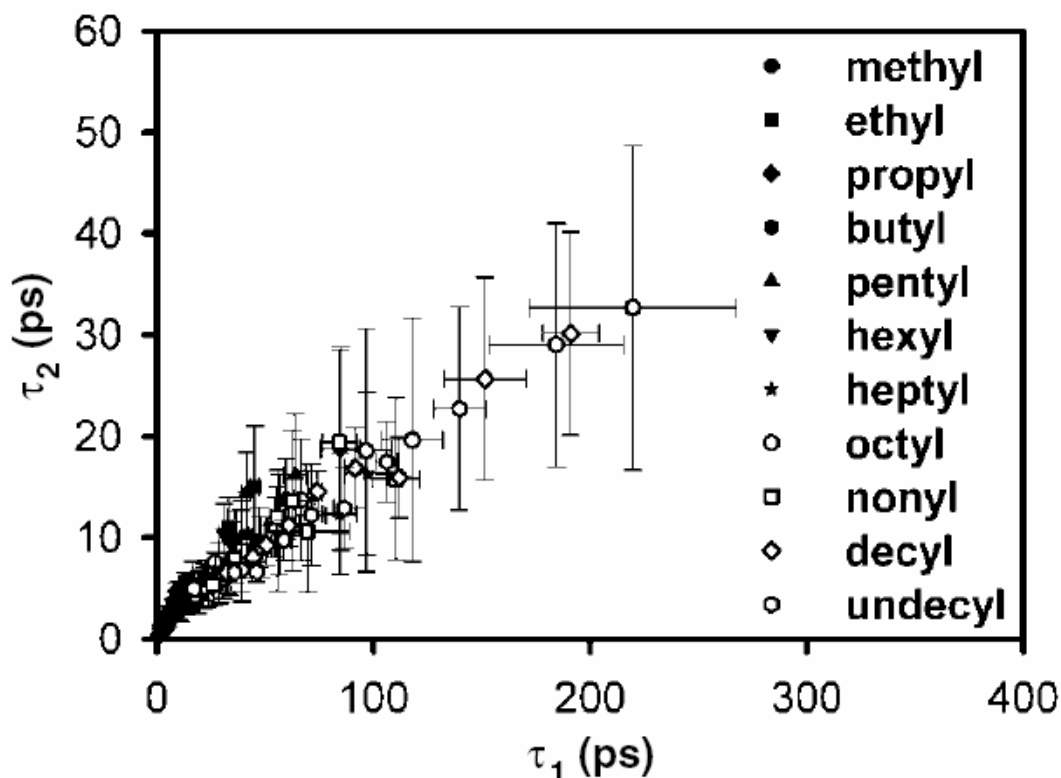


Figure 6.3. Plot of τ_2 versus τ_1 from all of the OKE decays reported previously for methyl cyanide and for all of those summarized here in tables 6-2 to 6-11.

volume of the reorienting molecule, k_B is Boltzmann's constant, and T is the temperature.

^{31, 32} There can be an additional factor in this equation to describe the tendency of the reorienting molecule to drag its neighbors with it, and there is also commonly a non-zero value offset that is often interpreted as the reorientational time at zero viscosity.³² In addition, this equation is intended to describe the orientational diffusion of probe molecules that are large compared to the molecules of the surrounding solvent. Nevertheless, in OKE studies of pure liquids the orientational correlation time is generally found to scale linearly with η/T with a slope that is consistent with reasonable

estimates of the hydrodynamic volume of the molecules. We have previously found this to be the case, for instance, in methyl cyanide.¹⁸

Shown in figure 6.4 is the DSE plot for butyl cyanide; the behaviour in this plot is typical of what is seen for most of the liquids studied here. At high temperature (low η/T) the plot is linear, and at a lower temperature there is a transition to a second linear region with a different slope. The slopes of the DSE plots for these liquids in the higher-temperature (slope 1) and lower-temperature (slope 2) regions are listed in table 6-1. Some of the liquids show signs of having a third region with another slope, whereas the longest-chain liquids exhibit only a single slope. However, we should also note that for the longer-chain liquids we could not investigate a significant portion of the liquid temperature range due to limitations in the maximum temperature attainable in our cryostat. As shown in figure 6.5, for shorter-chain alkyl cyanides the value of η/T at which the transition occurs decreases linearly with chain length. As the chain length increases the transition value of η/T increases again, but this may actually reflect a different transition than seen for the shorter-chain liquids (figure 6.4).

Before considering the source of the change in slope in the DSE plots, we should first consider what can be learned about the microscopic structure of these liquids based upon our OKE data. In particular, we can assess different models of the molecular structure by comparing the slope of the DSE plots to the hydrodynamic volume corresponding to that structure. In one structural extreme the molecules would be completely collapsed, whereas in the other extreme they would be completely extended.

In either of these extremes it is reasonable to believe that orientational diffusion would be described by a single exponential.

If the molecules are collapsed, then the hydrodynamic volume will be approximately equal to the volume per molecule. In figure 6.6 we plot the slopes from the DSE plots as a function of molecular volume. While there is clearly a correlation between the molecular volume and the DSE slope, the relationship is not a linear one. Using the molecular volume to approximate the hydrodynamic volume of a collapsed chain will work best for the molecules with longer alkyl chains, and so for the shorter chains the molecular volume is undoubtedly an underestimate of the hydrodynamic volume in a collapsed state. However, even taking this effect into account does not appear sufficient to linearize the data plotted in figure 6.6. We conclude that the alkyl chains are not fully collapsed, as would be expected.

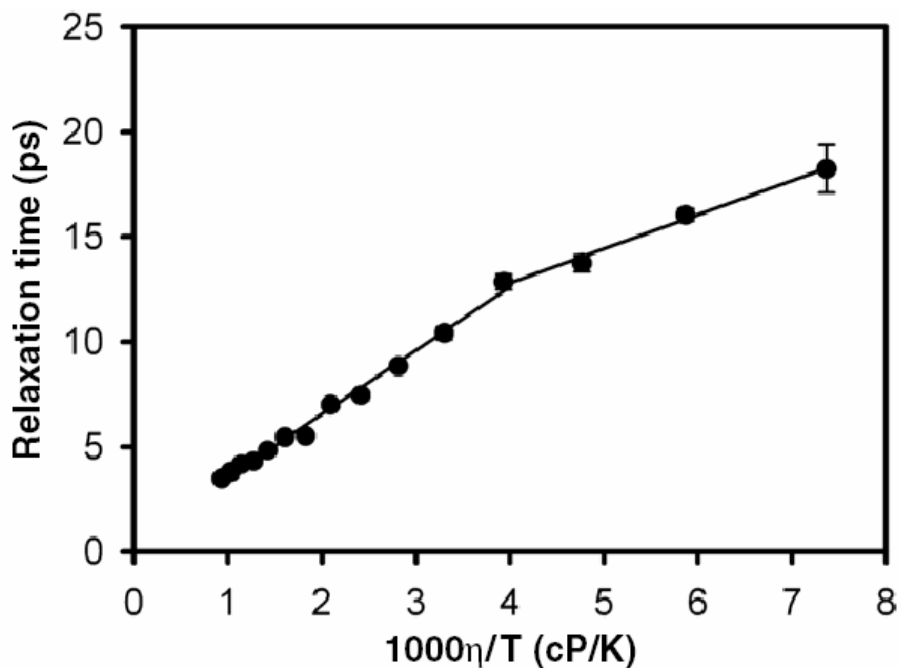


Figure 6.4. Debye–Stokes–Einstein plot for butyl cyanide.

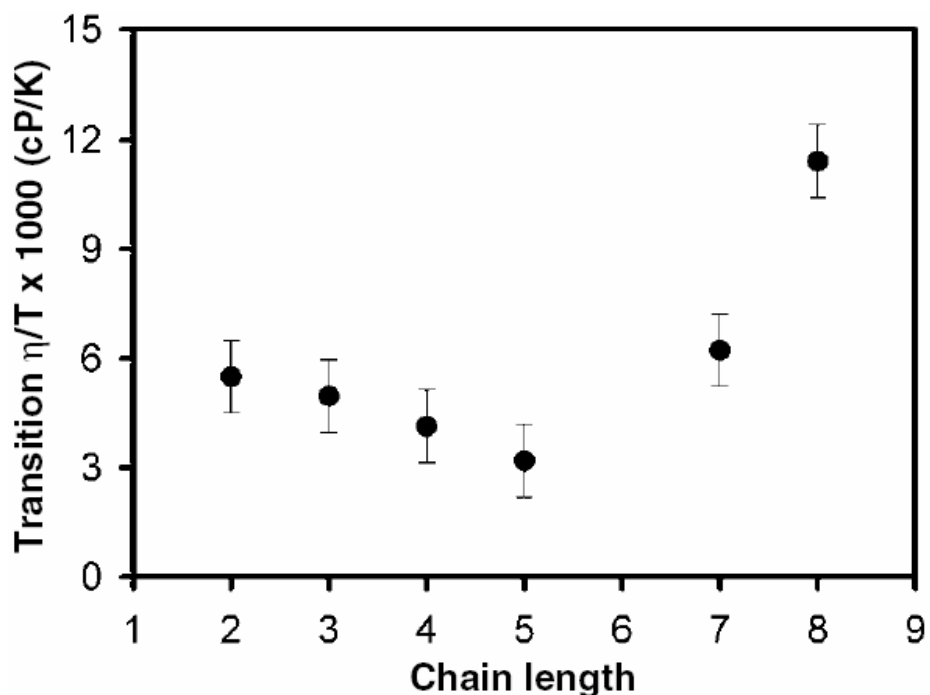


Figure 6.5. Value of η/T at the transition in slopes in the DSE plot for alkyl cyanides as a function of number of carbons in the alkyl chain.

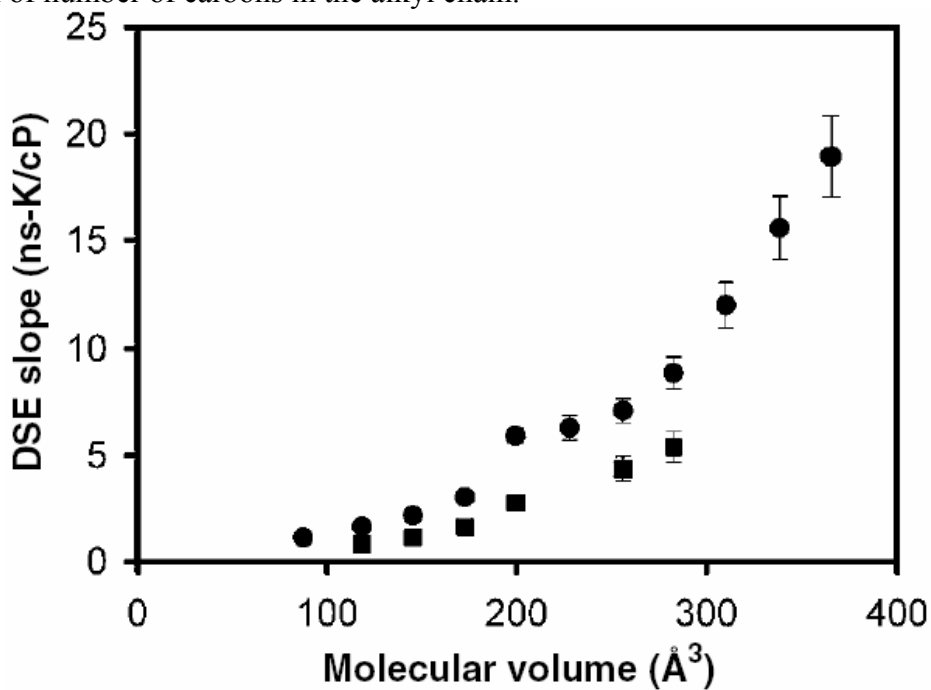


Figure 6.6. Slope of the DSE plots as a function of molecular volume for methyl cyanide and the liquids studied here. Circles denote slope 1 and squares slope 2.

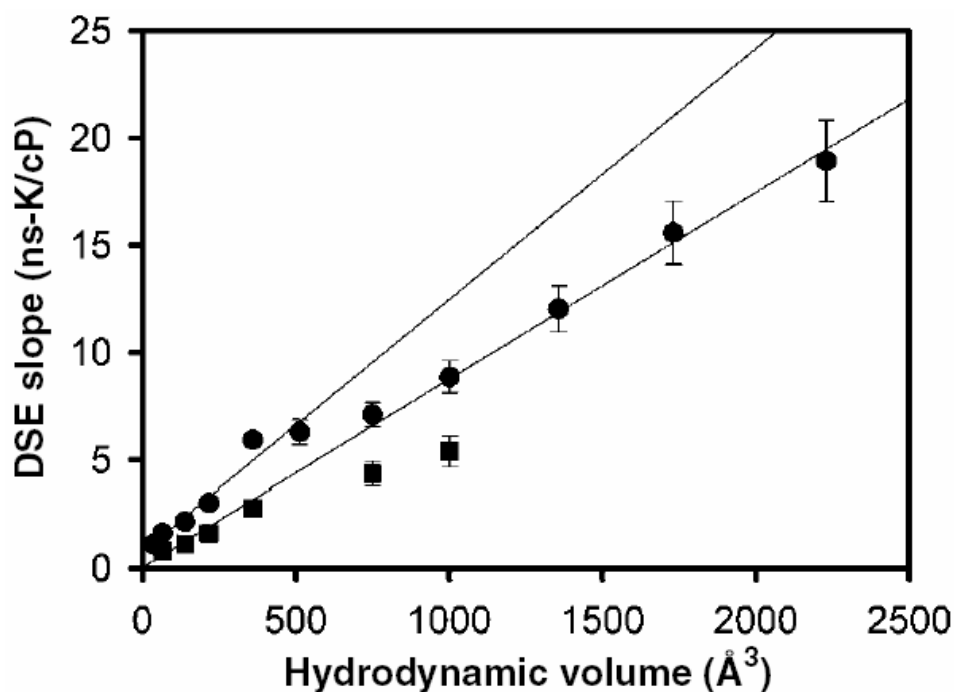


Figure 6.7. Slope of the DSE plots as a function of hydrodynamic volume assuming fully extended alkyl chains for methyl cyanide and the liquids studied here. Circles denote slope 1 and squares slope 2. The solid lines are linear least-squares fits.

To investigate the limit in which the molecules are fully extended, a molecular modeling program was employed to estimate the lengths of the molecules in this configuration.³³ The hydrodynamic volume was then estimated to be $\pi/6$ times the cube of this length. A plot of the DSE slope as a function of this hydrodynamic volume is shown in figure 6.7. It is clear that an extended structure is consistent with our OKE data. For the short-chain molecules, methyl cyanide to hexyl cyanide, slope 1 falls on a straight line on this plot. Similarly, slope 2 for ethyl cyanide to pentyl cyanide falls on a straight line along with slope 1 for heptyl cyanide to undecyl cyanide. The ratio between the slopes of these two linear fits is approximately 1.35. Slope 2 for heptyl and octyl cyanides does not fall on either of these lines.

The above results strongly suggest that the molecules of the alkyl cyanides studied here are extended in the liquid and that they reorient essentially as rigid rods. If the dynamics of the cyanide groups were to begin to decouple from those of the molecules as a whole with decreasing temperature, then the slope of the DSE plot would fall below that expected from the hydrodynamic volume calculated for an extended molecule. There is no sign of this happening even for the longest-chain liquids studied here. It is somewhat surprising that molecules with so much conformational flexibility would reorient in a rod-like manner, although this is not inconsistent with the results of previous OKE studies in which single-exponential decays have been observed for straight-chain alkanes.³⁴⁻³⁹

The ability of the molecules to reorient in this manner may be indicative of the underlying intermolecular structure of the liquid, which we will now consider. Despite their molecular simplicity, linear alkanes and their derivatives can exhibit rich phase behaviour. For instance, many linear alkanes form plastic crystals and exhibit rotator phases.⁴⁰⁻⁴⁵ This type of behaviour is used to advantage, for instance, in the creation of Shpol'skii matrices for high resolution spectroscopy at low temperature.⁴⁶ As another example, liquid alkanes and long-chain alcohols can exhibit surface freezing phenomena well above their bulk freezing points.⁴⁷ These phenomena are all manifestations of the propensity of linear alkanes and their derivatives to form aligned structures, even in the liquid phase. A tendency for local parallel alignment among the molecules in the liquids studied here would make the molecules tend to adopt extended conformations, and therefore could contribute to the apparent rod-like nature of their orientational diffusion.

We now consider the origin of the slope changes in the DSE plots observed in many of these liquids. The challenge is to explain why the slope decreases at lower temperatures, as most of the plausible mechanisms for a change in slope would tend to work in the opposite direction. For instance, it is possible that the change in slope reflects a decrease in the hydrodynamic volume of the molecules. However, this scenario is the opposite of what one would predict from the behaviour of n-alkanes and their monosubstituted derivatives.⁹⁻¹¹ Another possibility is that the boundary conditions for reorientation change as the temperature is lowered. However, this situation would require that the boundary condition change from stick at high temperature to slip at low temperature, which would not be expected. Furthermore, the magnitude of the difference in reorientation time due to such a change in boundary condition should be highly dependent on the aspect ratio of the molecules,⁴⁸ yet the variation of both DSE slopes is a linear function of hydrodynamic volume.

One factor that needs to be kept in mind is that OKE experiments measure a collective orientational correlation time, τ_{coll} , rather than a single-molecule orientational correlation time, τ_{sm} . These two correlation times are related by:

$$\tau_{coll} = \frac{g_2}{j_2} \tau_{SM} \quad (6.2)$$

where g_2 and j_2 are, respectively, the static and dynamic pair orientational correlation parameters.^{32,49} The former parameter is a measure of the degree of parallel ordering in a liquid, with higher values corresponding to a greater degree of order. The latter parameter is generally assumed to be approximately unity in simple liquids. Another possible

explanation for the decrease in the DSE slope at lower temperatures is therefore that there is a change in the intermolecular structure that leads to a decrease in g_2 . This idea seems counterintuitive at first, as the degree of parallel ordering of molecules would be expected to increase with decreasing temperature. At room temperature, g_2 for methyl cyanide is approximately 1.7,^{18, 50} and this parameter takes on a similar value across the entire liquid temperature range of this substance. We would therefore expect g_2 to take on a similar value for slope 1 in ethyl cyanide to hexyl cyanide, based on the data in figure 6.7. If the change in slope is due to a change in g_2 , then this parameter must take on a value of approximately 1.25 in the slope 2 region of ethyl to pentyl cyanides and in the slope 1 region of heptyl to undecyl cyanides, reflecting a lower degree of parallel ordering. However, because the polarizability of these molecules is largely localized on the cyanide groups, it is the parallel ordering of these moieties that is of prime importance in determining the value of g_2 . Thus, it is possible that while the liquids as a whole become more ordered with decreasing temperature, the ordering among cyanide groups actually decreases.

Based on room-temperature x-ray scattering studies of methyl, ethyl and propyl cyanide, it has been suggested that dipole–dipole interactions are the dominant force in determining the structure of these liquids.⁸ This idea is consistent with the relatively high value of g_2 found for methyl cyanide. We propose that dipole–dipole forces are also dominant in determining the structure of butyl, pentyl and hexyl cyanides at high temperature. However, we believe that interactions between the alkyl chains become increasingly important as the temperature is lowered, and that there is a transition point at

which these interactions dominate the liquid structure, leading to a decrease in the degree of parallel ordering of cyanide groups. The temperature at which the alkyl–alkyl interactions begin to dominate the liquid structure would be expected to increase with increasing chain length, as is observed. Furthermore, for long enough alkyl chains the interactions among cyanide groups may not be the dominant factor in determining the liquid structure at any temperature, which is again consistent with our observations. We should also note that the slope 2 data for heptyl and octyl cyanides may be indicative of yet another ordering transition.

6.5. Conclusions

We have presented detailed, temperature-dependent OKE studies of liquid n-alkyl cyanides. Based on the behaviour of the orientational diffusion in these liquids, we have been able to gain insights into their microscopic structure. The molecules of these liquids appear to adopt an extended conformation, and to reorient essentially in rod-like manner. Our data further point to the possibility of microscopic structural transitions in the alkyl cyanides with shorter chains. Decreases in the slope of DSE plots at low temperature lead us to propose that, while interactions among cyanide groups dominate the liquid structure at high temperatures, interactions between alkyl chains take on greater importance at reduced temperatures.

The microscopic structural transitions that we are proposing based on our data may not be full-fledged phase transitions. Although the proposed structural changes may in fact be subtle, they are reminiscent of the multiple phases that can be observed below the freezing point of many n-alkanes and their derivatives. We should note that there is

also an analogy to the cyanobiphenyl class of liquid crystals, in which the cyanide group appears to play a key role in the phase behaviour of the molecules.⁵¹ Alkyl cyanides are relatively unstudied compared to other monosubstituted linear alkanes, but it is clear from the results presented here that further temperature-dependent studies of these liquids with techniques such as calorimetry and x-ray or neutron scattering may be of great interest.

Chapter 6 References and Notes

- (1) Vauthey E *Chem. Phys. Lett.* **1993** 216 530–6
- (2) Vauthey E *Chem. Phys.* **1995** 196 569–82
- (3) Harju T O, Korppi-Tommola J E I, Huizer A H and Varma C *J. Phys. Chem.* **1996** 100 3592–600
- (4) Gumy J-C, Nicolet O and Vauthey E *J. Phys. Chem.* **1999** A 103 10737–43
- (5) Peters K S and Kim G *J. Phys. Chem.* **2001** A 105 4177–81
- (6) Yeow E K L and Braslavsky S E *Phys. Chem. Chem. Phys.* **2002** 4 239–47
- (7) Yoshihara T, Druzhinin S I, Demeter A, Kocher N, Stalke D and Zachariasse K A *J. Phys. Chem.* **2005** A 109 1497–509
- (8) Gorbunova T V, Shilov V V and Batalin G I *Zh. Fiz. Khim.* **1974** 48 2571–2
- (9) Rigby D and Roe R J *J. Chem. Phys.* **1988** 89 5280–90
- (10) Small D M *The Physical Chemistry of Lipids* (New York: Plenum) **1986**
- (11) Habenschuss A and Narten A H *J. Chem. Phys.* **1990** 92 5692–9
- (12) Righini R *Science* **1993** 262 1386–90
- (13) Smith N A and Meech S R *Int. Rev. Phys. Chem.* **2002** 21 75–100
- (14) Kinoshita S, Kai Y, Ariyoshi T and Shimada Y *Int. J. Mod. Phys. B* **1996** 10 1229–72
- (15) Fourkas J T *Nonresonant intermolecular spectroscopy of liquids* *Ultrafast Infrared and Raman Spectroscopy*, ed M D Fayer (New York: Dekker) **2001** pp 473–512
- (16) McMorrow D and Lotshaw W T *J. Phys. Chem.* **1991** 95 10395–406
- (17) Loughnane B J, Farrer R A, Scodinu A, Reilly T and Fourkas J T *J. Phys. Chem. B* **2000** 104 5421–9
- (18) Loughnane B J, Scodinu A, Farrer R A, Fourkas J T and Mohanty U *J. Chem. Phys.* **1999** 111 2686–94
- (19) Scodinu A and Fourkas J T *J. Phys. Chem. B* **2002** 106 10292–5

- (20) SigmaPlot v. 9.0 (Point Richmond, CA: Systat) **2004**
- (21) Viscosity of Liquids: Aliphatic Nitriles (London: Engineering Sciences Data Unit) **2002**
- (22) Berne B J and Pecora R *Dynamic Light Scattering* (New York: Wiley) **1976**
- (23) Lotshaw W T, McMorrow D, Kalpouzios C and Kenney-Wallace G A *Chem. Phys. Lett.* **1987** 136 323–8
- (24) Kalpouzios C, Lotshaw W T, McMorrow D and Kenney-Wallace G A *J. Phys. Chem.* **1987** 91 2028–30
- (25) Deeg F W, Stankus J J, Greenfield S R, Newell V J and Fayer M D *J. Chem. Phys.* **1989** 90 6893–902
- (26) McMorrow D and Lotshaw W T *Chem. Phys. Lett* **1991**. 178 69–74
- (27) Chang Y J and Castner E W Jr *J. Chem. Phys.* **1993** 99 113–25
- (28) Neelakandan M, Pant D and Quitevis E L *J. Phys. Chem. A* **1997** 101 2936–45
- (29) Smith N A and Meech S R *J. Phys. Chem. A* **2000** 104 4223–35
- (30) McMorrow D and Lotshaw W T *Chem. Phys. Lett.* **1993** 201 369–76
- (31) Debye P *Polar Molecules* (New York: Dover) **1929**
- (32) Kivelson D and Madden P A *Annu. Rev. Phys. Chem.* **1980** 31 523–58
- (33) Chem 3D Pro v. 5.0 (Cambridge, MA: CambridgeSoft) **1999**
- (34) Scodinu A and Fourkas J T *J. Phys. Chem. B* **2003** 107 44–51
- (35) Kalpouzios C, McMorrow D, Lotshaw W T and Kenney-Wallace G A *Chem. Phys. Lett.* **1988** 150 138–46
- (36) Kalpouzios C, McMorrow D, Lotshaw W T and Kenney-Wallace G A *Chem. Phys. Lett.* **1989** 155 240–2
- (37) McMorrow D, Thantu N, Melinger J S, Kim S K and Lotshaw W T *J. Phys. Chem.* **1996** 100 10389–99
- (38) Steffen T, Meinders N A C M and Duppen K *J. Phys. Chem. A* **1998** 102 4213–21
- (39) Hunt N T, Jaye A A and Meech S R *J. Phys. Chem. B* **2003** 107 3405–18
- (40) Sirota E B and Herhold A B *Polymer* **2000** 41 8781–9
- (41) Mukherjee P K *J. Chem. Phys.* **2000** 113 4472–5
- (42) Herhold A B, King H E Jr and Sirota E B *J. Chem. Phys.* **2002** 116 9036–50
- (43) Chazhengina S Y, Kotelnikova E N, Filippova I V and Filatov S K *J. Mol. Struct.* **2003** 647 243–57
- (44) Yamamoto T, Nozaki K and Hara T *J. Chem. Phys.* **1990** 92 631–41
- (45) Sirota E B and Wu X Z *J. Chem. Phys.* **1996** 105 7763–73
- (46) Plakhotnik T, Moerner W E, Irgartinger T and Wild U P *Chimia* **1994** 48 31–2
- (47) Penfold J *Rep. Prog. Phys.* **2001** 64 777–814
- (48) Hu C-M and Zwanzig R *J. Chem. Phys.* **1974** 60 4354–7
- (49) Keyes T, Kivelson D and McTague J P *J. Chem. Phys.* **1971** 55 4096–100
- (50) Loughnane B J, Farrer R A, Scodinu A and Fourkas J T *J. Chem. Phys.* **1999** 111 5116–23
- (51) Chandrasekhar S *Liquid Crystals* 2nd edn (Cambridge: Cambridge University Press) **1992**

Chapter 7

New OKE technique for microscopy

7.1. Introduction

Nonlinear optical (NLO) techniques are becoming an increasingly powerful means of performing three-dimensional imaging of and making spectroscopic measurements in small volumes of biological and other samples.¹⁻⁴ NLO techniques offer a number of important advantages as methods for microscopic imaging and spectroscopy for the following reasons. First, NLO techniques depend upon the laser intensity to the power of at least two, and so at appropriate incident intensities signal is generated only within the focal volume of the laser beam. Since the position of this volume can be controlled in three dimensions, these techniques can be used for optical sectioning of a sample. Second, NLO techniques can provide types of contrast that are unavailable from linear spectroscopic techniques; for instance, second-harmonic generation microscopy is sensitive only to regions in which a sample does not have inversion symmetry. Third, NLO techniques can offer considerably more species selectivity than is available in other types of microscopy, often without even requiring the use of labeling.

7.2. Experimental Section

Here we discuss the development of a new scheme for increasing the sensitivity and selectivity of OKE microscopy and microspectroscopy on Raman-active intermolecular and low-frequency intramolecular vibrational modes. This technique is

called antiresonant-ring Kerr Spectroscopy (ARKS). The layout of this instrument is shown in Fig. 7.1. The probe beam is incident on a polarizing beam cube (PBC), and the two portions of the split beam travel in opposite directions around the ring. The sample is placed between two matched microscope objectives with a shared focal point and this entire assembly sits on a translatable stage that lies near the middle of the ring. The probe beam is thus split into two equal pieces in a Sagnac interferometer, and the timing of the two probe beams are subject to different intensity and/or phase changes in the sample. The pump beam will be focused at the same spot in the sample but will not enter the ring (see Fig. 7.1). The key feature of this setup is that the two probe beams travel along exactly the same path and are subject to exactly the same distortions. Thus, in the absence of the pump beam, all of the energy should exit the ring in the direction that it entered. However, if the sample stage is positioned such that the two probe pulses arrive at different times in relation to the pump beam, the difference in the index of refraction experienced by the two pulses in the sample will allow light to leak through the beam splitter in the other direction, where it can be detected. In effect, this apparatus performs an optical subtraction of the counterpropagating probe pulses, which should allow for an extremely high sensitivity to be achieved.

An especially attractive feature of ARKS spectrometer is that it can generate contrast in a number of different ways depending on relative arrival times of the pump pulse and the two probe pulses. For instance, if one probe pulse arrives before the pump pulse and the other arrives at the same time as the pump pulse, contrast will be based upon the third-order electronic polarizability of the sample, which would be useful in

detecting especially polarizable molecules such as DNA. If one probe pulse arrives before the pump and the other arrives a few picoseconds afterwards, contrast is generated

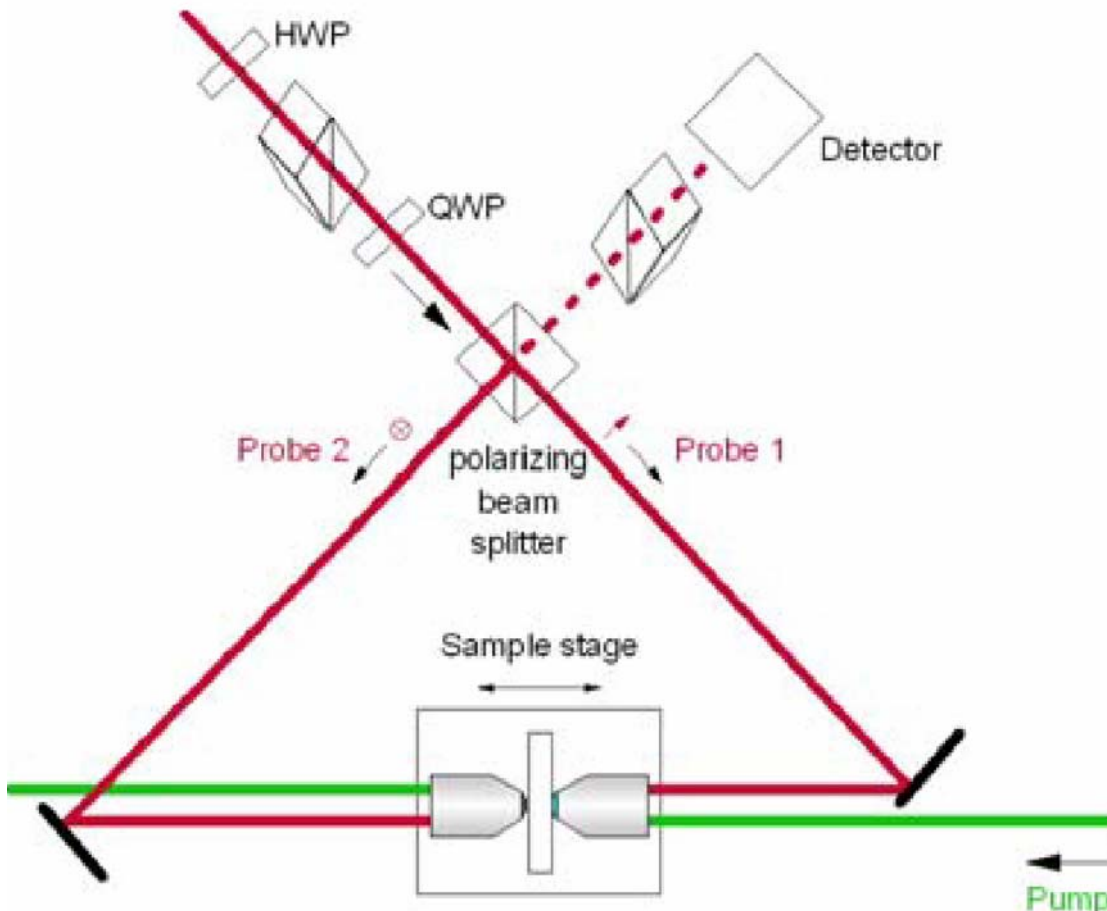


Figure. 7.1 First-generation antiresonant-ring OKE spectrometer.

via the ability to generate molecular alignment, which should be dependent on local water content. Yet another contrast mechanism is available in samples in which a low-frequency intramolecular Raman band appears in the OKE decay (such as a phosphate mode in DNA, for example). In this situation, both probe pulses can arrive after the pump

pulse, one at the maximum of a vibrational oscillation and one at the neighboring minimum. At times greater than a picosecond or so, the intermolecular signal will decay relatively slowly compared to half of the period of a vibrational oscillation, and so this technique could provide an effective means of performing Raman microscopy on low-frequency intramolecular modes with a single laser.

The major advantage of such a spectrometer is that it performs optical subtraction of the OKE signal generated by a single pump beam but interrogated by two different probe beams. The beams exit the ring at the input polarizer, and are sent to an analyzer polarizer that only lets light through if there is a phase difference between the two probe beams. The two beams traverse paths that are absolutely identical, but arrive at the sample at different times, and so any phase difference is due solely to the pump beam. This allows for the sensitive detection of many different tensor elements of the OKE signal. Furthermore, in the context of OKE microscopy, it allows for rapid switching among different contrast modes. For instance, to generate contrast via the electronic polarizability, one probe beam can arrive before the pump and the other can arrive simultaneously with the pump. For contrast based on a particular vibrational mode, one probe beam can arrive at the maximum of the vibrational oscillation and the other at the minimum. Similar ideas can be applied to generate contrast based on the reorientation time.

The first-generation design of the ARKS spectrometer had a significant, unanticipated problem: the OKE signal is quite different if the pump and probe beam counterpropagate rather than copropagate (or nearly copropagate). These experiments

were on hold temporarily during our relocation to the University of Maryland, but we took this opportunity to think carefully about the optimal design of a second generation spectrometer in light of what we have learned from the first-generation design. In addition to the original criteria that the probe beams travel along exactly the same paths and that detection be accomplished with a zero-background scheme, we now know that we have to implement a design in which the two probe beams propagate through the sample in the same direction as the pump.

We think about the second-generation antiresonant-ring OKE spectrometer. Our new scheme, which is shown in Fig. 3, draws upon an optical setup that was designed to produce a pair of OKE pump pulses of opposite polarization with controlled timing and intensity. The probe beam passes through a polarizer set to 45° , and then is incident on a polarizing beam cube that sends the vertically-polarized component in one direction and the horizontally-polarized component in a perpendicular direction. Both beams are steered by identical sets of optics, including a delay line that is adjustable in one leg. The beams are recombined at a second PBC that they exit collinearly. The beams are focused into a sample at the same spot as a pump beam that travels parallel to them. The probe beams are collimated after the sample and are sent back into the ring through the other face of the second PBC. The horizontally-polarized component follows the path that was originally traversed by the vertically-polarized component and vice versa. The beams exit the ring collinearly at the unused face of the first PBC.

Both probe beams follow exactly the same path, albeit in different directions. If the unsplit probe beam is polarized at 45° and if both probe beams experience the same conditions, then the light that exits the ring will also be polarized at 45° . A polarizer set to pass light at -45° is placed in the beam path, which should not allow any light to pass

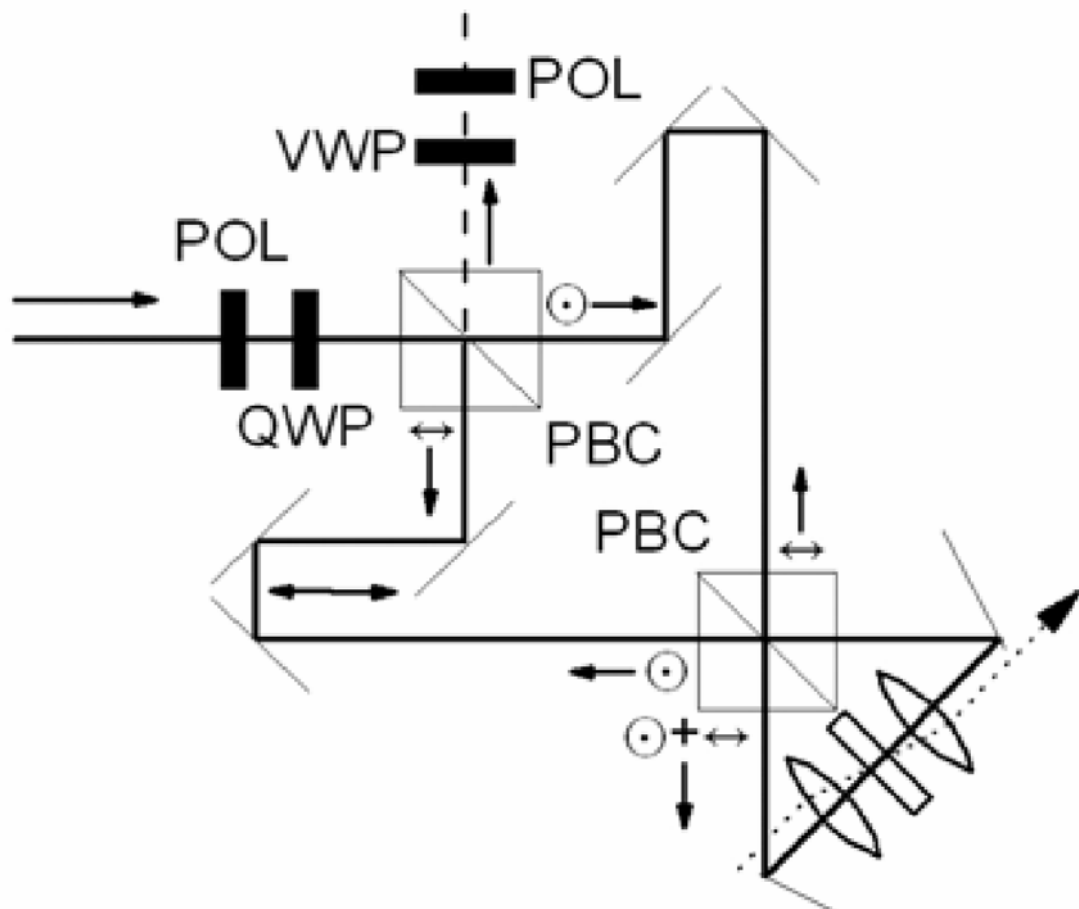


Figure. 7.2 Schematic diagram of the second-generation ARKS spectrometer. POL = polarizer; QWP = quarter-wave plate; PBC = polarizing beam cube; VWP = variable wave plate. The dotted line is the pump beam and the dashed line the output.

(note that the mirrors in the ring will have slightly different phase shifts for s and p polarizations, and so we will include a variable wave plate before the analyzer polarizer to compensate for this). Now, assume that one probe beam experiences a phase shift relative to the other probe beam because they arrive at the sample at different delay times relative to the pump beam. As a result, the output of the ring will have a slight degree of ellipticity, allowing some light to exit the analyzer polarizer. This light is exactly what we wish to collect.

7.3 Experimental results

This apparatus should offer a S/N ratio similar to that of a standard polarization-spectroscopy OKE spectrometer, while making it possible to measure different tensor elements of the OKE response (or differences between different tensor elements at given time delays in the context of generating contrast in microscopy). To see how this works, call the probe beam polarizations x and y . If the y -polarized probe beam arrives before an x -polarized pump beam and the other probe beam arrives after the pump beam, then the output is $R_{xxx}(\tau)$, where τ is the delay time. Using the same timing but polarizing the pump beam at the magic angle (m) or at y yields the $R_{xmm}(\tau)$ (isotropic) and the $R_{xyy}(\tau)$ (polarized) responses, respectively.. If the probe beams arrive at the same time and the pump beam has x polarization, then the output is $R_{xxx}(\tau) - R_{yyx}(\tau) = R_{xyy}(\tau)$, which is the depolarized response. I summarize the relationships in table 7-1.

We now turn to the sample CS_2 at room temperature. Shown in Figure 7.3 is the $R_{xxx}(\tau)$ output, and $R_{xyy}(\tau)$ is shown in Figure 7.4. By adjusting the pump polarization

Pump polarization	probe 1		probe 2		Tensor elements
	polarization	timing	polarization	timing	
x	y	Before pump	x	After pump	$R_{xxxx}(\tau)$
m	y	Before pump	x	After pump	$R_{xxmm}(\tau)$
y	y	Before pump	x	After pump	$R_{xyxy}(\tau)$
x	y	Same time	x	Same time	$R_{xyxy}(\tau)$

Table 7-1 The different tensor elements by changing the timing and polarization of all pulses

at the magic angle to one of the probe beams, the isotropic $R_{xxmm}(\tau)$ response is shown in Figure 7.5. When the two probe beams arrive the same time and pump beam has x polarization, then we get the depolarized response $R_{xyxy}(\tau)$, which is shown in Figure 7.6.

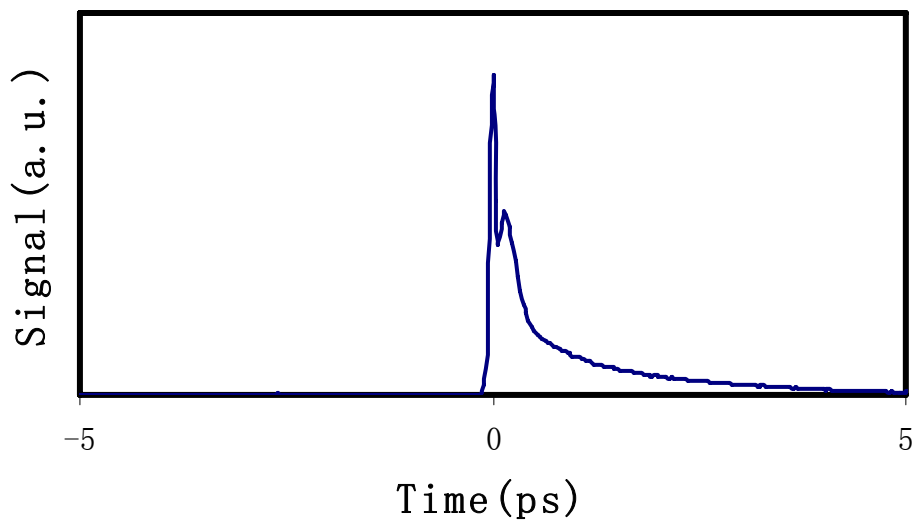


Figure 7.3 $R_{xxxx}(\tau)$ response of CS_2 at room temperature.

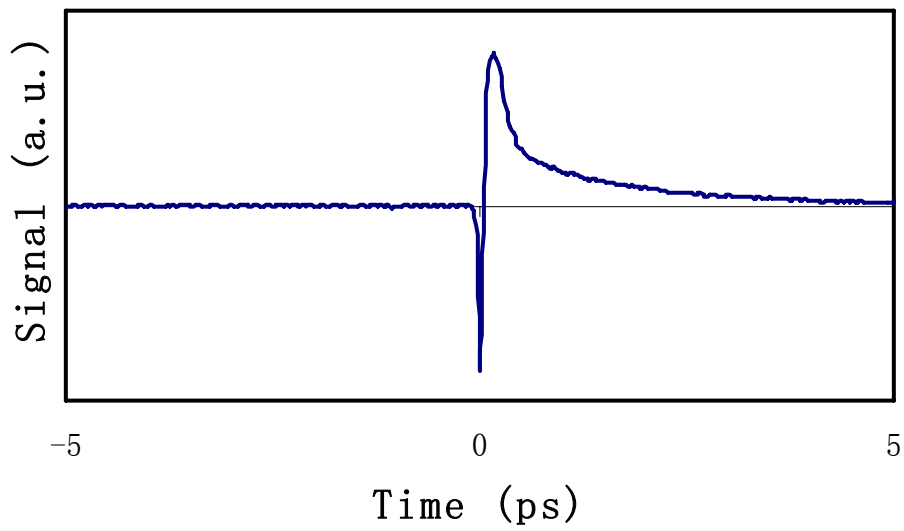


Figure 7.4 $R_{xyy}(\tau)$ response of CS_2 at room temperature.

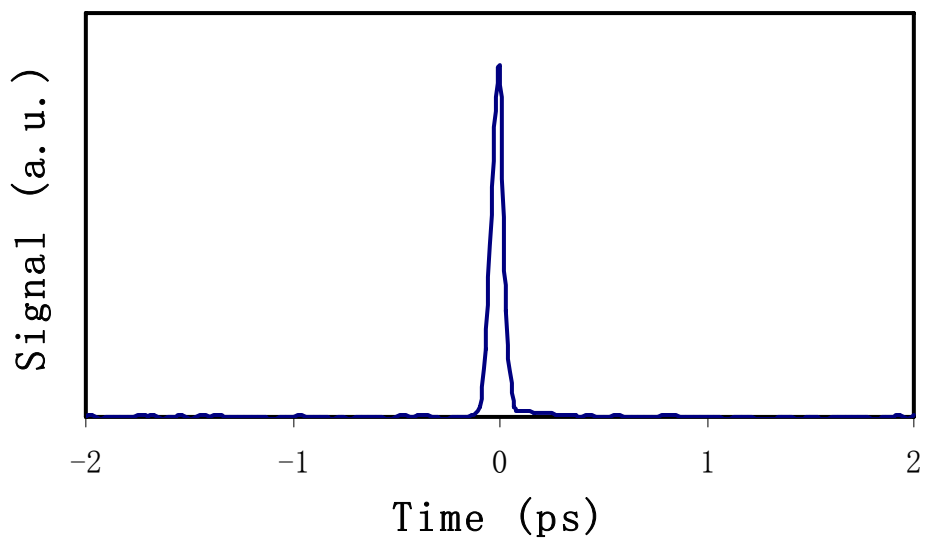


Figure 7.5 Isotropic $R_{xmm}(\tau)$ response of CS_2 at room temperature.

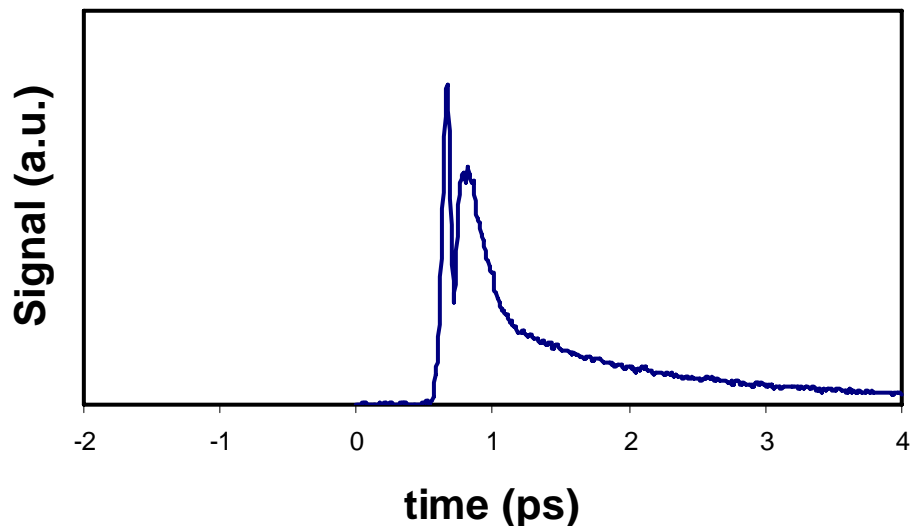


Figure 7.6 Depolarized $R_{xyxy}(\tau)$ response of CS_2 at room temperature.

7.4 Conclusions

The second-generation ARKS spectrometer make it possible to take advantage of different types of contrast mechanisms in OKE microscopy. One of the most useful types of contrast for many samples will be based on intramolecular vibrations. For modes with frequencies of 1000 cm^{-1} or less, OKE microscopy should provide a viable alternative to CARS microscopy. However, most samples are also likely to have many low-frequency intramolecular vibrations, and so it is desirable to employ techniques to further increase the sensitivity of OKE spectroscopy to desired vibrations. We undertook the work described in Chapter 2 in which two pump pulses were used to enhance the contribution of a selected vibrational mode to the OKE signal while simultaneously diminishing the contribution of other modes and of diffusive reorientation. In general, it

should be possible to suppress the contribution of n modes (or reorientational times) by using $n + 1$ or more pump pulses with appropriate timing, intensity, and polarization.⁵ We will implement this strategy for increasing the selectivity of OKE spectroscopy by using a programmable pulse shaper.

The combination of ARKS and techniques for mode-selective excitation will provide us with the ability to perform OKE microscopy with high contrast. Furthermore, as discussed above, this contrast can take on a number of different forms depending on the relative timing of the two probe pulses. Our goal will be to combine them in order to move from spectroscopy to microscopy.

Chapter 7 References and Notes

- (1) So, P. T. C.; Dong, C. Y.; Masters, B. R.; Berland, K. M. *Annu. Rev. Biomed. Eng.* **2000**, 2, 399.
- (2) Millard, A. C.; Fittinghoff, D. N.; Wiseman, P. W.; Muller, M.; Brakenhoff, G. J.; Squier, J. A.; Wilson, K. R. *Biophys. J.* **2000**, 78, 800.
- (3) Volkmer, A.; Cheng, J. X.; Xie, X. S. *Phys. Rev. Lett.* **2001**, 8702, 023901.
- (4) Potma, E. O.; de Boeij, W. P.; Wiersma, D. A. *J. Opt. Soc. Amer. B* **2000**, 17, 1678.
- (5) Zhu, X.; Farrer, R.A.; Fourkas, J.T. *J. Phys. Chem. B* **2005**, 109, 8481-8488

Chapter 8

Conclusions and future directions

I have demonstrated that by using two pump pulses with independently-controllable polarizations, intensity and timing, different contributions to the OKE signal in liquids can be enhanced and suppressed. When both pump pulses have the same polarization, intramolecular vibrations can be enhanced or suppressed without affecting the reorientational diffusion contribution to the signal significantly. Similar control can be exerted over intramolecular vibrations when the pump pulses are perpendicularly polarized, and under these conditions it is also possible to suppress the reorientational diffusion component of the signal completely. I also characterize in detail the perpendicularly-polarized pulses with controllable intensities and timing used for the excitation step in OKE spectroscopy. I examine the ratio of pump pulse intensities required to cancel the contribution of reorientational diffusion or of a Raman active intramolecular vibration to the signal as a function of the delay time between excitation pulses. These results indicate that the signal can be described well as arising from the sum of independent third-order responses initiated by each pump pulses.

To attain maximal contrast in OKE microscopy it would be useful to be able to suppress any unwanted contributions to the signal. This can be accomplished using the technique described in this thesis, which can be implemented readily in an OKE microscopy setup. Our work underscores the utility of using polarization as a factor in

the control scheme. Our experiments pave the way for using sequences of multiple pump pulses with controllable polarization, timing, and intensity to single out the contribution of a single mode of interest in a complex OKE decay. The combination of ARKS and this technique would be of great interest for performing mode-selective OKE microscopy with high contrast. We can expect OKE microscopy as implemented here to have resolution that is comparable to that of CARS microscopy and related nonlinear optical microscopies, on the order of 300 to 500 microns. Ultimately the use of pulse-shaping technology with amplitude and polarization control should be able to improve the spatial resolution significantly.

For the dynamics of nanoconfined benzene, we expected benzene to be far less influenced by confinement than are linear molecules based on its shape. OKE spectroscopy is sensitive only to the tumbling motions of a disk, and so we cannot observe the in-plane spinning motion of molecules that are flat on the pore surfaces. The disk-like shape leads to the prediction of a smaller hydrodynamic effect for reorientation off of the pore surfaces than is observed for linear molecules. Our expectations were not met. Benzene does exhibit a biexponential OKE decay in confinement. However, the faster decay component depends on pore size and is slower than the reorientational decay in the bulk liquid, and the slower decay component has a decay time that can be more than an order of magnitude larger and does not depend on pore size. The fallacy in our reasoning was the assumption that benzene wets silica only weakly. In fact, subsequent measurements demonstrated that the contact angle of benzene on silica is 6° , which is smaller than its contact angle on paraffin! Surprisingly, the contact angle of benzene- d_6

on silica is actually significantly greater than that of benzene. In agreement with this observation, the dynamics of benzene-d₆ are faster in confinement than those of benzene, despite the greater viscosity of the former liquid. We were also able to use literature NMR data on the behavior of benzene-d₆ in confinement to determine that there is significantly greater ordering of the liquid at the pore surfaces than in the bulk. Of the liquids that we have studied in confinement, the behavior of benzene bears closest resemblance to that of water, suggesting that there is significant cooperativity in the orientational relaxation of confined benzene. It will be of great interest to extend nanoconfined benzene studies to other confined aromatic systems and to make further comparisons with single-molecule orientation data.

For the dynamics of *n*-alkyl cyanides, we were interested in whether single-exponential orientational diffusion would continue to be observed in the bulk with lengthening of the alkyl chain. If the relaxation of the bulk liquid took on such a simple form, these liquids would be ideal candidates for studying the effects on dynamics in confinement of molecular length versus pore diameter. In plotting the OKE orientational relaxation time versus η/T (viscosity over temperature), we found linear behavior for each liquid at high temperatures. Furthermore, the slopes of these plots scaled exactly as would be predicted from the hydrodynamic volume for reorientation of extended molecules, reaffirming our conclusion. Even more interestingly, most of the liquids showed a sharp transition to a second, lower slope in the Debye-Stokes-Einstein plot at lower temperatures. We believe that this change in slope reflects an underlying structural transition in the liquids. Our theory is that at high temperature the microscopic structure

is determined largely by polar interactions among cyanide groups, but at lower temperature it is the alkyl chains that dominate local ordering. We know of no other liquids in which such a phenomenon has been observed above the melting point, although liquid-liquid phase transitions have been proposed in supercooled states of substances and in 2-D nitrile surface layers on water. This behavior is also reminiscent of transitions that occur in rotator phases of alkanes and *n*-alkyl alcohols below their melting points. Whether or not our observations are indicative of an actual phase transition is an open question that merits further investigation.

Appendix 1

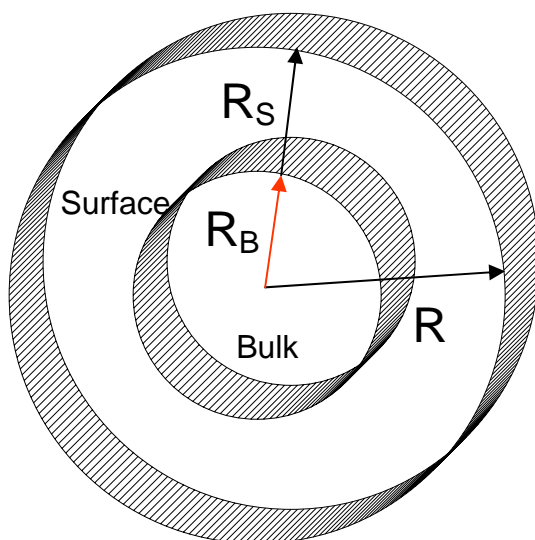


Figure A1.1 Schematic diagram of the cross-sectional area of a three dimensional cylindrical pore of radius R with a radius R_B of bulk-like molecules.

Figure A1.1 is a schematic diagram of bulk and surface population of molecules within a cylindrical pore of radius R . In order to calculate the surface thickness it is necessary to relate the population of molecules which are readily available from an OKE experiment to the bulk radius (R_B) and the surface radius (R_S). The total population of the molecules is given by

$$\mathbf{P}_{\text{Total}} = \mathbf{P}_B + \mathbf{P}_S, \quad (\text{A1.1})$$

where $\mathbf{P}_{\text{Total}}$, \mathbf{P}_B , and \mathbf{P}_S are the total, bulk and surface populations of molecules, respectively. Let's assume \mathbf{A} is the relative population of molecules with reorientational time τ in the bulk. Then,

$$A = \frac{P_B}{P_{Total}} . \quad (A1.2)$$

The bulk (V_B) to total volume (V_{Total}) ratio is given by

$$\frac{V_B}{V_{Total}} = \frac{\pi R_B^2}{\pi R^2} = \frac{P_B}{P_{Total}} \quad (A1.3)$$

By combining equations A1.2 and A1.3, the bulk (R_B) and surface thickness (R_S) are readily apparent.

$$R_B = R\sqrt{A} \quad (A1.4)$$

$$R_S = R - R_B = R(1 - \sqrt{A}) \quad (A1.5)$$

References

- (1) Denk, W.; Strickler, J. H.; Webb, W. *Science* **1990**, 248, 73.
- (2) Cheng, J. X.; Book, L. D.; Xie, X. S. *Opt. Lett.* **2001**, 26, 1341.
- (3) Potma, E. O.; de Boeij, W. P.; Wiersma, D. A. *Biophys. J.* **2001**, 80, 3019.
- (4) Squier, J. A.; Muller, M.; Brakenhoff, G. J.; Wilson, K. R. *Opt. Express* **1998**, 3, 315.
- (5) Righini, R. *Science* **1993**, 262, 1386.
- (6) Smith, N. A.; Meech, S. R. *Int. Rev. Phys. Chem.* **2002**, 21, 75.
- (7) Kinoshita, S.; Kai, Y.; Ariyoshi, T.; Shimada, Y. *Int. J. Mod. Phys. B* **1996**, 10, 1229
- (8) Loughnane, B. J.; Scodinu, A.; Farrer, R. A.; Fourkas, J. T.; Mohanty, U. *J. Chem. Phys.* **1999**, 111, 2686.
- (9) Righini, R. *Science* **1993**, 262, 1386.
- (10) Kinoshita, S.; Kai, Y.; Ariyoshi, T.; Shimada, Y. *Int. J. Mod. Phys. B* **1996**, 10, 1229.
- (11) Fourkas, J. T. Nonresonant Intermolecular Spectroscopy of Liquids In Ultrafast Infrared and Raman Spectroscopy; Fayer, M. D., Ed.; Marcel Dekker: New York, **2001**; Vol. 26, p 473.
- (12) Smith, N. A.; Meech, S. R. *Int. Rev. Phys. Chem.* **2002**, 21, 75.
- (13) Loughnane, B. J.; Scodinu, A.; Farrer, R. A.; Fourkas, J. T.; *J. Phys. Chem. B* **2000**, 104, 5421
- (14) McMorro, D.; Lotshaw, W. T.; Kenney-Wallace, G. A. *IEEE J. Quantum Electron.* **1998**, 24, 443
- (15) McMorro, D.; Thantu, N.; Kleiman, V.; Melinger, J. S.; Lotshaw, W. T. *J. Phys. Chem. A* **2001**, 105, 7960
- (16) Castner Jr., E. W.; Maroncelli, M. *J. Mol. Liq.* **1998**, 77, 1.
- (17) Cong, P.; Deuel, H. P.; Simon, J. D. *Chem. Phys. Lett.* **1995**, 240, 72
- (18) Neelakandan, M.; Pant, D.; Quitevis, E. L. *J. Phys. Chem. A* **1997**, 101, 2936.
- (19) Bartolini, P.; Ricci, M.; Torre, R.; Righini, R.; Santa, I. *J. Chem. Phys.* **1999**, 110, 8653.
- (20) Cang, H.; Novikov, V. N.; Fayer, M. D. *Phys. Rev. Lett.* **2003**, 90, 197401
- (21) Cang, H.; Novikov, V. N.; Fayer, M. D. *J. Chem. Phys.* **2003**, 118, 2800.
- (22) Ricci, M.; Wiebel, S.; Bartolini, P.; Taschin, A.; Torre, R. *Philos. Mag. B* **2004**, 84, 1491.
- (23) Torre, R.; Bartolini, P.; Righini, R. *Nature* **2004**, 428, 296.
- (24) Cang, H.; Li, J.; Fayer, M. D. *J. Chem. Phys.* **2003**, 119, 13017.
- (25) Giraud, G.; Gordon, C. M.; Dunkin, I. R.; Wynne, K. *J. Chem. Phys.* **2003**, 119, 464.
- (26) Hyun, B. R.; Dzyuba, S. V.; Bartsch, R. A.; Quitevis, E. L. *J. Phys. Chem. A* **2002**, 106, 7579.

- (27) Farrer, R. A.; Fourkas, J. T. *Acc. Chem. Res.* **2003**, 36, 605.
- (28) Hunt, N. T.; Jaye, A. A.; Meech, S. R. *J. Phys. Chem. B* **2003**, 107, 3405.
- (29) Hunt, N. T.; Jaye, A. A.; Hellman, A.; Meech, S. R. *J. Phys. Chem. B* **2004**, 108, 100.
- (30) McMorow, D.; Thantu, N.; Melinger, J. S.; Kim, S. K.; Lotshaw, W. T. *J. Phys. Chem.* **1996**, 100, 10389.
- (31) Steffen, T.; Meinders, N. A. C. M.; Duppen, K. *J. Phys. Chem. A* **1998**, 102, 4213.
- (32) Idrissi, A.; Ricci, M.; Bartolini, P.; Righini, R. *J. Chem. Phys.* **2001**, 114, 6774.
- (33) Hunt, N. T.; Meech, S. R. *Chem. Phys. Lett.* **2003**, 378, 195. PAGE EST: 7.3 H J. Phys. Chem. B
- (34) Scodinu, A.; Fourkas, J. T. *J. Phys. Chem. B* **2003**, 107, 44.
- (35) Wiewior, P. P.; Shirota, H.; Castner, E. W. *J. Chem. Phys.* **2002**, 116, 4643.
- (36) Shirota, H.; Castner, E. W. *J. Am. Chem. Soc.* **2001**, 123, 12877.
- (37) Eaves, J. D.; Fecko, C. J.; Stevens, A. L.; Peng, P.; Tokmakoff, A. *Chem. Phys. Lett.* **2003**, 376, 20.
- (38) Giraud, G.; Wynne, K. J. *Am. Chem. Soc.* **2002**, 124, 12110.
- (39) Giraud, G.; Karolin, J.; Wynne, K. *Biophys. J.* **2003**, 85, 1903.
- (40) Cang, H.; Li, H.; Fayer, M. D. *Chem. Phys. Lett.* **2002**, 366, 82.
- (41) Gottke, S. D.; Cang, H.; Bagchi, B.; Fayer, M. D. *J. Chem. Phys.* **2002**, 116, 6339.
- (42) Gottke, S. D.; Brace, D. D.; Cang, H.; Bagchi, B.; Fayer, M. D. *J. Chem. Phys.* **2002**, 116, 360.
- (43) Hyun, B. R.; Quitevis, E. L. *Chem. Phys. Lett.* **2003**, 373, 526.
- (44) Hunt, N. T.; Meech, S. R. *J. Chem. Phys.* **2004**, 120, 10828.
- (45) Potma, E. O.; de Boeij, W. P.; Wiersma, D. A. *Biophys. J.* **2001**, 80, 3019
- (46) Zhu, X.; Farrer, R. A.; Gershgoren, E.; Kapteyn, H. C.; Fourkas, J. T. *J. Phys. Chem. B* **2004**, 108, 3384.
- (47) Weiner, A. M.; Leaird, D. E.; Wiederrecht, G. P.; Nelson, K. A. *Science* **1990**, 247, 1317.
- (48) Weiner, A. M.; Leaird, D. E.; Wiederrecht, G. P.; Nelson, K. A. *J. Opt. Soc. Am. B* **1991**, 8, 1264.
- (49) Wiederrecht, G. P.; Dougherty, T. P.; Dhar, L.; Nelson, K. A.; Weiner, A. M.; Leaird, D. E. *Ferroelectrics* **1993**, 144, 1.
- (50) Wefers, M. M.; Kawashima, H.; Nelson, K. A. *J. Chem. Phys.* **1998**, 108, 10248
- (51) Gershgoren, E.; Vala, J.; Kosloff, R.; Ruhman, S. *J. Phys. Chem. A* **2001**, 105, 5081.
- (52) Hecht, E. *Optics* (Addison- Wesley Publishing Reading, MA) **1987**
- (53) Mayer; Gires *Compt. Rend.* **1964**, 258, 2039.
- (54) Duguay; Hansen, *Appl. Phys. Lett.* **1969**, 15, 192.
- (55) Ippen and Shank, *Appl. Phys. Lett.* **1975**, 26, 82.
- (56) Green, B. I.; Farrow, R. C. *Chem. Phys. Lett.* **1983**, 98, 273

- (57) Kalpuzos, C.; Lotshaw, W.T; McMorrow, D; Kenney-Wallace, G.A. *J. Phys. Chem.* **1987**,91,2028.
- (58) Ruhman, S.; William,L.; Joly, A.; Kohler, B.; Nelson K.A. *J.phys.Chem* **1987**, 91,2237
- (59) Ruhman, S.; Kohler, B.; Joly, A.; Nelson, K.A. *Chem.Phys. Lett.* **1987**, 14116.
- (60) Ruhman, S.; Nelson, K.A. *J.Chem.Phys.* **1991**, 94, 859.
- (61) McMorrow, D.; Lotshaw, W.T. *Chem. Phys. Lett.* **1990**, 171(1), 85
- (62) McMorrow, D.; Lotshaw, W.T. *J. Phys. Chem.* **1991**, 95, 10395
- (63) McMorrow, D.; Lotshaw, W.T. *J. Phys. Chem.* **1996**, 100, 10389
- (64) Dhar, L.; Rogers, J. A.; Nelson, K. A. *Chem. Rev.* **1994**, 94, 157
- (65) Wallen, S.L; Nikiel, L; Yi, J.; Jonas. J. *J. Phys. Chem.* **1995**, 99, 15421
- (66) Oogaz, F.;Rawson, H. *J.Non-Crystalline Solids* **1986**, 82, 57.
- (67) Ballard, C.C.; Broge, E.C.; Iler, R.K.; St. John; McWhorther; J.R. *J.Am.Chem. Soc.* **1960**, 60,20
- (68) Hair, M.L; hertl, W.; *J. Phys. Chem.* **1969**, 73,2372
- (69) Armistead, C.G.; Hockey, J.A. *Trans. Faraday Soc.* **1967**, 63, 2549
- (70) Sindorf, D.W; Maciel, G.E. *J. Phys. Chem.* **1983**, 87, 5516
- (71) Majors, R.E.J. *Chroma. Sci.* **1974**, 12, 767.
- (72) Brinker,C.J.; Scherer, G.W. *Sol-gel Science: The Physics and Chemistry of Sol-Gel processing* Academic Press: San Diego, CA, **1990**
- (73) Iler, R.K. *The Chemistry of Silica*; (Wiley, New York) **1979**
- (74) Gregg, S. J.; Sing, K.S.W. *Adsorption, Surface Area, and Porosity* (Academic Press, London) **1967**
- (75) Brunauer, S; Emmett, P.H; Teller, E. *J.Am.Chem. Soc* **1938**, 60, 309
- (76) Langmuir, I *J. Am.Chem. Soc.* **1918**, 40, 1961
- (77) Dhar, L.; Rogers, J. A.; Nelson, K. A. *Chem. Rev.* **1994**, 94, 157
- (78) Fourkas, J. T.; Fayer, M. D. *Acc. Chem. Res.* **1992**, 25, 227.
- (79) Weiner, A. M.; Leaird, D. E.; Wiederrecht, G. P.; Nelson, K. A. *Science* **1990**, 247, 1317
- (80) Weiner, A. M.; Leaird, D. E.; Wiederrecht, G. P.; Nelson, K. A. *J. Opt. Soc. Amer. B* **1991**, 8, 1264.
- (81) Gershgoren, E.; Bartels, R. A.; Fourkas, J. T.; Tobey, R.; Murnane, M. M.; Kapteyn, H. C. *Opt. Lett.* **2003**, 28, 361.
- (82) Zhu, X.; Farrer, R. A.; Gershgoren, E.; Kapteyn, H. C.; Fourkas, J. T. *J. Phys. Chem. B* **2004**, 108, 3384
- (83) Wefers, M. M.; Kawashima, H.; Nelson, K. A. *J. Chem. Phys.* **1998**, 108, 10248
- (84) McMorrow, D.; Lotshaw, W. T. *J. Phys. Chem.* **1991**, 95, 10395.
- (85) Hellwarth, R. W. *Prog. Quantum Electron.* **1977**, 5, 1
- (86) Murry, R. L.; Fourkas, J. T. *J. Chem. Phys.* **1997**, 107, 9726
- (87) Berne, B. J.; Pecora, R. *Dynamic Light Scattering*; Wiley: New York, **1976**.
- (88) Wurrey, C. J.; Bucy, W. E.; Durig, J. R. *J. Phys. Chem.* **1976**, 80, 1129.

- (89) Frankiss, S. G. *J. Mol. Struct.* **1968**, 2, 271.
- (90) So, P. T. C.; Dong, C. Y.; Masters, B. R.; Berland, K. M. *Annu. Rev. Biomed. Eng.* **2000**, 2, 399.
- (91) Millard, A. C.; Fittinghoff, D. N.; Wiseman, P. W.; Muller, M.; Brakenhoff, G. J.; Squier, J. A.; Wilson, K. R. *Biophys. J.* **2000**, 78, 800Plat.
- (92) Volkmer, A.; Cheng, J. X.; Xie, X. S. *Phys. Rev. Lett.* **2001**, 8702, 023901.
- (93) Potma, E. O.; de Boeij, W. P.; Wiersma, D. A. *J. Opt. Soc. Amer. B* **2000**, 17, 1678.
- (94) Klar, T. A.; Jakobs, S.; Dyba, M.; Egner, A.; Hell, S. W. *Proc. Nat. Acad. Sci. USA* **2000**, 97, 8206.
- (95) Potma, E. O.; de Boeij, W. P.; Wiersma, D. A. *Biophys. J.* **2001**, 80, 3019.
- (96) Eaves, J. D.; Fecko, C. J.; Stevens, A. L.; Peng, P.; Tokmakoff, A. *Chem. Phys. Lett.* **2003**, 376, 20.
- (97) Brixner, T.; Gerber, G. *Opt. Lett.* **2001**, 26, 557.
- (98) Ulness, D. J.; Kirkwood, J. C.; Albrecht, A. C. *J. Chem. Phys.* **1998**, 108, 3897.
- (99) Blank, D. A.; Kaufman, L. J.; Fleming, G. R. *J. Chem. Phys.* **1999**, 111, 3105.
- (100) Tanimura, Y.; Mukamel, S. *J. Chem. Phys.* **1993**, 99, 9496.
- (101) Berne, B. J.; Pecora, R. *Dynamic Light Scattering*; Wiley: New York, **1976**.
- (102) Weiner, A. M.; Leaird, D. E.; Wiederrecht, G. P.; Nelson, K. A. *Science* **1990**, 247, 1317.
- (103) Weiner, A. M.; Leaird, D. E.; Wiederrecht, G. P.; Nelson, K. A. *J. Opt. Soc. Amer. B* **1991**, 8, 1264.
- (104) Brixner, T.; Gerber, G. *Opt. Lett.* **2001**, 26, 557.
- (105) Etchepare, J.; Kenney-Wallace, G. A.; Grillon, G.; Migus, A.; Chambaret, J. P. *IEEE J. Quantum Electron.* **1982**, QE-18, 1826.
- (106) Etchepare, J.; Grillon, G.; Chambaret, J. P.; Hamoniaux, G.; Orszag, A. *Opt. Commun.* **1987**, 63, 329.
- (107) Deeg, F. W.; Fayer, M. D. *J. Chem. Phys.* **1989**, 91, 2269.
- (108) McMorro, D.; Lotshaw, W. T. *J. Phys. Chem.* **1991**, 95, 10395.
- (109) Vauthey E. *Chem. Phys. Lett.* **1993** 216 530–6
- (110) Vauthey E. *Chem. Phys.* **1995** 196 569–82
- (111) Harju T O, KorppiTomola J E I, Huizer A H and Varma C. *J. Phys. Chem.* **1996** 100 3592–600
- (112) Gumy J-C, Nicolet O and Vauthey E. *J. Phys. Chem.* **1999** A 103 10737–43
- (113) Peters K S and Kim G. *J. Phys. Chem.* **2001** A 105 4177–81
- (114) Yeow E K L and Braslavsky S E. *Phys. Chem. Chem. Phys.* **2002** 4 239–47
- (115) Yoshihara T, Druzhinin S I, Demeter A, Kocher N, Stalke D and Zachariasse K A. *J. Phys. Chem.* **2005** A 109 1497–509
- (116) Gorbunova T V, Shilov V V and Batalin G I. *Zh. Fiz. Khim.* **1974** 48 2571–2
- (117) Rigby D and Roe R J. *J. Chem. Phys.* **1988** 89 5280–90
- (118) Small D M. *The Physical Chemistry of Lipids* (New York: Plenum) **1986**
- (119) Habenschuss A and Narten A H. *J. Chem. Phys.* **1990** 92 5692–9

- (120) Righini R *Science* **1993** 262 1386–90
- (121) Smith N A and Meech S R *Int. Rev. Phys. Chem.* **2002** 21 75–100
- (122) Kinoshita S, Kai Y, Ariyoshi T and Shimada Y *Int. J. Mod. Phys. B* **1996** 10 1229–72
- (123) Fourkas J T *Nonresonant intermolecular spectroscopy of liquids* *Ultrafast Infrared and Raman Spectroscopy*. ed M D Fayer (New York: Dekker) **2001** pp 473–512
- (124) McMorro D and Lotshaw W T *J. Phys. Chem.* **1991** 95 10395–406
- (125) Scodinu A and Fourkas J T *J. Phys. Chem. B* **2002** 106 10292–5
- (126) SigmaPlot v. 9.0 (Point Richmond, CA: Systat) **2004**
- (127) *Viscosity of Liquids: Aliphatic Nitriles* (London: Engineering Sciences Data Unit) **2002**
- (128) Berne B J and Pecora R *Dynamic Light Scattering* (New York: Wiley) **1976**
- (129) Lotshaw W T, McMorro D, Kalpouzou C and Kenney-Wallace G A *Chem. Phys. Lett.* **1987** 136 323–8
- (130) Kalpouzou C, Lotshaw W T, McMorro D and Kenney-Wallace G A *J. Phys. Chem.* **1987** 91 2028–30
- (131) Deeg F W, Stankus J J, Greenfield S R, Newell V J and Fayer M D *J. Chem. Phys.* **1989** 90 6893–902
- (132) McMorro D and Lotshaw W T *Chem. Phys. Lett* **1991**. 178 69–74
- (133) Chang Y J and Castner E W Jr *J. Chem. Phys.* **1993** 99 113–25
- (134) Neelakandan M, Pant D and Quitevis E L *J. Phys. Chem. A* **1997** 101 2936–45
- (135) Smith N A and Meech S R *J. Phys. Chem. A* **2000** 104 4223–35
- (136) McMorro D and Lotshaw W T *Chem. Phys. Lett.* **1993** 201 369–76
- (137) Debye P *Polar Molecules* (New York: Dover) **1929**
- (138) Kivelson D and Madden P A *Annu. Rev. Phys. Chem.* **1980** 31 523–58
- (139) Chem 3D Pro v. 5.0 (Cambridge, MA: CambridgeSoft) **1999**
- (140) Scodinu A and Fourkas J T *J. Phys. Chem. B* **2003** 107 44–51
- (141) Kalpouzou C, McMorro D, Lotshaw W T and Kenney-Wallace G A *Chem. Phys. Lett.* **1988** 150 138–46
- (142) Kalpouzou C, McMorro D, Lotshaw W T and Kenney-Wallace G A *Chem. Phys. Lett.* **1989** 155 240–2
- (143) Steffen T, Meinders N A C M and Duppen K *J. Phys. Chem. A* **1998** 102 4213–21
- (144) Hunt N T, Jaye A A and Meech S R *J. Phys. Chem. B* **2003** 107 3405–18
- (145) Sirota E B and Herhold A B *Polymer* **2000** 41 8781–9
- (146) Mukherjee P K *J. Chem. Phys.* **2000** 113 4472–5
- (147) Herhold A B, King H E Jr and Sirota E B *J. Chem. Phys.* **2002** 116 9036–50
- (148) Chazhengina S Y, Kotelnikova E N, Filippova I V and Filatov S K *J. Mol. Struct.* **2003** 647 243–57
- (149) Yamamoto T, Nozaki K and Hara T *J. Chem. Phys.* **1990** 92 631–41

- (150) Sirota E B and Wu X Z *J. Chem. Phys.* **1996** 105 7763–73
- (151) Plakhotnik T, Moerner W E, Irgartinger T and Wild U P *Chimia* **1994** 48 31–2
- (152) Penfold J *Rep. Prog. Phys.* **2001** 64 777–814
- (153) Hu C-M and Zwanzig R *J. Chem. Phys.* **1974** 60 4354–7
- (154) Keyes T, Kivelson D and McTague J P *J. Chem. Phys.* **1971** 55 4096–100
- (155) Loughnane B J, Farrer R A, Scodinu A and Fourkas J T *J. Chem. Phys.* **1999** 111 5116–23
- (156) Chandrasekhar S *Liquid Crystals* 2nd edn (Cambridge: Cambridge University Press) **1992**
- (157) So, P. T. C.; Dong, C. Y.; Masters, B. R.; Berland, K. M. *Annu. Rev. Biomed. Eng.* **2000**, 2, 399.
- (158) Millard, A. C.; Fittinghoff, D. N.; Wiseman, P. W.; Muller, M.; Brakenhoff, G. J.; Squier, J. A.; Wilson, K. R. *Biophys. J.* **2000**, 78, 800.
- (159) Volkmer, A.; Cheng, J. X.; Xie, X. S. *Phys. Rev. Lett.* **2001**, 8702, 023901.
- (160) Potma, E. O.; de Boeij, W. P.; Wiersma, D. A. *J. Opt. Soc. Amer. B* **2000**, 17, 1678.
- (161) Zhu, X; Farrer, R.A; Fourkas, J.T. *J. Phys. Chem. B* **2005**, 109, 8481-8488
- (162) Drake, J. M.; Klafter, J., Eds.; *Molecular Dynamics in Restricted Geometries*; Wiley: New York, **1989**.
- (163) Drake, J. M.; Klafter, J.; Kopelman, R.; Awschalom, D.D., Eds.; *Dynamics in Small Confining Systems*; Materials Research Society: Pittsburgh, **1993**; Vol. 290, pp 377.
- (164) Drake, J. M.; Klafter, J.; Kopelman, R.; Troian, S. M., Eds.; *Dynamics in Small Confining Systems II*; Materials Research Society: Pittsburgh, **1995**; Vol. 366, pp 466.
- (165) Drake, J. M.; Klafter, J.; Kopelman, R., Eds. *Dynamics in Small Confining Systems III*; Materials Research Society: Pittsburgh, **1997**; Vol. 464, pp 388.
- (166) Drake, J. M.; Grest, G. S.; Klafter, J.; Kopelman, R., Eds.; *Dynamics in Small Confining Systems IV*; Materials Research Society: Warrendale, PA, **1999**; Vol. 543, pp 372.
- (167) Farrer, R. A.; Loughnane, B. J.; Fourkas, J. T. *J. Phys. Chem. A* **1997**, 101, 4005.
- (168) Drake, J. M., Klafter, J., Kopelman, R., Eds.; Temperature-Dependent Dynamics of Microconfined CS₂. In *Dynamics in Small Confining Systems III*; Materials Research Society: Pittsburgh, **1997**; Vol. 464; pp 263.
- (169) Loughnane, B. J.; Farrer, R. A.; Fourkas, J. T. *J. Phys. Chem. B* **1998**, 102, 5409.
- (170) Loughnane, B. J.; Fourkas, J. T. *J. Phys. Chem. B* **1998**, 102, 10288.
- (171) Loughnane, B. J.; Farrer, R. A.; Fourkas, J. T. Rotational Diffusion of Microconfined Liquids. In *Dynamics in Small Confining Systems IV*; Materials Research Society: Pittsburgh, **1999**; pp 33.

- (172) Loughnane, B. J.; Scodinu, A.; Fourkas, J. T. *J. Phys. Chem. B* **1999**, 103, 6061.
- (173) Loughnane, B. J.; Farrer, R. A.; Scodinu, A.; Fourkas, J. T. *J. Chem. Phys.* **1999**, 111, 5116.
- (174) Loughnane, B. J.; Scodinu, A.; Fourkas, J. T. *Chem. Phys.* **2000**, 253, 323.
- (175) Loughnane, B. J.; Farrer, R. A.; Scodinu, A.; Reilly, T.; Fourkas, J. T. *J. Phys. Chem. B* **2000**, 104, 5421.
- (176) Scodinu, A.; Fourkas, J. T. *J. Phys. Chem. B* **2002**, 106, 10292.
- (177) Farrer, R. A.; Fourkas, J. T. *Acc. Chem. Res.* **2003**, 36, 605.
- (178) Scodinu, A.; Farrer, R. A.; Fourkas, J. T. *J. Phys. Chem. B* **2002**, 106, 12863.
- (179) Brinker, C. J.; Scherer, G. W. *Sol-Gel Science: The Physics and Chemistry of Sol-Gel Processing*; Academic Press: San Diego, CA, **1990**.
- (180) Majors, R. E.; Hopper, M. J. *J. Chromat. Sci.* **1974**, 12, 767.
- (181) Righini, R. *Science* **1993**, 262, 1386.
- (182) Fourkas, J. T. Nonresonant Intermolecular Spectroscopy of Liquids. *In Ultrafast Infrared and Raman Spectroscopy*; Fayer, M. D., Ed.; Marcel Dekker: New York, **2001**; Vol. 26; pp 473.
- (183) Kinoshita, S.; Kai, Y.; Ariyoshi, T.; Shimada, Y. *Int. J. Mod. Phys. B* **1996**, 10, 1229.
- (184) Loughnane, B. J.; Scodinu, A.; Farrer, R. A.; Fourkas, J. T.; Mohanty, U. *J. Chem. Phys.* **1999**, 111, 2686.
- (185) McMorrow, D.; Lotshaw, W. T. *J. Phys. Chem.* **1991**, 95, 10395.
- (186) Chang, Y. J.; Castner Jr., E. W. *J. Phys. Chem.* **1996**, 100, 3330.
- (187) Neelakandan, M.; Pant, D.; Quitevis, E. L. *Chem. Phys. Lett.* **1997**, 265, 283.
- (188) Ricci, M.; Bartolini, P.; Chelli, R.; Cardini, G.; Califano, S.; Righini, R. *Phys. Chem. Chem. Phys.* **2001**, 3, 2795.
- (189) Chelli, R.; Cardini, G.; Ricci, M.; Bartolini, P.; Righini, R.; Califano, S. *Phys. Chem. Chem. Phys.* **2001**, 3, 2803.
- (190) Ratajska-Gadomska, B.; Gadomski, W.; Wiewior, P.; Radzewicz, C. *J. Chem. Phys.* **1998**, 108, 8489.
- (191) Ricci, M.; Wiebel, S.; Bartolini, P.; Taschin, A.; Torre, R. *Philosoph. Mag.* **2004**, 84, 1491.
- (192) Berne, B. J.; Pecora, R. *Dynamic Light Scattering*; Wiley: New York, **1976**.
- (193) Irons, E. *J. Philosoph. Mag.* **1943**, 34, 614.
- (194) Battaglia, M. R.; Buckingham, A. D.; Williams, J. H. *Chem. Phys. Lett.* **1981**, 78, 421.
- (195) Ma, J. C.; Dougherty, D. A. *Chem. Rev.* **1997**, 97, 1303.
- (196) Narten, A. H. *J. Chem. Phys.* **1977**, 67, 2102.
- (197) Cabaco, M. I.; Danten, Y.; Besnard, M.; Guissani, Y.; Guillot, B. *J. Phys. Chem. B* **1997**, 101, 6977.
- (198) Bacon, G. E.; Curry, N. A.; Wilson, S. A. *Proceeding of the Royal Society (London) Series A* **1964**, 279, 98.

- (199) Gaines, G. L., Jr.; Le Grand, D. G. *Colloids and Surfaces, A: Physicochemical and Engineering Aspects* **1994**, 82, 299.
- (200) Yi, J.; Jonas, J. *J. Phys. Chem.* **1996**, 100, 16789.
- (201) Kivelson, D.; Madden, P. A. *Annu. Rev. Phys. Chem.* **1980**, 31, 523.
- (202) Madden, P. A.; Battaglia, M. R.; Cox, T. I.; Pierens, R. K.; Champion, J. *Chem. Phys. Lett.* **1980**, 76, 604.